Title
LOW-TEMPERATURE TOUGHNESS OP BCC Fe-Ni-Ti ALLOYS

Author
Sasaki, Go.

Publication Date
1973-07-01

LBL-1493

c.1

LOW-TEMPERATURE TOUGHNESS OF BCC Fe-Ni-Ti ALLOYS

Go Sasaki
(D. Eng. Thesis)

July 1973

Prepared for the U. S. Atomic Energy Commission
under Contract W-7405-ENG-48

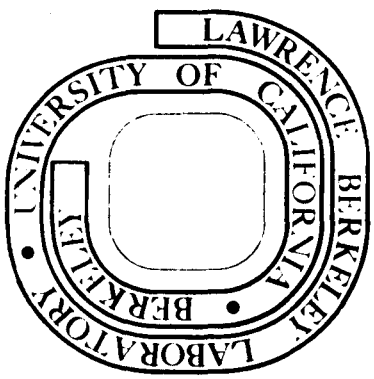

LBL-1493

DISCLAIMER

TABLE OF CONTENTS

LOW-TEMPERATURE TOUGHNESS OF BCC Fe-Ni-Ti ALLOYS

Go Sasaki

Inorganic Materials Research Division, Lawrence Berkeley Laboratory and Department of Materials Science and Engineering, College of Engineering; University of California, Berkeley, California

ABSTRACT

The microstructural and kinetic factors controlling low-temperature toughness such as recystallization, substructure, grain size, precipitation hardening, austenite formation and retained austenite were systematically investigated on interstitial-free bcc Fe-Ni-Ti alloys. Among these factors, the grain size was found to be most influential. The enhancement of low-temperature toughness by controlling these microstructural factors was successfully accomplished. As a result, a new cryogenic alloy with the extraordinary combination of strength and toughness was developed. The Fe-12Ni-0.5Ti alloy has a yield stress of ~ 200 ksi and a V-notch impact energy of ~ 100 ft-lbs at - 267°C (6°K). Up to this date, no comparable results have been reported.

The effect of the grain size on the ductile-brittle transition temperature, T_c, was also investigated. There exists a shift from a low grain size dependence on T_c to a high grain size dependence at grain size ~ 5μ. When the grain size is reduced to less than 3μ, the ductile-brittle transition is suppressed to a lower temperature and does not appear even at temperatures very close to absolute zero. Hence, having the bcc structure in iron alloys is a necessary condition for the presence of the transition, but not a sufficient one.

I. INTRODUCTION

Is the brittle behavior of bcc iron alloys inevitable and unavoidable? This is a question that engineers and scientists have asked themselves since the discovery that iron can exist in two different crystal structures. Brittle failures continue to occur in oil tankers, airplanes, pipelines, etc. with alarming frequency.[1,2] This study will answer the long-pending, difficult question: can bcc iron be made to behave in a ductile manner at cryogenic temperatures.

Let us compare the mechanical properties associated with the two most common crystal structures, fcc and bcc. It is now well established that the stress-strain curve of bcc single crystals can be divided into three distinct stages. Stage I, in which the work hardening rate is approximately linear, is called "easy glide." In Stage II the work hardening rate is also linear, but much greater than that of Stage I, of the order of G/300. Stage III shows a region in which the work hardening rate decreases continuously with increasing strain. Polycrystalline fcc metals and alloys do not show Stage I and deform primarily in a way equivalent to Stage III in a single crystal deformation.

The stress-strain curve of annealed polycrystalline bcc is characterized by an upper yield point, a lower yield point and a Lüders strain range. It is, however, also true that many polycrystalline bcc crystals, especially interstitial-free materials, do not show these phenomena, nor do quenched and tempered steels. T. E. Mitchell, et al.[3]

found the stress-strain curve for zone melted high purity Nb single crystals to be similar to those characteristic of fcc crystals. The three-stage hardening curve has since been observed in many bcc metals, iron,[4-6] tantalum[7] and molybdenum.[8] In spite of this increased knowledge, the stress-strain behavior of bcc crystals is not yet clearly understood.

There exist two important differences in mechanical behavior between polycrystalline bcc and fcc metals when they are tested at low temperatures ($T < 0.2\ Tm$). The first is a strong temperature dependence of flow stress in bcc crystals, while there is a much smaller temperature dependence for fcc metals. D. F. Stein and J. R. Low[9] reported that the temperature dependence of the flow stress in bcc iron could be decreased as the impurity level, especially interstitial element impurities, is lowered. However, even when impurity levels were extrapolated to zero, there still exists a relatively strong temperature dependence.

The flow stress consists of two components, a thermal component σ^* and an athermal component σ_μ. In the polycrystalline fcc crystals, σ_μ is the larger component, accounting for more than 70 percent of the total stress. On the other hand, in the polycrystalline bcc, σ^* is the larger component at very low temperatures. Analyzing the activation energy and activation volume for dislocation motion, H. Conrad[10] indicated that the thermal component σ^* is associated with the overcoming of a high Peierls-Nabarro force in the bcc crystals.

The second difference is that bcc materials undergo the ductile to brittle transition, whereas there is no such transition in fcc metals. The embrittlement of bcc materials occurs over a relatively small temperature range, the ductile-brittle transition temperature, T_c.

The T_c is known to be strain rate and stress concentration sensitive. The T_c determined by Charpy impact test is usually higher than that by conventional tensile test, due mainly to the two reasons, its higher strain rate and the presence of a notch. Consequently, the materials can be used when the safety parameter, T_c, determined in the same service conditions of the materials, is always scrupulously kept below the sevice temperature.

T_c is also the temperature where a relatively temperature-insensitive fracture stress, σ_F becomes equal to the flow stress, σ_f, as measured by a conventional tensile test. Hence, for a given strain rate, T_c can be lowered by

1) raising the fracture stress level
2) decreasing the thermal component of flow stress σ^*
3) decreasing the athermal component of flow stress σ_μ

Several major ways to achieve a decrease in the transition temperature have been suggested:

a) use of uniformly distributed fine ductile precipitates
b) thermomechanical treatment
c) decrease in grain size
d) ultra-high purification
e) use of a getter to remove interstitials

The fracture stress level can be raised by a), b) and c). Both σ^* and σ_μ can be reduced by d) and e).

A group research effort was conducted to design and develop a superior high strength alloy, especially for cryogenic service. The Fe-Ni-Ti ternary system was found to be excellent for this purpose for five reasons. First, the structure with high dislocation density (in equiaxed alpha or massive martensite, α') can be obtained when the alloy is quenched from the austenite region. Secondly, the ferrite, α, which is an annealed α', can provide the sites for precipitation to occur. Thirdly, ultrafine grain size can be achieved by thermal and thermomechanical treatment utilizing the $\alpha' \rightarrow \gamma$ reverse transformation. All of these factors will raise the fracture stress level. Fourthly, the use of the purest possible raw materials of substitutional elements such as nickel and titanium act to decrease σ^*. Finally, small amounts of titanium can act as a getter of not only the interstitials such as carbon and nitrogen but also oxygen.

Earlier work done in this laboratory by W. Horwood has demonstrated that a ternary Fe-12 wt.% Ni-0.5 wt.% Ti alloy exhibits a remarkable combination of strength and toughness at - 196°C. The properties of this alloy are superior to those of the presently existing commercial alloys, such as 9Ni steel and 304L.[11,12] There are several factors which will affect the mechanical properties of the Fe-Ni-Ti ternary alloys, and the mechanism responsible for the combination of high toughness and high strength is considered to be due to complex interactions of these factors. Hence, it was felt important to study

each factor separately and then to consider the mixed effects of combinations.

The objective of this study was to elucidate the mechanism responsible for the high toughness of the Fe-Ni-Ti alloys, by using alloys with three different nickel contents (8%, 12% and 16%).

This study was divided into two parts. In part 1, the mechanical properties of the Fe-Ni-Ti alloys at - 196°C were systematically investigated. The microstructural factors controlling the low temperature toughness were studied and, as a result, tremendous improvement in low-temperature toughness was obtained by controlling the microstructural constituents.

In part 2, the effects of grain size on the ductile-brittle transition temperature were investigated, and the results were compared with existing theories.

II. EXPERIMENTAL PROCEDURE

A. Materials Preparation

1. Alloy Composition

The alloys used for the investigation were prepared by induction melting in an argon atomsphere. The raw materials were electrolytic iron (99.9%), high purity nickel (99.9%) and sponge titanium (99.9%). The melts were cast into 20 lb. ingots (1.75 in. diameter by ~ 10 in. length), which were homogenized for 72 hrs. at 1100°C. The ingots were cross forged to a 1.75 in. by 2.50 in. shape at 1000°C.

The specimens for chemical analysis were cut from the center of the forged billet, the results of which are given in Table 1. The flow stress and the toughness of bcc iron are known to be greatly influenced by impurities such as carbon, nitrogen and oxygen.[9,13] The alloys used showed impurity levels of C ~ 40 ppm max., N ~ 100 ppm max. and O ~ 400 ppm max. The mechanical properties of concern were those of the 8Ni-0.5Ti, 12Ni-0.5Ti and 16Ni-0.5Ti alloys. The binary alloy 12Ni was used to check the role of titanium. The weight percent is given unless otherwise mentioned.

2. Processing and Heat Treatment

In order to investigate the effect of prior structure on the mechanical properties of the 12Ni-0.5Ti alloy, three processings were applied. The first processing was a standard treatment (STD) in which

the forged billets were cut into a 0.625 in. by 2.50 in. plate, and annealed at 900°C for 2 hrs.

Without cutting, the other forged billets were directly annealed at 900°C for 2 hrs. and used for the second and third processings. The second processing was warm rolling to 0.625 in. by 2.50 in. plate at 680°C (WR), which was the middle of the A_s (austenite start temperature) and A_f (austenite finish temperature). The third was cold rolling at room temperature to 0.625 in. by 2.50 in. plate (CR). The reduction of ~ 60% was chosen so that cold working penetrated into the center; the reheated structures were uniform throughout the section.

The heating and cooling curves were obtained by using specimens of the same size as those used for the mechanical tests. The thermocouple was attached into a 0.063 in. diameter 0.500 in. deep hole, made at the center the specimen. After processing, the 0.625 in. by 0.50 in. specimens were cut, heat treated in an air furnace (±5°C) and quenched into 0°C water.

The 0.125 in. by 0.125 in. by 0.125 in. specimens, cut from the plates already processed, were used for aging studies.

B. Mechanical Testing

1. Hardness Tests

A Wilson Rockwell Hardness Tester was employed for hardness measurements; the "C" scale was used. At least five hardness impressions were made on each specimen for Charpy impact test and aging studies, and the hardness values reported are average values.

2. Charpy Impact Tests

When the Charpy specimens were machined, the specimen number and notch direction were marked for each specimen, and the bars were then heat treated. Figure 1 illustrates sectioning of the specimens and the notch direction. Standard Charpy-V-notch specimens (Fig. 2a) were used, except for the test at -266°C in which case shorter specimens, 51 mm in length instead of 55 mm (2.165 in.)(2.009 in.), were used. The tests were conducted on a 223 ft-lbs capacity Charpy impact testing machine between the temperatures 25°C (room temperature) and - 267°C (liquid He temperature).

Methyl alcohol (99%) bath cooled by dry ice was used for the test at -77°C; isopentane bath cooled by liquid nitrogen was used for temperatures between -120°C and -170°C. Liquid nitrogen was the coolant for the -196°C test. ASTM Specification E-23-64 was carefully followed throughout the test. Specimens were kept at least 15 min. in the cooling bath, and were impacted within 3 sec. after removal.

The impact test at -267°C was conducted using a 0.50 in. by 0.50 in. by 2.50 in. lucite box in which the specimen was placed with styrofoam and liquid helium was directly inserted. By this method, which is described by S. Jin, et al.,[14] the specimen was cooled to -266°C within 3 min. and kept at that temperature for an additional minute before the impact.

3. Tensile Tests

The 1.000 in. gage length, 0.250 in. diameter round specimens shown in Fig. 2b were used for determining the tensile properties except for the test at -267°C, in which case, the 0.500 in. gage length, 0.125 in. diameter subsize round specimens were used.

An 11,000 lb capacity Instron Testing Machine was used at a cross head speed of 0.05 cm/min (~0.02 in./min) which gives a strain rate of 10^{-4}/sec.

The testing temperatures were 25°C (room temperature) and three lower temperatures, -77°C, -196°C and -267°C. In the latter three cases, the tests were conducted in baths of 1) methyl alcohol (99%) cooled by dry ice, 2) liquid nitrogen and 3) liquid helium, respectively.

C. Dilatometry

Dilatometric studies were carried out to determine the As, Af, M_s (martensite start temperature) and M_f (martensite finish temperature) and also to investigate the martensite-austenite reverse transformation characteristics. The dilatometer was especially designed and made so that it not only give the heating and cooling rate of 3°C/min, but also simulate exactly the same heat treatment condition (~50°C/min) as the specimens used for mechanical tests. Figure 3 shows the outline of the equipment and the specimen dimensions.

When the isothermal study was being performed, the set of the dilatometry including LVDT (linear variable differential transformer), glass tubes and the specimen was charged into the vertical furnace at

a predetermined temperature. The thermocouple was attached to a 0.063 in. diameter and 0.125 in. deep hole in the middle of the specimen. The steady-state conditions were obtained within a minute. During heat treatment, high purity argon gas was charged from the bottom of the furnace throughout the test in order to prevent possible scale formation on the specimen surface which could lead to an error in reading. After the test, the set was taken from the furnace and the M_s and M_f values were measured.

A length change during the exposure at the three phase ($\alpha + \gamma +$ ppt) range, $\Delta\ell$, was compared with that of a length change $\Delta\ell_o$ in the austenite range.

D. X-Ray Analysis

The amount of the retained austenite was determined using a Norelco type 12045 diffractometer with $CuK_{\alpha 1}$ ($\lambda = 1.54050$Å) radiation and monochrometer.

The specimen was polished and slightly etched. The intensities of 110, 200 and 211 reflections from bcc and 111, 200, 220 reflections from fcc were determined and compared.

E. Microscopy

1. Optical Microscopy

Specimens prepared for optical microscopy were polished with energy paper and 1.0μ diamond paste and finished with 0.5μ Al_2O_3 particles. The etchant used was a freshly mixed solution of 50%

Kalling solution and 50% nital. Observations were made on transverse sections for all specimens and both transverse and longitudinal sections for warm rolled and cold rolled specimens.

2. Scanning Electron Microscopy

The fracture surface of selected charpy impact and tensile specimens was examined with Jeolco JSM-U3 scanning electron microscope (SEM) with secondary emission at 25 kV.

A technique in which the polished and etched surface, and also the fracture surface can be observed simultaneously was developed and utilized to correlate the microstructure directly to the fracture path. The specimens were mounted by transoptic powder so that the fracture surface will be at an obtuse angle with respect to the would-be polished surface. The specimens were heavily etched after polishing and broken off mechanically from the mounts. The observation was made under SEM with the specimen tilted to obtain optimal focus and contrast conditions in the picture.

3. Transmission Electron Microscopy

Thin foils were observed with a Hitachi HU-125 electron microscope and a Siemens Elmiskop 1A microscope both operated at 100 kV. Foil preparation consisted of cutting 20 mil sections from bulk samples, chemical thinning to 2 ~ 4 mils, followed by either jet polishing or window technique. The chemical thinning solution was 5% hydrofluoric acid in hydrogen peroxide. The polishing solution was an electrolyte of 75 g of CrO_3 in 400 cc of acetic acid and 20 cc of H_2O.

III. RESULTS

A. Phase Transformation

The phase transformation temperatures were determined by using the dilatometer which is shown in Fig. 3. The specimens used were previously austenitized at 900°C for 2 hours and then air cooled. The heating and cooling rates were 3°C/min. The austenite start and finish temperatures, A_s and A_f, and the martensite start and finish temperatures, M_s and M_f are listed in Table 2.

The equilibrium phase diagram was constructed from dilatometric and metallographic studies, as illustrated in Fig. 4. The structure of high dislocation density, equiaxed alpha or massive martensite (both bcc structures) can be obtained when the iron-rich Fe-Ni-Ti alloys are cooled to room temperature from austenite, γ. This quenched structure is referred to as the alpha prime phase, α'. As the structure is reheated again to higher temperatures the reverse $\alpha' \rightarrow \gamma$ transformation occurs. In the intermediate temperatures, α' transforms to austenite, γ; ferrite, α; and the precipitate phase, ppt. The austenite γ thus formed transforms to α' during quenching while α remains unchanged. In the lower temperature range, α' changes to α and the precipitate phase, ppt. In the phase diagram by R. Vogel and H. J. Wallbanm,[15] the precipitation of Laves phase $(FeNi)_2Ti$ appears only in the lower temperature range. Our observation, however, shows the evidence of the precipitation in the intermediate temperature range as well as in the lower temperature range. G. R. Speich[16] also reported

the three phase range at the intermediate temperatures. The identity of the precipitates is still controversial. This problem will be discussed in Chapter III, F.

B. Mechanical Tests at - 196°C (77°K)

1. Effects of Prior Structure

As described in the material preparation section, three processings were applied to investigate the effects of the prior structure on the mechanical behavior of the alloys. They were a) standard treatment, annealing at 900°C (STD), b) warm rolling 60% at 680°C which is approximately the center of A_s and A_f temperatures (WR), and c) cold rolling at room temperature with a reduction of 60% (CR). The purpose of the second and the third processings was to increase the fracture stress level, which could lead to a decrease in the ductile-brittle transition temperature, T_c. After these processings the alloys were reheated at intermediate temperatures (600°C ~ 900°C) for an hour and quenched into 0°C water.

The V-notch Charpy impact energies were measured at liquid nitrogen temperature, - 196°C. The results are shown in Figs. 5, 6 and 7 for STD, WR and CR, respectively. The hardness readings at room temperature and the effective grain diameter, d*, are also indicated in the figures. The effective grain diameter indicates the grain size of the quenched structure and does not necessarily mean the austenite grain size. This topic will be discussed in detail in section III, F.

The tensile properties of the 12Ni-0.5Ti alloys at - 196°C are listed in Table 3. As the reheating temperature increased, the strength followed the same pattern, independent of processings, though the strength levels for CR and WR conditions were higher than that of STD. The strength was at a peak at 600°C, and it gradually decreased to 700°C where it leveled off. The tensile at - 196°C did not show any brittle behavior.

The V-notch Charpy impact tests, on the other hand, showed both brittle and ductile fractures. The impact energy values of high toughness were quite similar (100-130 ft-lbs) for the three processings treatments, but the width of the high toughness plateaus were sensitive to the processings. The plateau was narrow, only a few degrees at 700°C for STD. For the WR and CR specimens, however, it extended between 700 ~ 800°C. The toughness at lower temperatures (600, 650°C) of the WR specimens remained comparatively higher, whereas that of the STD and CR specimens was lower. W. Horwood[11] observed the high toughness plateau between 700 and 750°C in the 12Ni-0.5Ti alloy. The different prior structures changed the kinetics of the reverse $\alpha' \rightarrow \gamma$ phase transformation producing the different microstructures which affected the mechanical response of the material.

2. Effects of Ni Content

The effects of Ni content on the mechanical properties in the Fe-Ni-Ti ternary alloys were investigated using the 8Ni-0.5Ti, 12Ni-0.5Ti and 16Ni-0.5Ti alloys. Figures 8 and 9 show the results of the Charpy tests at the liquid nitrogen temperature, - 196°C, for

the STD and CR specimens, respectively. The hardness readings are again indicated on the same graph. The tensile properties of the alloys were determined at - 196°C, as shown in Table 4. The yield strength was found to increase remarkably as the nickel increased from 8% to 16% for both STD and STD - 700 specimens.

As shown in Figs. 8 and 9, the impact energies changed drastically according to the increase in nickel. The STD specimen of the 8Ni-0.5Ti alloy, did not show any peak; the 12Ni-0.5Ti showed a narrow peak, and the 16Ni-0.5Ti showed an extended peak. In the case of CR specimens, the 8Ni-0.5Ti alloy did show a small peak, the 12Ni-0.5Ti a wide peak and the 16Ni-0.5Ti an extended peak. These facts clearly negate the validity of the original explanation[11,12] that high toughness plateau corresponded to the three phase ($\alpha + \gamma$ + ppt) range.

C. Mechanical Test at - 267°C (6°K)

The V-notch Charpy tests and the tensile tests were carried out at liquid helium temperature, - 267°C, by the method described in section II. As shown in Table 5, the impact energy values are high. Both specimens of WR-700 and WR-700 cycle, did not show any transition from ductile to brittle even as low as - 267°C. The impact values of 92 ~ 101 ft-lbs at - 267°C were the highest values attained. The specimens of WR - 700 cycle were prepared by warm rolling and multi-thermal cycling (five times) at 700°C followed by 0°C water quenching. The thermal cycling was used to reduce the effective grain diameter.

The tensile tests did not reveal any brittle failure, as illustrated in Table 5. The strength increased from ~ 140 ksi to 200 ksi and the tensile ductilities remained almost the same as the testing temperature was decreased from -196°C down to - 267°C.

Investigating the mechanical properties of the Fe-12Ni-0.25Ti alloy, S. Jin et.al.[62] very recently reported the impact energy values which exceeds the authors values in the Fe-12Ni-0.5Ti alloy. The yield stress of the Fe-12Ni-0.5Ti alloy (~ 200 ksi), however, is superior to the Fe-12Ni-0.25Ti alloy (~ 185 ksi). To the authors knowledge, no comparable results have ever been reported in the literature.

As illustrated in one of the curves in Figs. 10 to 12, the stress strain curves of specimens tested at - 267°C showed the serrations after yielding. This serration phenomenon is not uncommon at testing temperatures very close to absolute zero.[17,18,19] There have been a number of explanations for the cause of this phenomenon such as deformation twinning, martensite formation, etc., although now it is generally agreed that the serration are caused by adiabatic heating.[17,18]

D. Mechanical Tests at - 77 and 25°C

Specimens with various sizes of recrystallized austenite grains were selected from the 12Ni-0.5Ti alloy, and tensile tests and Charpy impact tests were carried out at dry ice temperature, - 77°C, and at room temperature, 25°C. The results for -77°C and 25°C are shown in Table 5 and 6, respectively. No brittle failure was observed.

E. Temperature Dependence of Mechanical Properties

It is of importance to investigate a wide range of properties to obtain an overall picture and an understanding of the principles involved. It is especially important for bcc materials such as the alloys used in this investigation, because they demonstrate strong strain rate and temperature dependencies.

In the tensile tests, the strain rate was kept constant at 10^{-4}/sec, and the stronger effect of the temperature dependence on the mechanical properties was investigated. Figures 10 to 12 show typical engineering stress strain curves at the various testing temperatures. Several serrations were observed just after yielding in the stress strain curve for - 267°C. The stress strain curves for the - 196°C, -77°C tests and those made at 25°C showed a small work hardening, but no yield drop.

The effect of the testing temperature on both tensile and impact properties differs with processing treatment. Figures 13 to 15 show such effects for the STD, STD-700 and WR-700 specimens. The yield stress and ultimate tensile strength increased slowly from testing temperature, 25°C to -100°C, and rather rapidly there after, as the testing temperature decreased. The tensile elongation increased slightly with decreasing testing temperatures of 25°C to -196°C, and then decreased as the temperature was further lowered toward -267°C. The reduction of area curve had a peak at -77°C, and decreased rather rapidly as the testing temperature decreased.

The tensile tests did not reveal any ductile-brittle transition even at -267°C. The transition was observed in the Charpy impact tests where the strain rate is high. As shown in Fig. 13, the STD specimen has the ductile-brittle transition temperature of -170°C in Charpy tests. When the grain size was decreased, the ductile-brittle transition temperature decreased (Fig. 14) and finally, the transition did not occur in the Charpy tests (Fig. 15). The effect of grain size will be discussed in detail in Section IV.

F. Metallographic Studies

Metallographic studies are especially important for correlating mechanical properties with microstructures. Optical microscopy and transmission electron microscopy were extensively used to identify the microstructural features. Scanning electron microscopy was successfully used to relate the microstructure to fracture path.

1. Optical Microscopy

The optical micrographs of the 12Ni-0.5Ti alloys are shown in Figs. 16-18. Figure 16 illustrates the microstructures of a series of STD specimens,

(a) STD (annealed at 900°C for 2 hrs.)

(b) STD-600 (reheated at 600°C for an hour and quenched into 0°C water)

(c) STD-650 (reheated at 650°C for an hour and quenched into 0°C water)

(d) STD-700 (reheated at 700°C for an hour and quenched into 0°C water)

(e) STD-750 (reheated at 750°C for an hour and quenched into 0°C water)

(f) STD-800 (reheated at 800°C for a hour and quenched into 0°C water).

The microstructure of the STD specimen consists of both jagged boundaries, typical of so called "massive martensite," and rather smooth boundaries, typical, of equiaxed alpha structure. The detail on the substructure will be discussed in section IV, A.

The term, "packet size" is sometimes used to express the size of the martensitic structure. This terminology is, however, not applied to the equiaxed structure. Hence, the term, "effective grain diameter" was felt most adequate to describe the size of the quenched structure. When the alloy was treated at 600 or 650°C, prior austenite grains boundaries can be revealed. Figures 16b, c show such micrographs. Using the intercept method,[20] the prior austenite grain size and the effective grain diameter were measured as 50μ and 24μ, respectively. The microstructure of the STD-650 specimen (Fig. 16c) indicates the presence of duplex structure of α and α'. As shown in Figs. 16d, e, f. The STD-700, STD-750 and STD-800 treatments produce the well recrystallized structures.

The microstructures of the WR and CR specimens are shown in Figs. 17 and 18, respectively. Both warm rolling and cold rolling produced the fine recrystallized structures at 700°C (See Fig. 17d and 18d) and the structures remained small compared to the STD specimen with the same reheating temperatures such as 750, 800 and 850°C.

The effective grain diameter, d*, was measured for all recrystallized specimens, STD-700, STD-750, STD-800, WR-700, WR-750, CR-700, CR-750, etc., and the results are plotted in Figs. 5-7.

The microstructures of the 8Ni-0.5Ti and 16Ni-0.5Ti alloys, both STD specimens, are illustrated in Figs. 19 and 20, respectively. The annealing conditions, at 900°C for 2 hrs, were selected to enable all three alloys to start with the same grain size. Comparisons can be made by observing Figs. 16a,b, Figs. 19a,b and Figs. 20a,b. The structure of the 8Ni-0.5Ti alloy (Fig. 19a) consisted of both smooth and jagged boundaries indicating a mixed structure of massive martensite and equiaxed alpha. The annealed structure of the 16Ni-0.5Ti alloy (Fig. 20a) showed only massive martensite.

The STD-700, and STD-750 specimens of the 8Ni-0.5Ti alloy (Figs. 19d,e) had duplex structures of α and α'. It wasn't until 800°C that a recrystallized structure could be obtained (Fig. 19f), for the A_s and A_f of the 8Ni-0.5Ti alloys are shifted to higher temperatures. For the 16Ni-0.5Ti alloy, massive phase transformation takes place, especially at the prior austenite boundaries, at 650°C (Fig. 20c), and the alloy recrystallizes at 700°C (Fig. 20d).

2. Transmission Electron Microscopy

The purpose of the transmission electron microscopy work was to observe the precipitate and the substructure.

A large number of fine rod-shaped precipitates which are regularly oriented to the matrix, were found in the STD-600 and STD-650 specimens of the 12Ni-0.5Ti alloy, as shown in Figs. 21 and 22, respectively.

The dimensions of the particles range from a cross section of 40 to 100Å in diameter and length of 100 to 1,000Å. Such particles had not been observed in the recrystallized specimens (such as the STD-700, STD-750, etc.). Attempts to determine the crystal structure of the precipitates was unsuccessful; the particles were too small to be extracted. The phase diagram[15,16] suggests that a Laves phase $(FeNi)_2Ti$ is more likely to form, but NiTi[21] and Ni_3Ti[22,23,24] have been reported to form in the Fe-Ni-Ti ternary system.

The substructure of the annealed 12Ni-0.5Ti alloys consisted of both long parallel laths, typical of massive martensite, and large tangled dislocation structures, typical of equiaxed alpha structure. Subsequent heat treatment at 700°C to 800°C produce more round boundaries as well as long lath boundaries, indicating the presence of both mixed structures of massive martensite and equiaxed alpha. The substructural change among the recrystallized specimens, i.e., STD-700, STD-750 and STD-800, was too small to make a quantitative measurement. This was also true for the recrystallized structures of the WR and CR specimens. Figures 23 and 24 shows the typical substructures of the STD-700 and STD-750 specimens, respectively.

3. Fractrography

A technique in which one can simultaneously observe both polished and etched surface and fracture surface under the SEM was developed, and extensively used to correlate the microstructure directly to the fracture path. Figures 25 to 27 show such pictures for Charpy impact

specimens of the 12Ni-0.5Ti alloy tested at -196°C. The observation was made on the entire fracture surface, but the pictures were taken from the center part of the fractured specimens.

Figure 25a indicates that brittle fracture actually occurred at the massive martensite boundaries in the annealed (STD) specimen. Fracture mode was mostly quasi-cleavage. Figure 25b shows the ductile dimple structure of the STD-700 specimen which has the Charpy impact energies of ~ 120 ft-lbs at -196°C. There seemed to be no clear relationship between the microstructure and fracture path in the ductile specimen, in which numerous holes always existed below the fracture surface, often as far as 2 mm from the surface.

In Fig. 25a, the STD-600 specimen indicated that fracture occurred mostly at the prior austenite grain boundaries, suggesting the fracture mode of intergranular fracture, less cleavage. This was due to the preferred formation of austenite at the prior austenite grain boundaries. (See Fig. 16b) On the other hand, the WR-600 in which the prior austenite structure was small (of the magnitude of 5μ) indicated the ductile dimple structure as shown in Fig. 26b.

In case of the STD-650, austenite forms not only at the prior austenite grain boundaries, but also at the martensite boundaries, and the duplex structure of α and α' becomes dominant (Fig. 16c). As illustrated in Fig. 27a, the fracture mode of the STD-650 specimen, was a mixture of cleavage and intergranular fracture. The WR-650 specimen, however, fractured in a ductile manner as shown in Fig. 27b.

The effect of the testing temperature on the fracture mode was investigated by observing the fracture surfaces of the Charpy specimens tested at 25°C, -77°C, -196°C and -267°C under SEM. Figures 28 and 29 show scanning electron micrographs of fractured surfaces for the STD-700 and WR-700 multicycled specimens. The effective grain size for the former was 5.5μ and 1.7μ for the latter. The dimple sizes do not seem to be affected by the grain size difference. The dimple sizes of the specimens fractured at 25°C seems to be a little larger than those fractured at -77 and -196°C.

IV. DISCUSSIONS

This section will be divided into two parts. In Part 1, the discussion will focus on the microstructural factors controlling the low-temperature toughness of the Fe-Ni-Ti alloy. The discussion will be further extended to demonstrate how an improvement in toughness can be achieved by controlling these microstructural factors. In Part 2, the effects of the effective grain size on the ductile-brittle transition temperature are investigated and the results compared with existing theories.

PART 1

A. Microstructural Factors Controlling Low-Temperature Toughness

There are several factors which control the mechanical properties of the Fe-Ni-Ti alloys, and the mechanism responsible for high strength and high toughness is considered to be the complex effects of these factors. The effects of these controlling factors on the low temperature toughness are schematically show in Fig. 30 for the reheating temperature range (600 to 900°C). The impact energies at -196°C are also shown for three different prior processings. These effects intricately overlap at a certain temperature. Hence, to elucidate the mechanism of low-temperature toughness, it is of importance to isolate each factor from other factors.

In this section, six microstructural factors which control the low-temperature toughness will be independently discussed. The

mechanism will be explored in the next two sections. The six factors are as follows:

1) recrystallization and recovery
2) substructure
3) grain size
4) precipitation hardening
5) formation of austenite, duplex structure
6) retained austenite

The discussion will be based on the results of the 12Ni-0.5Ti alloy, unless otherwise stated.

1. Recrystallization and Recovery

The microstructures of the specimen reheated at 700°C and above for all three processings, i.e., STD, WR and CR showed clear recrystallized structures. (See Figs. 14-16) The duplex structure did not show consistently higher toughness; the WR-600 and WR-650 remained comparatively high in toughness whereas the toughness was low for the STD-600, STD-650, CR-600 and CR-650 specimens. The 8Ni-0.5Ti alloy recrystallized at 850°C, but the structure became coarse. However, the 16Ni-0.5Ti recrystallized at 700°C and the structure remained fine to temperatures as high as 900°C. (Figs. 17 and 18). Hence, the recrystallized structure is a sufficient condition for high toughness but not a necessary one.

Recovery is important for the cold rolled specimens. Investigating the effect of cold working on the microstructures of 9Ni steel,

R. L. Miller[25] reported that cold working prior to annealing resulted in a new uniformly distributed equiaxed grain structure, whereas without prior cold work, the microstructure retained the acicular appearance of the original martensite. Many factors, such as precipitation hardening and duplex structure, operate at the recovery temperature, ~ 600°C, of the alloy. An attempt has been made to isolate each of the factors and this will be discussed in section IV, C.

2. Substructure--Massive Structure

The so called "massive" structure in iron-base alloys is misleading since the definition of the terminology varies from one researcher to another. For example, Parr's group[26,27] divides the morphology of the substructure in iron-base alloys into three structures, i.e., equiaxed ferrite, massive and martensitic. On the other hand, Owen's group[28-30] proposes that a massive structure in iron-base alloys can be divided into two in view of the transformation mechanism. According to Owen's group, one of the structures is formed by short-range diffusion across an incoherent, or possibly semi-coherent, interface with no resulting shape change. It is called equiaxed alpha structure, which corresponds to the massive structure in the Parr's terminology. The second structure, the massive martensite, is produced by a martensitic process involving shear. This is simply called martensitic in Parr's terminology.

A. Gilbert and W. S. Owen[28] first observed the massive structure in ferrous alloys and pointed out its resemblance to the massive alpha structure in nonferrous alloys. For the above reason, the use of the

Owen's group's terminology and definition was felt adequate in this study. Furthermore, the word "massive martensite" is now widely used (see the survey by G. Krauss and A. R. Marder[31]).

Three kinds of substructure result when Fe-Ni alloys are quenched from austenite range, as shown in Figs. 31a, b, and c.[32] The first picture shows an equiaxed alpha structure which appeared in the Fe-8Ni alloy. This structure consists of approximately equiaxed grains, although the grain boundary contours are more irregular than in a fully annealed metal.[27] No surface relief effects are observed and the crystal structure is bcc.

The second structure, observed in Fe-12Ni alloy is called "massive martensite." The crystal structure is bcc and the interfaces of this structure become very jagged with many straight traces of planes intersected by the polished surface.[27] The transformation is accompanied by a shape change, and it is classified as a martensitic transformation. Figure 31c represents "acicular martensite" which is characterized by the existence of midribs and internal twins. The crystal structure of acicular martensite is bct and there is always an appreciable volume fraction of retained austenite.[27]

The morphology of the quenched structure in the Fe-Ni alloys is affected by several factors such as chemical composition, cooling rate and austenitizing temperature. First, the effect of the chemical composition will be discussed.

Summarizing all available papers[29,33-35] on the effects of alloy chemistry on the morphology of substructure in ferrous alloys, it can be stated that the substructure in Fe-Ni alloys changes with nickel content as follows:

Ni(%) < 10 equiaxed
Ni(%) 10 ~ 29 massive martensite
Ni(%) > 29 acicular martensite

This morphology change is, however, greatly influenced by the carbon content. In a simple Fe-Ni-C ternary system (Ni < 29), the effect of carbon on the martensite morphology is as follows:

C(%)0.0 ~ 0.6 massive martensite
C(%) > 0.3 acicular martensite

The effect of carbon on the transition from equiaxed alpha structure to massive martensite has not been established. As demonstrated by C. L. Magee and R. G. Davis,[35] depending on the nickel and carbon content, a wide range of mix structures of both massive and acicular martensite can be observed. The 9Ni steel, a commercial cryogenic steel containing 0.10C shows massive martensite with internal twins but only the massive martensite is observed when the 9Ni steel carbon level is decreased to 0.01%.[36]

A small amount of titanium in the Fe-8Ni-Ti alloys was found to enhance massive transformation.[32]

All discussions thus far are based on the observation of a regular cooling rate such as water quenching (~ 10^2 °C/sec) and air cooling (~ 10 °C/sec). W. D. Swan and J. G. Parr[26] investigated the effect of cooling rate (from 80 °C/sec up to 60,000 °C/sec) on the substructure

and discovered two transformations, i.e., on equiaxed alpha and massive martensite in Fe-Ni alloys with nickel content from zero to seven percent. At a regular cooling rate, equiaxed structure is likely to form in Fe-Ni with nickel up to seven percent, and massive martensite with ten percent nickel.

The annealed structures of the Fe-Ni-Ti alloys follow a similar pattern. The substructure of the 8Ni-0.5Ti alloy showed the mixed structure of equiaxed alpha and massive martensite (Fig. 19a), and that of the 12Ni-0.5Ti showed the same mixed structure but in this latter case there was more massive martensite (Fig. 16a). The substructure of the 16Ni-0.5Ti alloy, on the other hand, was completely massive martensite (Fig. 20a). The formation of the mixed structure is probably as follows: on continuous cooling, a specimen may transform partially by the short range diffusion, equiaxed alpha type transformation, and at lower temperatures completes the transformation martensitically.

3. Grain Size

The now well known Hall-Petch relationship demonstrates that the flow stress, σ_f is a function of the reciprocal square root of slip band length or grain size, d.

$$\sigma_f = \sigma_o + kd^{-1/2} \qquad (1)$$

where σ_o, the frictional stress, and k, the Hall-Petch slope, are constant. The original models proposed by E. O. Hall[37] and N. J. Petch[38] are based on a pileup of dislocations at the grain boundaries. The lack of direct evidence of dislocation pileups in bcc materials, however, has lead to the development of non pileup theories on yielding.

Recently this subject was critically reviewed by J. C. M. Li and Y. S. Chou.[39] According to H. Conrad,[10] N. J. Petch[40] and A. H. Cottrell[41,42] give rather good support to the relationship

$$\sigma_F \propto \left(\frac{E\gamma}{d}\right)^{1/2} \qquad (2)$$

where σ_F is the fracture stress, E is Young's modulus, γ the surface energy and d the grain size. The fracture stress level can be raised by decreasing the grain size, which decreases the brittle-ductile transition temperature, T_c. The effects of the grain size on the mechanical properties were extensively studied and critically discussed in part II.

4. Precipitation Hardening

The effect of precipitates on the low-temperature toughness is not clearly understood. A massive precipitation at the grain boundaries is alway harmful to toughness. However, introducing fine ductile uniformly distributed precipitates may possibly lead to increased toughness. These precipitates limit the dislocation motion, which can increase the fracture stress level and decrease the T_c.

The Laves phase Fe_2Ti was found to deform partially in a ductile manner, which indicates a ductile compound.[43] The Ni_3Ti is also believed to be a ductile compound.

The thin foil work showed fine rod-shaped precipitates in the specimens reheated at 600 or 650°C (Figs. 21 and 22). The WR-600 and WR-650 specimens did show high toughness at - 196°C. There still

exists more room to further enhance the strength and toughness by introducing more particles.

5. Formation of Austenite--Duplex Structure

The austenite in the iron rich Fe-Ni-Ti alloy with nickel ~ 10% is so unstable that it transforms completely to α' when the alloy is quenched from the austenite region to room temperature. No existence of retained austenite was observed. The result agrees with other works.[28,29,30] This is closely related to the fact that the crystal structure of massive martensite or equiaxed alpha is not bct but bcc.

When the alloy is treated in the three phase ($\alpha + \gamma$ + ppt) range, the formation of austenite and precipitation hardening occur simultaneously. Nickel partitions also occur in α and γ phases, and there exists the possibility of the existence of retained austenite when the alloy is quenched from the three phase range. This subject is described in the next section.

Small but noticeable contractions were observed approximately 100°C below A_s temperature in the dilatometric curves of the 12Ni-0.5Ti and 16Ni-0.5Ti alloys. This slight shift is due to the formation of austenite, suggesting that the first austenite forms about 100°C below the A_s temperature. Similar observations have been reported in the works[36,44,45] on the commercial 9Ni steels.

The formation of austenite is a time and temperature dependent phenomenon. The austenite first forms at the prior austenite and massive martensite grain boundaries, and then in the matrix. The alloy gradually develops a duplex structure of α with precipitates

and γ, which later transforms into α' or possibly is retained.

In order to understand the mechanical properties of the specimen treated at the three phase range, quantitative study of the amount of both α and α' is a necessity. Three methods can be applied to measure the volume fraction of austenite (or α'). The difficulty lies in the fact that α and α' are both bcc.

One method is the use of X-ray diffractometer with high temperature camera. Two groups of researchers applied this method to measure the volume fraction of austenite in 18Ni maraging steel,[31,32] but one of them reported temperature variations of as much as 40°C from one location to another on the sample surface. Hence, this method presents difficulties.

Another possible approach is a metallographic method using the extraction replica technique. α and α' are distinguishable because α will become decorated with precipitates whereas α' will be free from precipitates. This method, however, is not alway reliable. For example, in the early stages of precipitation, this technique does not reveal visible precipitates in replicas.

The best method is to measure a length change, $\Delta\ell$ during the exposure at the three phase range and compare it with a length change $\Delta\ell_o$ in the γ range by the use of a dilatometer. By this method it is also possible to investigate the kinetics of phase transformation. As indicated in Section II, the dilatometer can simulate the same heating conditions as in the heat treatment of the mechanical test specimens. The isochronal phase transformation is shown in Fig. 32. Notice that

a fair amount of austenite formed at 600°C which is 30°C below the A_s.

Cold working prior to annealing increased the rate of austenite formation. This effect is shown in Fig. 33. Notice that the slope of the heating curve of the CR-750 gradually decreases compared with that of the STD-750. R. L. Miller[25] also reported the marked increase in the rate of austenite formation by the effect of cold working.

6. Retained Austenite

The high toughness of the Fe-Ni-Ti alloys can not be explained in the same way as that of a commercial cryogenic material, 9Ni steel, even though the 9Ni steel has been found[45,47] to show a similar high toughness peak. The 9Ni steel develops optimum toughness when treated in the temperature range 500 to 600°C, whereas the optimal temperature for 2Ni-0.5Ti alloys is in the range of 700 to 800°C. The typical A_s and A_f for the 9Ni steel are 615 and 720°C,[36] which are almost the same as the 12Ni-0.5Ti alloys. The high toughness of the 9Ni steels is closely related to the formation of well-dispersed, fine stable austenite, which remains even after quenching and acts as a shock absorber.[45]

The retained austenite was measured on a series of STD specimens of the 12Ni-0.5Ti alloy by using an X-ray defractometer. No retained austenite was observed except some noticeable (111) and (200) peaks from austenite in the STD-600 specimen. The amount was less than 3 percent. This study indicates that the mechanism of high toughness of the Fe-Ni-Ti alloys is not due to the retained austenite.

This does not mean that the retained austenite is detrimental for the Fe-Ni-Ti alloy. When the alloy is treated in the three phase ($\alpha + \gamma$ + ppt) range long enough so that the partition of nickel in the α and γ phases occurs, there is the possibility of existence of retained austenite which may contribute to increase the toughness. This occurs only when the nickel in the γ phase exceeds ~ 25 percent.

B. Toughness Transition-Higher Temperature Side

The Charpy tests at -196°C of the 12Ni-0.5Ti alloy revealed high toughness plateaus for three kinds of processings, i.e., STD, WR and CR. (Figs. 5 to 7) Figure 30 clearly indicates that the microstructural factors controlling the toughness transition at the higher temperature side are a) recrystallization b) substructure and c) grain size. Since the specimen reheated at 700°C or higher showed well recrystallized structures, only two factors, b) and c), remain. First let us discuss factor b), substructure.

Investigating the effect of austenitizing temperature on the transformation temperatures in the Fe-10Ni alloy, W. S. Owen and E. A. Wilson[30] reported that there is an abrupt change in transformation made from the equiaxed alpha to the massive martensite type at the austenitizing temperature of ~ 1050°C. The specimen austenitized below approximately 1050°C transformed at 510°C to equiaxed alpha but those austenitized between 1050 and 1200°C transformed to massive martensite at a much lower temperature of 450°C. They attributed this result to the change in grain size, although the grain sizes were not given.

The recrystallized structures of the 12Ni-0.5Ti alloys did not show any abrupt change in substructure. (Figs. 16d, e, f; 17d, e, f and 18d, e, f) All of them were mixed structures of massive martensite and equiaxed alpha structure. But the amount of massive martensite tended to increase slightly as the reheating temperature was increased. The changes were, however, too small to make a quantitative analysis, as shown in the transmission electron micrographs (Figs. 23 and 24). The highest reheating temperature for this study was 900°C. This is substantially lower than the critical austenitizing temperature of 1050°C in Owen and Wilson's work.[30] Furthermore, during the $\gamma \rightarrow \alpha'$ transformation, the M_s temperatures obtained by dilatometric studies (cooling rate is ~ 50°C/min) for the STD-700, STD-750, STD-800 specimens did not show any abrupt change. Hence, the effect of substructure change in the temperature range from 700°C to 900°C is considered to be insignificant.

Let us now discuss factor c), the grain size. Figure 34 shows the effect of effective grain diameter, d* of the recrystallized specimens on the V-notch Charpy impact energies at - 196°C. There clearly exists a toughness transition when d* approaches the critical value of $d_c^* \sim 6.5\mu$. When the effective grain diameter, d* is plotted against 1/T where T is the absolute temperature, (Fig. 35), $d_c^* \sim 6.5\mu$ falls in the temperature range where the toughness transition occurs for the three processings, i.e., STD, WR and CR. Figure 35 is the direct evidence that the effective grain diameter is controlling toughness transition. The WR and CR processings prior to reheating

were found to refine the grain structure substantially compared with the STD processing.

Figure 35 also provides another interesting insight. The slope of the curve indicates the activation energy for the grain growth if the relationship between the effective grain diameter d^*, and austenite grain diameter d, is linear. In the initial part of the curve, d^* increases rather slowly between 700° and 800°C, which indicates that grain growth is retarded by the phase transformation. Also, in the section of the curve above 800°C, the slope is the same for the three different processings, indicating that the grain growth at 800°C or higher occurs by the same mechanism for the three processings treatments.

C. Toughness Transition-Lower Temperature Side

The toughness transition at the lower temperature side is more complicated. Figure 30 indicates that the microstructural factors controlling the toughness transition at the lower temperature side are a) recrystallization, c) grain size--prior austenite grain size, d) precipitation hardening, e) formation of austenite--duplex structure, and f) retained austenite.

The recrystallization factor is a sufficient condition for high toughness, but not a necessary one since the WR-650 specimen which is not a recrystallized structure (Fig. 17c) maintained high toughness on the average of 90 ft-lbs.

The remaining factors are c) grain size--prior austenite grain size, d) precipitation hardening, e) formation of austenite--duplex structure, and f) retained austenite. Since these factors are important in a similar temperature range, it is almost impossible to isolate each of these factors through isochronal studies.

Therefore, isothermal studies were carried out by measuring the hardness change at 600 and 650°C for, STD, WR and CR of the 12Ni-0.5Ti alloy. In order to isolate the effect of titanium, the 12Ni alloy which was previously annealed at 900°C was included for the study. The results for 600 and 650°C are shown in Figs. 36 and 37. The characteristics of the curve did not change between the isothermal treatment at 600 and 650°C except that the strength level for 600°C was higher than that for 650°C. In STD, the hardness drops first and then gradually reaches a maximum at about at 60 min. and then slowly decreases. In WR and CR, however, the hardness first increases to a maximum and then slowly decreases. The hardness drops sharply first and gradually increases and levels off for the 12Ni alloy. The first hardness drop in the STD specimen is due to the formation of austenite, as can be estimated from the curve of the 12Ni alloy. Precipitation hardening is considered to be responsible for the increase in hardness thereafter.

The hardness increase in the WR and CR specimens is due to the overall effect of both the formation of austenite which works as a negative factor, and to precipitation hardening, which does as a

positive effect. Both processings provide a lot of nucleation sites for both formation of austenite and precipitation and accelerate both reactions.

The Charpy tests were carried out at - 196°C for the specimens treated for 100 hrs (6,000 min.), to compare the results of the as processed specimen and the 1 hr reheated specimen. The STD-700 specimen with smaller grain size was tested instead of the STD specimen since the larger prior austenite grain boundaries was found to be detrimental to low-temperature toughness (Figs. 26 and 27). As shown in Figs. 36 and 37, toughness did not improve by prolonged time exposure. The fracture paths of both WR and STD-700 specimens which were treated at 650°C for 100 hrs. are shown in Fig. 38. The fracture surface of the STD-700 specimen (Fig. 38a) appears to consist of the mixed structure of quasi cleavage and dimples. The irregularity of intersection between the polished surface and the fractured one indicates that the fracture was somewhat hindered by the duplex structure though not enough to fail in ductile manner. It is not clear whether or not the fracture path follows the prior austenite grain boundaries. It seems to so follow in some locations but does not elsewhere. The fracture surface of the WR specimen shows a typical ductile fracture (Fig. 38b). Figure 39 shows the higher magnification of the dimple rupture. The matrix structure consists of duplex structure of α decorated with rod-shaped precipitates and α' without precipitate.

Retained austenite was measured by using an X-ray diffractometer on the hardness specimens treated at 600 and 650°C for 1 hr and also 100 hrs for three kinds of processings. No retained austenite was observed except for a small amount (less than 3%) in the STD-600 specimen. In the 12Ni alloy, however, 30 ~ 50% of retained austenite was observed in the specimens exposed for 100 hrs. Possible explanations are as follows: In the WR and CR specimens of the 12Ni-0.5Ti alloy, the precipitation occurs nearly simultaneously with the formation of austenite, and the nickel can be absorbed in the precipitates as well as in the austenite. Hence, the nickel content in austenite thus formed does not exceed ~ 25%, which is the nickel content of the Fe-Ni-Ti alloy with M_f of room temperature, and austenite is not likely to be retained. In the STD specimen, the austenite forms first and then precipitation occurs. The partition of nickel in the early stage of the exposure produced a small amount of austenite. In the 12Ni alloy, on the other hand, the partition of nickel in ferrite and austenite continues to occur until it reaches a state of equilibrium.

From the above discussions, the factor f), retained austenite, is not a main factor controlling toughness.

Factor d), precipitation hardening, is obviously not a positive factor, but nor is it a negative factor. For the WR-650 and WR-600, specimens showed comparatively high toughness.

Let us discuss the remaining factors, c) grain size--prior austenite grain size, and e) formation of austenite--duplex structure.

The observations on the polished and etched surface in Figs. 38 and 39 indicate that the ratio of α and α' in the duplex structure is about 2 to 3 and that the shape of the α' is oval. Hence factor e) is much the same among the specimens with prolonged exposure for WR and STD-700.

The difference of the prior structures, WR (Fig. 17a) and STD-700 (Fig. 16d) is not only the grain size, but also the grain boundary structure and the matrix structure. The matrix structure of the WR specimen is partially recrystallized whereas that of the latter is totally recrystallized. The effective grain size is 2.1μ for the WR specimens and 5.5μ for the latter. The grain boundary for the WR specimens is therefore much greater in area and is thought to be higher in energy so that the kinetics of phase transformation and precipitation are much faster than that for the STD-700 specimen. When the grain of the prior structure is large, grain boundaries form an envelope of α' along which the fracture occurs (Figs. 26 and 27). A close observation of the fracture path structure in the STD-700 specimen with prolonged time exposure (Fig. 38a) indicates that the fracture size is roughly the same order of magnitude for the STD-600 and STD-650 specimens. This may suggest that the structure prior to the 700°C treatment, the STD treatment, is affecting the fracture path. The isothermal treatment at 700°C the duplex structure develops first and recrystallization is delayed in case of heating rate of $\sim$ 50 °C/min.[11] For that reason, it is quite possible that the orientation of the grains in the STD treatment remains relatively unchanged

even after recrystallized structure is developed by reheating at 700 for 1 hr.

The author thus far has attempted to demonstrate and discuss the importance of the grain size in controlling toughness. However, a more systematic research study needs to be done to explore the mechanism of the high toughness plateau at the low temperature side.

D. Enhancement of Toughness by Grain Size Control

It is well established that the grain refinement increases both strength and toughness in unhardened steel.[49] This study has demonstrated that one of the main microstructural factors controlling low-temperature toughness is the effective grain diameter. In this section, the discussion will focus on how the low-temperature toughness is enhanced through grain size control.

1. Thermomechanical Treatment and Thermal Cycling

The thermomechanical treatment including cold working and the thermal cycling are the two major techniques to refine the structure of the material.[49] Both warm working and cold working were applied in this study. The effects of these two processings on the low-temperature toughness have already been discussed in section III,B; IV,A and IV,B. Figure 40 shows how the grain refining occurs at 750°C in the CR specimen and this is compared with that of the STD. Large number of nucleation sites are observed in the CR specimen during the early stage of reheating. The grain in the CR specimens remains fine even as the reheating temperature increases (Fig. 35).

Multithermal cycling was also applied to enhance the low-temperature toughness through grain size effect. As indicated in Fig. 41, the WR-700 cycle specimen which were previously cycled five times at 700°C was tougher at - 267°C (6°K) than the WR-700 specimen and did not show any ductile-brittle transition. Upon examination, the effective grain diameter was found to be reduced from 2.8μ to 1.7μ by multicycling.

2. Two-Step Heat Treatment

The $\alpha' \rightarrow \gamma$ reverse transformation of the Fe-Ni alloy with Ni ~ 30% have been reported to occur by a diffusionless process[54,55] or both by diffusionless, and nucleation growth processes[56,57] depending on the heating rate. The direct observation of the transformation is easily accomplished in the Fe-30Ni alloy, in which the austenite thus transformed can be retained at the room temperature since its M_s is below zero. Two types of the reverse transformation may be possible in a low nickel Fe-Ni alloy. In such an alloy, however, the direct observation of the $\alpha' \rightarrow \gamma$ reverse transformation is difficult since the reversed austenite transforms again into α' during cooling.

The effect of the heating rate on the microstructure was investigated, as shown in Fig. 42. The slower heating rate of ~ 10 °C/min. was found to produce a much finer structure compared with the more rapid heating rate of ~ 50 °C/min. Utilizing this idea, the two-step heat treatment was designed to produce a similar effect. In the two-step heat treatment, the specimen is treated at 650°C for one hour as a first step and then reheated at the higher temperature.

As shown in Fig. 43, the microstructures were substantially refined by the two-step heat treatment. The results of Charpy impact test at -196°C demonstrated that the high toughness plateau was extended to between 700 to 750°C.

The mechanism of the grain refinement through the two step heat treatment is different from that of the thermomechanical treatment. There exist two phases, α and α', with different nickel contents after the first step treatment (650°C × 1 hr.). When this structure is reheated to 750°C, each phase transforms into austenite with different A_s and A_f temperature. This effect can clearly be seen in the dilatometric study (Fig. 33). The fact that the A_f was increased to 730°C (regular A_f = 718°C) indicates that the recrystallization was suppressed until a higher temperature and as a result grain structure was refined.

PART II

A. Hall-Petch, Yield Stress-Grain Size Relation

The original mechanism of Hall-Petch relation involved a dislocation pileup at the grain boundaries, as discussed in Part 1A. Many theoretical studies have been done since their work to correlate dislocation mechanics to the experimentally derived Hall-Petch relation. This includes non pileup mechanisms such as work hardening theories and grain boundary source theories as well as many pileup mechanisms.

There have been no data available on the Hall-Petch relation for the interstitial free substitutional alloys except the recent report[50] on the iron with dilute amount of substitutional elements. In order to check the validity of the Hall-Petch relation in a interstitial-free substitutional alloy an attempt to correlate the yield stress to the effective grain diameter has been made in the 12Ni-0.5Ti alloy using the tensile data (Tables 3, 5-7). The yield stress--effective grain diameter relation was plotted for the four testing temperatures, 25°C, -77°C, -196°C and -267°C, as shown in Fig. 44. At room temperature the data was in excellent agreement with the Hall-Petch equation, whereas data scattered both at -77 and -196°C. A simple Hall-Petch relation did not hold at -267°C. For -267°C, it appears that the curve consists of two independent curves, each with different Hall-Petch slopes, suggesting that two different deformation mechanisms could be involved.

The frictional stress, σ_o and Hall-Petch slope, k for 25°C, -77°C and -196°C were determined and listed in Table 8. The value of k for 25°C, 0.15 ksi/mm$^{-1/2}$ was unusually small compared to the reported values of the Hall-Petch slope, which were

2.26 ksi/mm$^{-1/2}$ for the Fe-3Ni alloys[50]

2.0 ksi/mm$^{-1/2}$ for 9Ni steel[25]

~ 2.0 ksi/mm$^{-1/2}$ for mild steels[52]

Even if the yield stress is plotted against the prior austenite grain diameter, the value of k remains unchanged. The reason for the unusual small value of k is not known, but it could be due to a different deformation mechanism. The values of k for testing temperatures of -77°C and -196°C were found to be nearly the same and approximately 4 times larger than the value for 25°C.

B. Effect of Grain Size on Ductile-Brittle Transition Temperature

The specimens with a variety of effective grain diameters were prepared and Charpy tests were conducted at various temperatures to determine the ductile-brittle transition temperature, T_c. The results are shown in Fig. 41. T_c were determined to be -174°C, -189°C and -207°C for the specimens with the effective grain diameters, 24, 11.5 and 5.5μ, respectively.

As reported earlier in Section III, no brittle failure was observed in the tensile test at the various testing temperatures (25°C to -267°C). The ductile-brittle transition temperature, T_c measured in the Charpy

impact test differs from that of the tensile test due mainly to two reasons. First, the strain rate of the impact test is of the order of 10^3/sec whereas the strain rate of our tensile test is of the order of 10^{-4}/sec. The increase in strain rate raises the flow stress level with the fracture stress unaffected, so that T_c increases. Secondly, the sharp notch in the Charpy test specimen raises the T_c value.

A. H. Cottrell[42] developed theories on the ductile-brittle transition both for the tensile and Charpy tests. Cottrell's theories were later modified by R. W. Armstrong,[58-60] Experimentally, however, the effect of grain size on T_c for the Charpy test can be expressed by[53,61] either

$$T_c = A + B \ell nd^{-1/2} \tag{3}$$

or

$$T_c = A + B\, d^{-1/2} \tag{4}$$

where A and B are constant.

The relationship between T_c and the effective grain diameter, d^* were plotted according to the Eqs. (3) and (4) as shown in Figs. 45 and 46, respectively. Both figures clearly indicate that at least the two deformation mechanisms are involved in controlling T_c. Curve 1 indicates the small grain size dependence for relatively larger grains ($6 \sim 25\mu$) and curve 2 shows the larger grain size dependence for ultra fine grains ($< 5\mu$). Data[51] for the Fe-1.84Ni alloy are also indicated in Fig. 46. The slope of this alloy is close to curve 1 in the

12Ni-0.5Ti alloy, suggesting that the deformation mechanism may be the same. A possible explanation for the shift from the curve 1 to 2, is as follows: when the grain diameter is large, toughness, plastic flow is probably enhanced by the motion of the dislocations in the grains. When the grain diameter is of the order of a few microns, the dislocations are generated from the source at the grain boundaries under a shock load, and a large plastic flow may be produced by the motion of the dislocation along the grain boundaries rather than in the grains.

This is of course a simple qualitative explanation. Almost no theoretical studies on the deformation process in a ultra fine structure has been done except some studies in the field of superplasticity. The author felt strongly that a mechanism is needed to explain the deformation in a ultra fine structure.

V. SUMMARY

1. A new cryogenic alloy with extraordinary combination of high strength and high toughness was developed. The interstitial-free bcc Fe-12Ni-0.5Ti alloy has a yield stress of ~ 200 ksi and a V-notch Charpy impact value of ~ 100 ft-lbs at -267°C (6°K). As far as the values of the yield stress and the impact energy are concerned, no comparable results have been reported up to this date.
2. The ductile-brittle transition commonly occurs in bcc metals. The bcc 12Ni-0.5Ti alloy with grain size 2.8 and 1.7μ did not show any transition. When the grain diameter was reduced to a few microns, the ductile-brittle transition temperature is suppressed to a lower temperature and does not appear even at temperatures approaching absolute zero.
3. The grain diameter is the main microstructural factor controlling low temperature toughness.
4. The high toughness plateau in the isochronal study at -196°C can be extended by either thermomechanical treatment or two-step heat treatment. Both processes refine the structure, but by different mechanisms.
5. Hall-Petch, yield stress-grain size relation held for 25°C, -77°C and -196°C. Hall-Petch slope, k for the 12Ni-0.5Ti alloy was found to be one order of magnitude lower than the reported values.
6. When the grain size is larger than ~ 5μ, the effect of the grain size d on the ductile-brittle transition temperature T_c can be expressed by either

$$T_c = A + B\,\ell_{nd}^{1/2}$$

or

$$T_c = A + Bd^{-1/2}$$

7. The grain size dependence on T_c was shifted from a small dependence to a large one when the grain size was reduced to ~ 5μ, suggesting that two deformation mechanisms are involved.

ACKNOWLEDGEMENTS

The author wishes to express his deepest gratitude to Professors Victor Zackay and Earl Parker for their personal guidance, encouragement and support throughout the course of this work. Without their strong recommendation of continuing authors graduate studies beyond the M.S. level, this work would not have been accomplished. His appreciation is extended to Professor Richard Fulrath for helpful discussions and advice in designing the dilatometer, and to Professor Frank Hauser for his review of this manuscript. An appreciation is also extended to Dr. Michael Yokota for many valuable discussions and suggestions. The author is grateful to many of his colleagues, especially to Wade A. Horwood and Benjamin Francis. He is also very grateful to Sungho Jin for helping the mechanical tests at liquid helium temperature.

The assistance of the support staff of the Inorganic Materials Research Division of the Lawrence Berkeley Laboratory is acknowledged. In particular, the author wishes to recognize Brian Pope (melting), Ed Edwards, Julien Patenaude, Duane Newhart (machining), John Holthuis (alloy preparation), Lee Johnson (metallography), George Georgakopoulos (scanning electron microscope), Doug Kreitz (photography), Gloria Pelatowski (line drawings), and Alice Ramirez (typing).

The author also wishes to thank Hitachi Metals, Ltd for the continuous encouragement and the financial support through the Nakamura Fund.

Finally, his personal gratitude and thanks are reserved for his wife, Kay and his parents in Japan. They have shared a long and hard years at Berkeley with me.

This research was performed under the auspices of the U. S. Atomic Energy Commission, through IMRD of the Lawrence Berkeley Laboratory.

REFERENCES

1. E. R. Parker, Brittle Behavior of Engineering Structures, John Wiley and Sons, 1957.
2. E. R. Parker, Creating New Metals to Meet Society's Needs, The 60th Annual Faculty Research Lectures, University of California, Berkeley 1973.
3. T. E. Mitchell, R. A. Foxall, and P. B. Hirsch, Phil. Mag. 9, 1895, 1963.
4. A. S. Keh and Y. Nakada, Canad. J. Phys. 45, 1101, 1967.
5. A. S. Keh, Phil. Mag. 12, 9, 1965.
6. H. Bilger, Phil. Stat. Sol. 18, 637, 1966.
7. T. E. Mitchell and W. A. Spitzig, Act. Met. 13, 1169, 1965.
8. F. Guin and P. L. Pratt, Phys. Stat. Sol. 15, 539, 1966.
9. D. F. Stein and J. R. Low, Jr, Act. Met. 14 1183, 1966.
10. H. Conrad, The Cryrogenic Properties of Metals, Ch. 11 in High Strength Materials, V. F. Zackay, ed., John Wiley, 1965.
11. W. A. Horwood, M.S. thesis, University of California, Berkeley, December, 1972.
12. E. R. Parker and V. F. Zackay, LBL-832, April 1972.
13. J. R. Rellick and C. J. McMahon, Jr, Met. Trans. 1, 929, 1970.
14. S. Jin, W. A. Horwood, J. W. Morris, Jr. and V. F. Zackay; LBL-1483, University of California, Berkeley, Lawrence Berkeley Lab., 1972.
15. R. Vogel and H. T. Wallbaum, Arch. Eisenhüttenwesen, 12, 299, 1938.

16. G. R. Speich, Trans. AIME, 227, 754, 1963.

17. Z. S. Basinski, The Instability of Plastic Flow of Metals at Very Low Temperature, Proceedings, Royal Society of London, Series A, 240, 229, 1957.

18. E. B. Kula and T. S. DeSisto, Behavior of Materials at Cryogenic Temperatures, ASTM STP 387 Am. Soc. Testing Mats., 3, 1966

19. E. T. Wessel, ibid, 32, 1966.

20. G. L. Kehl, Principle of Metallographic Laboratory Practice, 292, McGraw-Hill, 1949.

21. V. M. Kardonskiy and M. D. Perkas, Fiz. Metal. Metalloved. 19, 298, 1965.

22. A. H. Yedeneral, V. M. Kardonskiy and M. D. Perkas, ibid, 24, 669, 1967.

23. J. K. Abraham and T. L. Wilson, Advances in X-ray Analysis, 11, 434, 1968.

24. J. K. Abraham, J. K. Jackson and L. Leonard, Trans. ASM, 61, 233, 1968.

25. R. L. Miller, Met. Trans, 3, 905, 1972.

26. W. D. Swanson and J. G. Parr, J1S1, 104, Feb. 1964.

27. R. J. Ackert and J. G. Parr, J1S1, 912, Nov. 1971.

28. A. Gilbert and W. S. Owen, Act. Met. 10, 45, 1962.

29. W. S. Owen, E. A. Wilson, and T. Bell, The Structure and Properties of Quenched Iron Alloys, Ch. 5 in High Strength Materials, V. F. Zackay ed., John Wiley and Sons, 1965.

30. W. S. Owen and E. A. Wilson, Physical Properties of Martensite and Bainite, Special Report 93 of the Iron and Steel Institute, Lo London, 53, 1965.

31. G. Krauss and A. R. Marder, Met. Trans, 2, 2356, 1971.

32. G. Sasaki, unpublished.

33. G. Thomas, Met. Trans, 2, 2373, 1971.

34. G. Krauss and A. R. Marder, Met. Trans. 2 2243, 1971.

35. C. L. Magee and R. G. Davies, Act. Met. 19, 345, 1971.

36. T. Ooka and K. Sugino, Kinzoku-gakkai-Shi, 30, 435, 1966.

37. E. O. Hall, Proc. Phys. Soc. London B64, 747, 1951.

38. N. J. Petch, J1S1, 174, 25, 1953.

39. J. C. M. Li and Y. T. Chou, Met. Trans. 1, 1145, 1970.

40. N. J. Petch, Fracture, John Wiley & Sons New York, 54, 1959.

41. A. H. Cottrell, ibid, 20

42. A. H. Cottrell, Trans. AIME, 212, 192, 1958.

43. G. Sasaki, The mechanical Properties of Laves Phases, University of California, Berkeley UCRL-20301, Dec. 1970.

44. G. R. Brophy and A. J. Miller, Trans. of ASM, 41, 1185, 1949.

45. C. W. Marshall, R. F. Hehemann and A. R. Troiano Trans. of ASM, 55, 135, 1962.

46. T. Ooka, H. Mimura, S. Yano, K. Sugino and T. Toizumi, Kinzoku-gakkai-Shi, 30, 442, 1966.

47. A. J. Sedrilcs and J. V. Craig, J1S1, 286, Mar. 1965.

48. R. C. Hall, G. N. Melnnis and S. Kluz, ibid, 1310, Oct. 1969.

49. R. A. Grange, Trans. ASM 59, 27, 1966.

50. W. B. Morrison and W. C. Leslie, Met. Trans. 4, 379, 1973.

51. I. Gupta, Met. Trans. 2, 323, 1971.

52. A. Crackwell and N. J. Petch, Act. Met. 3, 186, 1955.

53. W. C. Leslie, Met. Trans. 2, 1989, 1971

54. Ya. M. Golovchiner, Phys. Met. and Metallog. 15, No. 4, 54, 1963.

55. V. G. Gorback and E. D. Butakova, ibid, 16, No. 2, 112, 1963.

56. H. Kessler and W. Pitch, Act. Met. 15, 401, 1967.

57. S. Jana and C. M. Wayman, Trans. AIME, 239, 1187, 1967.

58. R. W. Armstrong, Phil. Mag. 9, 1063, 1964.

59. R. W. Armstrong, Met. Trans. 1, 1169, 1970.

60. R. W. Armstrong, Second International Conference on Fracture, 314, 1969.

61. N. S. Stoloff, Fracture, Vol. 6, H. Luebowitz ed., Acadimic Press 1969.

62. S. Jin, J. W. Morris, Jr. and V. F. Zackay; LBL-1484, University of California, Berkeley, Lawrence Berkeley Laboratory, 1973.

Table I. Chemical Composition (wt.%) of the Alloys Used

Alloys \ Chemical element	Ni	Ti	C	N_2	O_2	Mn	S	
12Ni	12.07	0.01	0.001	0.006	0.040	-	-	bal
8Ni-0.5Ti	8.07	0.52	< 0.001	0.010	0.029	< 0.005	0.004	bal
12Ni-0.5Ti	12.00	0.32	0.004	0.004	0.029	< 0.005	0.004	bal
16Ni-0.5Ti	15.50	0.34	0.003	0.002	0.016	< 0.005	0.004	bal

Table 2. Phase transformation temperatures, °C (heating and cooling rate ~ 3°C/min).

Alloys	A_s	A_f	M_s	M_f
12Ni	622	700	475	415
8Ni-0.5Ti	670	762	544	442
12Ni-0.5Ti	632	718	444	347
16Ni-0.5Ti	595	683	338	167

Table 3. Mechanical Properties of the 12Ni-0.5Ti Alloys at - 196°C

Specimen No.	Processing and heat treatment	Yield stress 0.2% offset ksi	Ultimate Tensile Strength ksi	Elongation %	Reduction of Area %	V-notch Charpy Impact Energy ft-lbs
STD	Standard (900°Cx2 hrs) AC	130.9	141.6	34.9	65.8	14.4, 11.1
STD-600	Standard 600°Cx1 hr WQ	139.8	148.3	35.3	58.4	8.4, 10.4
STD-700	Standard 700°Cxlhr WQ	134.9	143.8	36.4	65.4	121.2,103.6
WR	Warm Roll	140	152.1	38.8	66.8	109.9, 93.8
WR-600	Warm Roll 600°Cxlhr WQ	145.1	159.4	36.5	61.0	60.2, 64.0
WR-700	Warm Roll 700°Cxlhr WQ	135.8	146.7	34.9	66.2	116.3,117.8
WR-800	Warm Roll 800°Cxlhr WQ	130.0	140.0	34.3	69.9	115.9,112.5

Table 3 (continued)

Specimen No.	Processing and heat treatment	Yield stress 0.2% offset ksi	Ultimate Tensile Strength ksi	Elongation %	Reduction of Area %	V-notch Charpy Impact Energy ft-lbs
CR	Cold Roll(60%)	169.4	171.6	25.9	57.2	23.0, 19.7
CR-600	Cold Roll 600°Cx1hr WQ	153.9	165.9	30.8	54.7	33.3, 36.1
CR-700	COLD Roll 700°Cx1hr WQ	133.0	143.7	38.9	69.9	114.8, 90.4
CR-800	Cold Roll 800°Cx1hr WQ	129.0	140.0	35.9	70.6	91.1 ,126.8
CR-850	Cold Roll 850°Cx1hr WQ	132.5	141.6	36.9	69.9	24.8, 31.0
WR-700 Cycle	Warm Roll 700°Cx1hr.WQ 5 times cycling	133.4	142.4	35.6	71.8	108.2,112.7

Table 4. Mechanical properties of the Fe-Ni-Ti alloys at -196°C.

Alloys	Processing and heat Treatment	Yield Stress 0.2% Offset Ksi	Ultimate Tensile Strength Ksi	Elongation %	Reduction of Area %	V-Notch Charpy Impact Energy ft-lbs
8 Ni-0.5 Ti	STD (900°C×2hrs AC)	123.8	135.3	39.4	65.3	2.4 2.3
	STD 700°C×1 hr WQ	112.3	124.6	44.3	72.0	2.8 3.0
12 Ni-0.5 Ti	STD (900°C×2hrs AC)	130.9	141.6	34.9	65.8	14.4 11.1
	STD 700°C 1×hr WQ	134.9	143.8	36.4	65.4	121.2 103.6
16 Ni-0.5 Ti	STD (900°C×2hrs AC)	144.1	152.9	28.7	68.7	38.9 38.4
	STD 700°C×1 hr WQ	155.6	164.4	26.9	71.7	96.6 85.3

Table 5. Mechanical Properties of the 12 Ni-0.5 alloy at -267°C (6°K)

Specimen No.	Processing and Heat Treatment	Yield Strength Ksi	Ultimate Tensile Strength Ksi	Elongation %	Reduction of Area %	V-Notch Charpy Impact Energy ft-lbs
STD	Standard (900°C×2 hrs AC)	177.0	187.7	28.8*	63.9*	-- , --
STD-700	Standard 700×1° WQ	196.4	203.2	20.2	65.0	20.7 , 18.6
WR-700	Warm Roll 700×1° WQ	197.8	212.2	24.6	53.7	77.8 , 88.2
WR-700 Cycle	Warm Roll 700 1° WQ 5× cycling	193.8	204.5	22.8	65.0	91.8 ,101.4

*Reference values (testing temperature was increased at the last part of the test).

Table 6. Mechanical properties of the 12 Ni-0.5 alloy at -77°C.

Specimen No.	Processing and Heat Treatment	Yield Stress 0.2% Offset ksi	Ultimate Tensile Strength Ksi	Elongation %	Reduction of Area %	V-Notch Impact Energy ft-lbs
STD	Standard (900°C×2 hrs AC)	93.7	105.8	29.8	78.0	128.2
STD-700	Standard 700°C×1 hr WQ	98.2	106.2	31.2	75.3	161.0
WR-700	Warm Roll 700°C×1 hr WQ	99.6	108.2	31.8	75.9	-----
CR-850	Cold Roll 850°C×1 hr WQ	96.3	104.3	30.3	74.2	118.2
WR-700 Cycle	Warm Roll 700°C×1 hr WQ 5× Cycling	98.2	105.9	29.1	75.9	144.4

Table 7. Mechanical properties of the 12 Ni-0.5 alloy at 25°C.

Specimen No.	Processing and Heat Treatment	Yield Stress 0.2% Offset ksi	Ultimate Tensile Strength Ksi	Elongation %	Reduction of Area %	V-Notch Impact Energy ft-lbs
STD	Standard	85.1	92.1	25.7	74.2	170.0
STD-700	Standard 700°C×1 hr WQ	86.5	92.6	25.4	79.1	173.1
WR-700	Warm Roll 700°C×1 hr WQ	86.9	93.3	27.7	78.7	171.0
CR-850	Cold Roll 850°C×1 hr WQ	85.7	90.6	24.9	78.1	152.1

Table 8. Hall-Petch parameters of the 12Ni-0.5 alloy

Parameter \ Testing Temperature	25°C	-77°C	-196°C
$K(ksi/mm^{-1/2})$	0.15	0.55	0.56
σ_o(ksi)	84	90	128

FIGURE CAPTIONS

Fig. 1. Sectioning of mechanical test specimens.

Fig. 2. Mechanical test specimens.

(a) Charpy V-notch specimen

(b) Round tensile specimen

Fig. 3. Dilatometric apparatus

(a) Schematic View of the Furnace

(b) Specimen

(c) Specimen Dimensions.

Fig. 4. Fe-Ni System with Ti=0.5% constant.

Fig. 5. V-notch Charpy impact energies at -196°C of the 12Ni-0.5Ti alloy, annealed at 900°C for 2 hrs, (STD) and reheated at intermediate temperatures for an hour and quenched into a 0°C water.

Fig. 6. V-notch Charpy impact energies at -196°C of the 12Ni-0.5Ti alloy, annealed at 900°C for 2 hrs, warm rolled at 600°C (WR) and reheated at intermediate temperatures for an hour and quenched into a 0°C water.

Fig. 7. V-notch Charpy impact energies at -196°C of the 12Ni-0.5Ti alloy, annealed at 900°C for 2 hrs., cold rolled with a reduction of 60% (CR) and reheated at intermediate temperatures for a hour and quenched into a 0°C water.

Fig. 8. Effects of nickel content on the V-notch Charpy impact energies at -196°C in the Fe-Ni-Ti alloys, annealed at 900°C for 2 hrs. (STD) and reheated at intermediate temperatures for an hour and quenched into a 0°C water.

Fig. 9. Effects of nickel content on the V-notch Charpy impact energies at -196°C in the Fe-Ni-Ti alloys, annealed at 900°C for 2 hrs, cold rolled with a reduction of 60% (CR) and reheated at intermediate temperatures for an hour and quenched into a 0°C water.

Fig. 10. Engineering stress-strain curves for the 12Ni-0.5Ti alloy annealed at 900°C for 2 hrs. (STD). The specimens were tested at 25°C, -77°C, -196°C and -267°C. Strain rate was 10^{-4}/sec.

Fig. 11. Engineering stress-strain curves for the 12Ni-0.5Ti alloy, annealed at 900°C for 2 hrs (STD) and reheated at 700°C for an hour and quenched into a 0°C water. The specimens were tested at 25°C, -77°C, -196°C and -267°C. Strain rate was 10^{-4}/sec.

Fig. 12. Engineering stress-strain curves for the 12Ni-0.5Ti alloy, annealed at 900°C for 2 hrs., warm rolled at 680°C (WR) and reheated at 700°C for an hour and quenched into a 0°C water. The specimens were tested at 25°C, -77°c, -196°C and -267°C. Strain rate was 10^{-4}/sec.

Fig. 13. Effect of the testing temperature on the mechanical properties in the 12Ni-0.5Ti alloy annealed at 900°C for 2 hrs. (STD).

Fig. 14. Effect of testing temperature on the mechanical properties in the 12Ni-0.5Ti alloy, annealed at 900°C for 2 hrs. and reheated at 700°C for an hour and quenched into a 0°C water.

Fig. 15. Effect of testing temperature on the mechanical properties in the 12Ni-0.5Ti alloy, annealed at 900°C for 2 hrs., warm rolled at 680°C (WR) and reheated at 700°C for an hour and quenched into a 0°C water.

Fig. 16. Optical micrographs of the series of the STD specimens in the 12Ni-0.5Ti alloy --Transverse section.

(a) As STD (900°C × 2 hrs. AC)
(b) STD-600 (900°C × 2 hrs AC and 600°C × 1 hr. WQ)
(c) STD-650 (900°C × 2 hrs AC and 650°C × 1 hr. WQ)
(d) STD-700 (900°C × 2 hrs AC and 700°C × 1 hr. WQ)
(e) STD-750 (900°C × 2 hrs AC and 750°C × 1 hr. WQ)
(f) STD-800 (900°C × 2 hrs AC and 800°C × 1 hr. WQ)

Fig. 17. Optical micrographs of the series of the WR specimens in the 12Ni-0.5Ti alloy--Transverse section.

(a) As WR (warm roll at 680°C)
(b) WR-600 (warm roll at 680°C and 600°C × 1 hr WQ)
(c) WR-650 (warm roll at 680°C and 650°C × 1 hr WQ)
(d) WR-700 (warm roll at 680°C and 700°C × 1 hr WQ)
(e) WR-750 (warm roll at 680°C and 750°C × 1 hr WQ)
(f) WR-850 (warm roll at 680°C and 850°C × 1 hr WQ)

Fig. 18. Optical micrographs of the series of the CR specimens in the 12Ni-0.5Ti alloy--Transverse section.

(a) As CR (cold roll with 60% reduction)
(b) CR-600 (cold roll with 60% reduction and 600°C × 1 hr WQ)
(c) CR-650 (cold roll with 60% reduction and 650°C × 1 hr WQ)
(d) CR-700 (cold roll with 60% reduction and 700°C × 1 hr WQ)
(e) CR-750 (cold roll with 60% reduction and 750°C × 1 hr WQ)
(f) CR-850 (cold roll with 60% reduction and 850°C × 1 hr WQ)

Fig. 19. Optical micrographs of the series of the STD specimens in the 8Ni-0.5Ti alloy--Transverse section.

(a) As STD (900°C × 2 hrs AC)
(b) STD-600 (900°C × 2 hrs AC and 600°C × 1 hr WQ)
(c) STD-650 (900°C × 2 hrs AC and 650°C × 1 hr WQ)
(d) STD-700 (900°C × 2 hrs AC and 700°C × 1 hr WQ)
(e) STD-750 (900°C × 2 hrs AC and 750°C × 1 hr WQ)
(f) STD-800 (900°C × 2 hrs AC and 800°C × 1 hr WQ)

Fig. 20. Optical micrographs of the series of the STD specimens in the 16Ni-0.5Ti alloy --Transverse section.

(a) As STD (900°C × 2 hrs AC)
(b) STD-600 (900°C × 2 hrs AC and 600°C × 1 hr WQ)
(c) STD-650 (900°C × 2 hrs AC and 650°C × 1 hr WQ)
(d) STD-700 (900°C × 2 hrs AC and 700°C × 1 hr WQ)
(e) STD-750 (900°C × 2 hrs AC and 750°C × 1 hr WQ)
(f) STD-800 (900°C × 2 hrs AC and 800°C × 1 hr WQ)

Fig. 21. Transmission electron micrographs of the STD-600 specimen in the 12Ni-0.5Ti alloy. The specimen was annealed at 900°C for 2 hrs., and reheated at 600°C for an hour and quenched into a 0°C water.

Fig. 22. Transmission electron micrographs of the STD-650 specimen in the 12Ni-0.5Ti alloy. The specimen was annealed at 900°C for 2 hrs., and reheated at 650°C for an hour and quenched into a 0°C water.

Fig. 23. Transmission electron micrographs of the STD-700 specimen in the 12Ni-0.5Ti alloy. The specimen was annealed at 900°C for 2 hrs, and reheated at 700°C for an hour and quenched into a 0°C water.

Fig. 24. Transmission electron micrographs of the STD-750 specimen in the 12Ni-0.5Ti alloy. The specimen was annealed at 900°C for 2 hrs., and reheated at 750°C for an hour and quenched into a 0°C water.

Fig. 25. Scanning electron micrographs of fracture path in the Charpy specimen of the 12Ni-0.5Ti alloy tested at -196°C.

(a) STD (900°C × 2 hrs AC)
(b) STD-700 (900°C × 2 hrs AC and 700°C × 1 hr WQ)

Fig. 26. Scanning electron micrographs of fracture path in the charpy specimen of the 12Ni-0.5Ti alloy tested at -196°C.

(a) STD-600 (900°C × 2 hrs AC and 600°C × 1 hr WQ)
(b) WR-600 (warm roll at 680°C and 600°C × 1 hr WQ)

Fig. 27. Scanning electron micrographs of fracture path in the Charpy specimen of the 12Ni-0.5Ti alloy tested at -196°C.

(a) STD-650 (900°C × 2 hrs AC and 650°C × 1 hr WQ)
(b) WR-650 (900°C × 2 hrs AC and 650°C × 1 hr WQ)

Fig. 28. Scanning electron micrographs of the fractured surface in the tensile test of the STD specimen in the 12Ni-0.5Ti alloy tested at

(a) 25°C
(b) -77°C
(c) -196°C(77°K)
(d) -267°C(6°K)

Fig. 29. Scanning electron micrographs of the fractured surface in the tensile test of the WR-700 specimen in the 12Ni-0.5Ti alloy tested at

(a) 25°C,
(b) -77°C
(c) -196°C
(d) -267°C

Fig. 30. Microstructural factors controlling low-temperature toughness.

Fig. 31. Optical micrographs of three different kinds of substructure in Fe-Ni alloys.[32]

(a) Equiaxed structure in a Fe-8Ni alloy (200x)
(b) Massive martensite in a Fe-12Ni alloy (200x)
(c) Accicular martensite in a Fe-28Ni-0.3C alloy (200x), Courtesy of D. Bhandarkar.

Fig. 32. Isothermal phase transformation in the 12Ni-0.5Ti alloy by dilatometric study. The heating and cooling rate was ~ 50°C/sec.

Fig. 33. Characteristics of phase transformation in the 12Ni-0.5Ti alloy by dilatometric study. The heating and cooling rate was ~ 50°C/sec.

Fig. 34. The relationship between the Charpy impact energies at -196°C and the effective grain diameter.

Fig. 35. The relationship between the effective grain diameter and the inverse of the absolute temperature.

Fig. 36. The hardness change of the 12Ni-0.5Ti alloy during the isothermal treatment at 600°C for three kinds of processings, STD, WR, and CR. The data of the 12Ni alloy is included.

Fig. 37. The hardness change of the 12Ni-0.5Ti alloy during the isothermal treatment at 650°C for three different processings, STD, WR and CR. The data of the 12Ni is included.

Fig. 38. Scanning electron micrographs of fracture path in the Charpy specimen of the 12Ni-0.5Ti alloy tested at -196°C.

(a) STD-700-650L(900°C × 2 hrs AC, 700°C × 1 hr AC and 650°C × 100 hrs WQ)
(b) WR-650L(warm roll at 680°C and 650°C × 100 hrs WQ)

Fig. 39. Magnified micrographs of the Fig. 38b.

Fig. 40. Grain refinement at 750°C of the CR and STD specimens water quenched after heating at 750°C for the following time-- Longitudinal section.

(a) 6 minutes. The CR specimen. Temperature is approximately 600°C.
(b) 9 minutes. The CR specimen. Temperature is approximately 700°C.
(c) 15 minutes. The CR specimen. Temperature is 750°C
(d) 20 minutes. The CR specimen. Temperature is 750°C
(e) 6 minutes. The STD specimen. Temperature is approximately 600°C.
(f) 15 minutes. The STD specimen. Temperature is 750°C

Fig. 41. The effect of the effective grain diameter on the Charpy impact energies in the 12Ni-0.5Ti alloy, tested over a wide range of temperatures (-267°C to 25°C).

Fig. 42. The effect of the heating rates on the microstructure of the 12Ni-0.5Ti alloy.

Fig. 43. The effect of the two-step heat treatment on the microstructure of the 12Ni-0.5Ti alloy.

Fig. 44. Yield stress-grain size relationships in the 12Ni-0.5Ti alloy for tour testing temperatures, 25°C, -77°C, -196°C and -267°C.

Fig. 45. The effect of the effective grain diameter, d^* on the ductile-brittle transition temperature, T_c. The plots were made in accordance with the equation, $T_c = A + B\ell nd^{1/2}$ where A and B are constant.

Fig. 46. The effect of the effective grain diameter, d^* on the Ductile-Brittle transition temperature, T_c. The plots were made in accordance with the equation, $T_c = A + Bd^{-1/2}$ where A and B are constant.

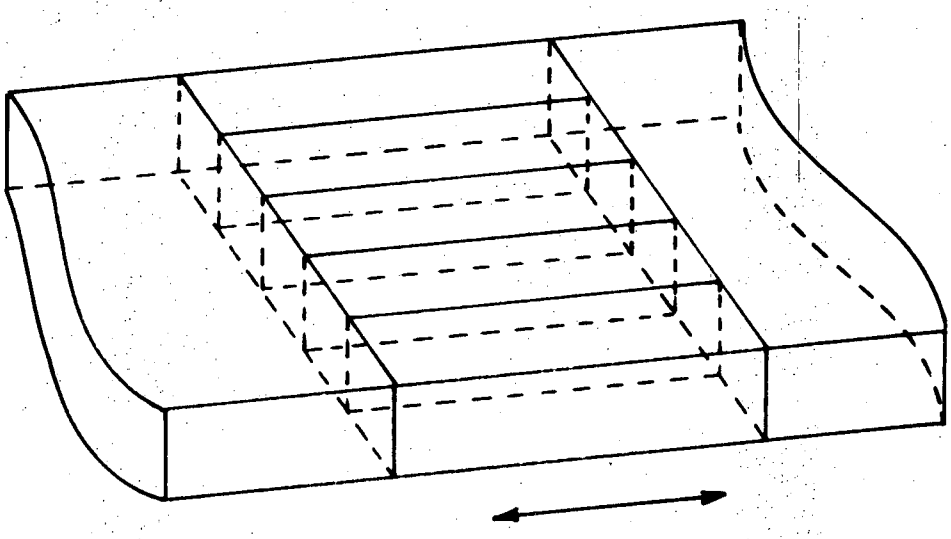

Rolling Direction

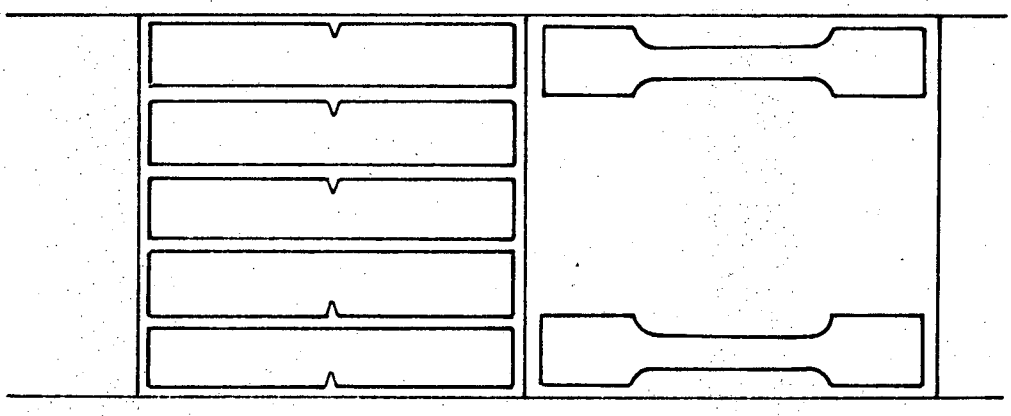

Charpy V-notch Specimen

Round Tensile Specimen

XBL 736-6282

Fig. 1.

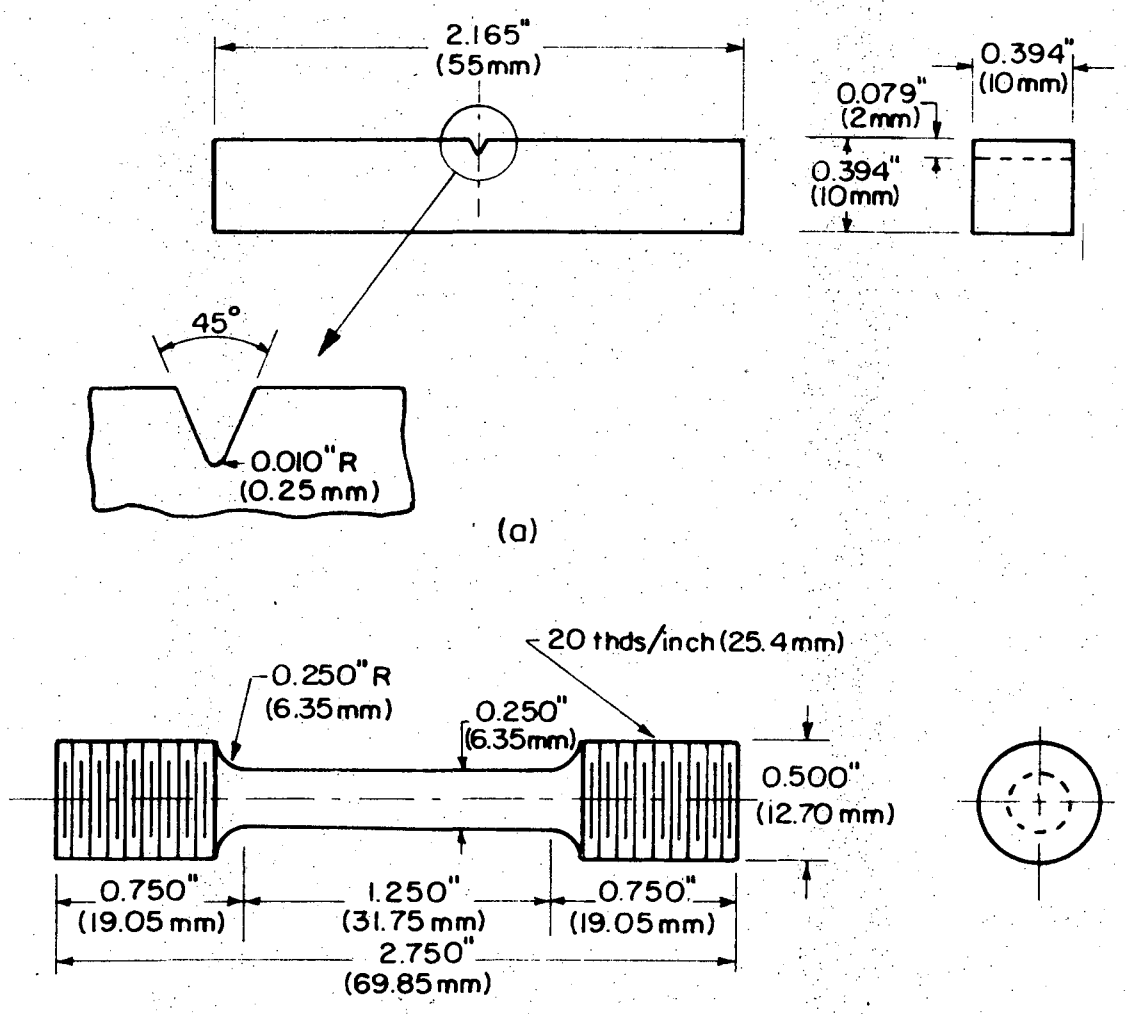
2.165"
(55mm)
0.394"
(10mm)
0.079"
(2mm)
0.394"
(10mm)
45°
0.010"R
(0.25mm)
(a)
20 thds/inch (25.4mm)
0.250"R
(6.35mm)
0.250"
(6.35mm)
0.500"
(12.70mm)
0.750"
(19.05mm)
1.250"
(31.75mm)
0.750"
(19.05mm)
2.750"
(69.85mm)
(b)
XBL 736-6280

Fig. 2.

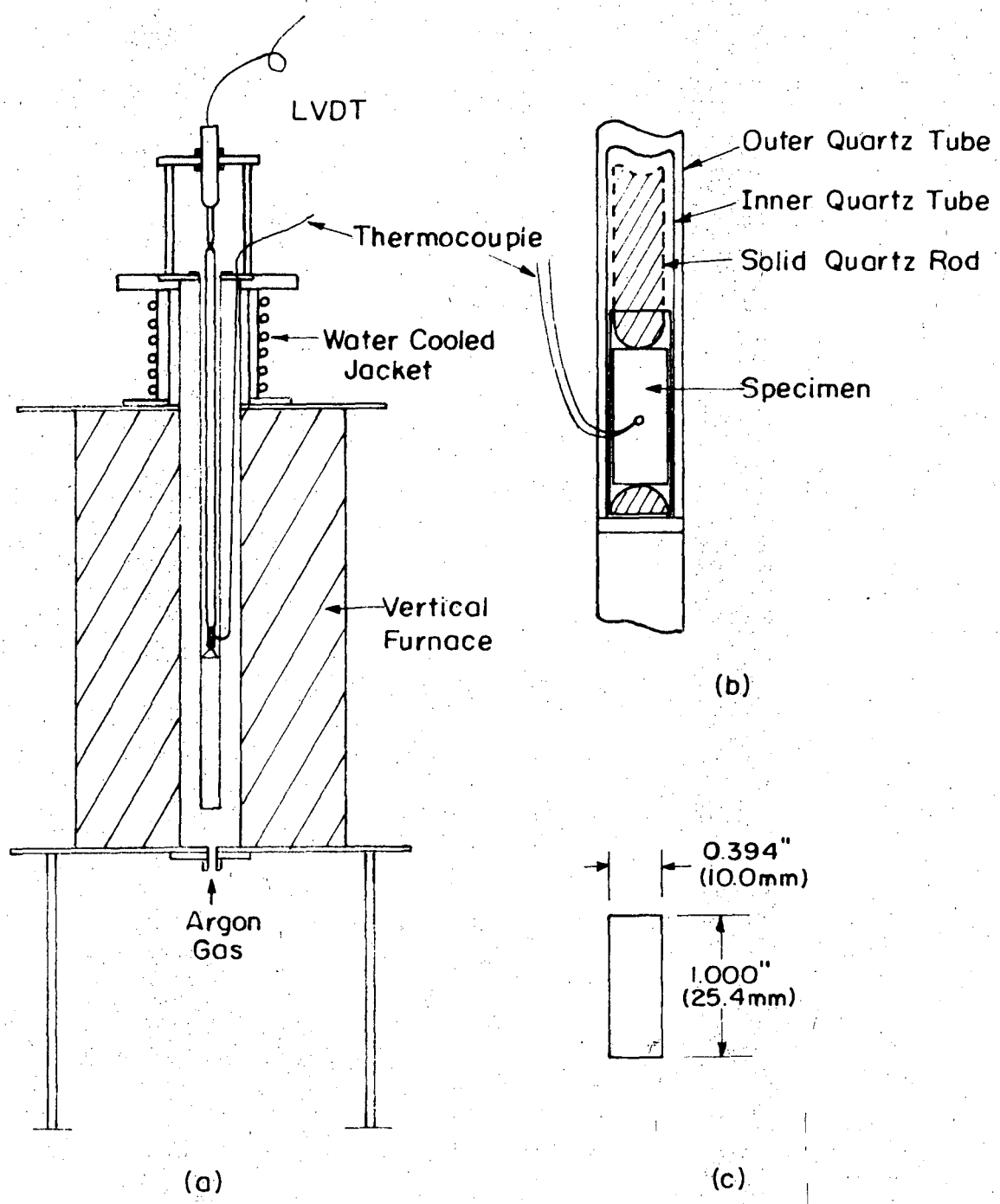

Fig. 3.

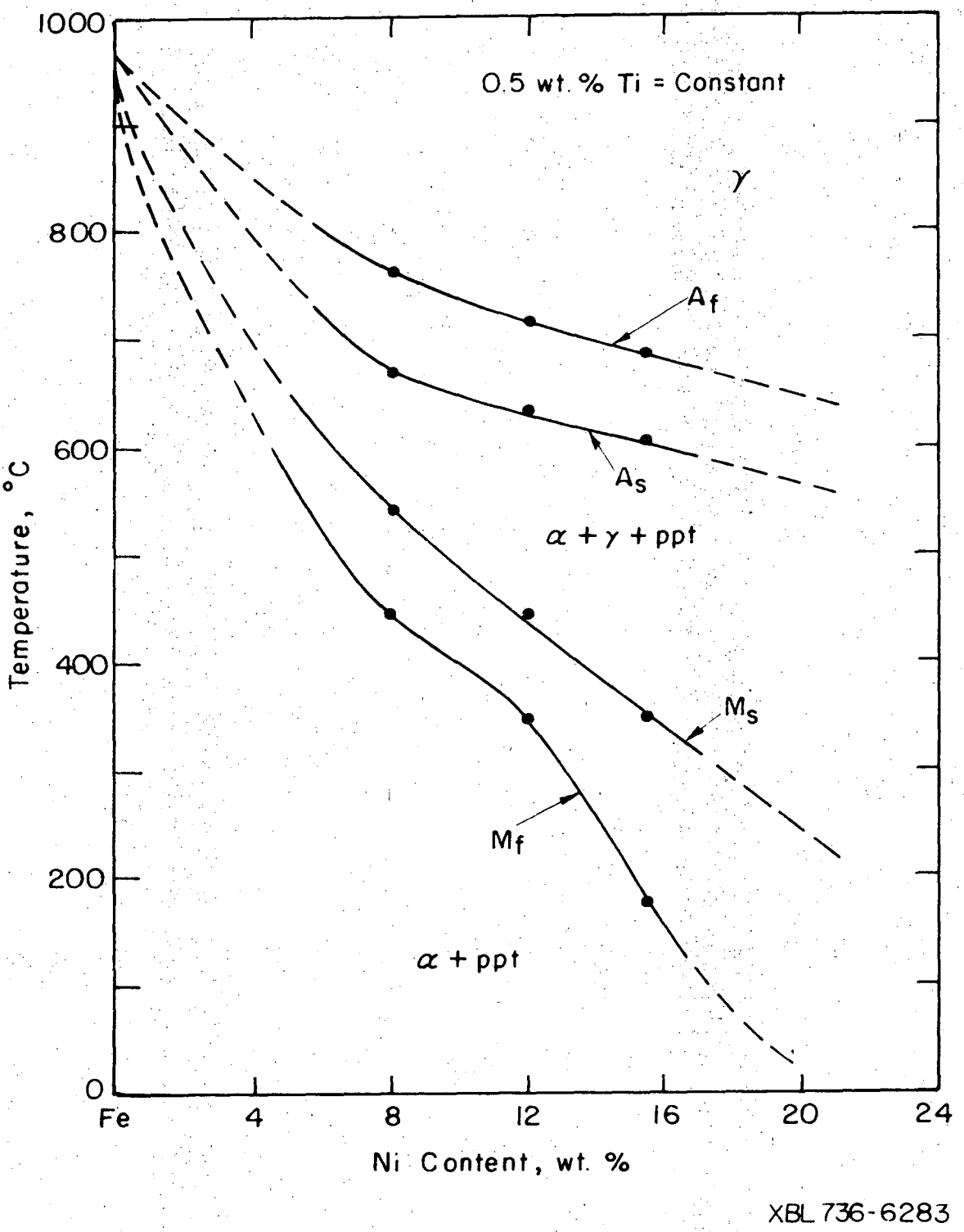
1000
800
600
400
200
0
Temperature, °C
0.5 wt. % Ti = Constant
γ
A_f
A_s
α + γ + ppt
M_s
M_f
α + ppt
Fe
4
8
12
16
20
24
Ni Content, wt. %
XBL 736-6283

Fig. 4.

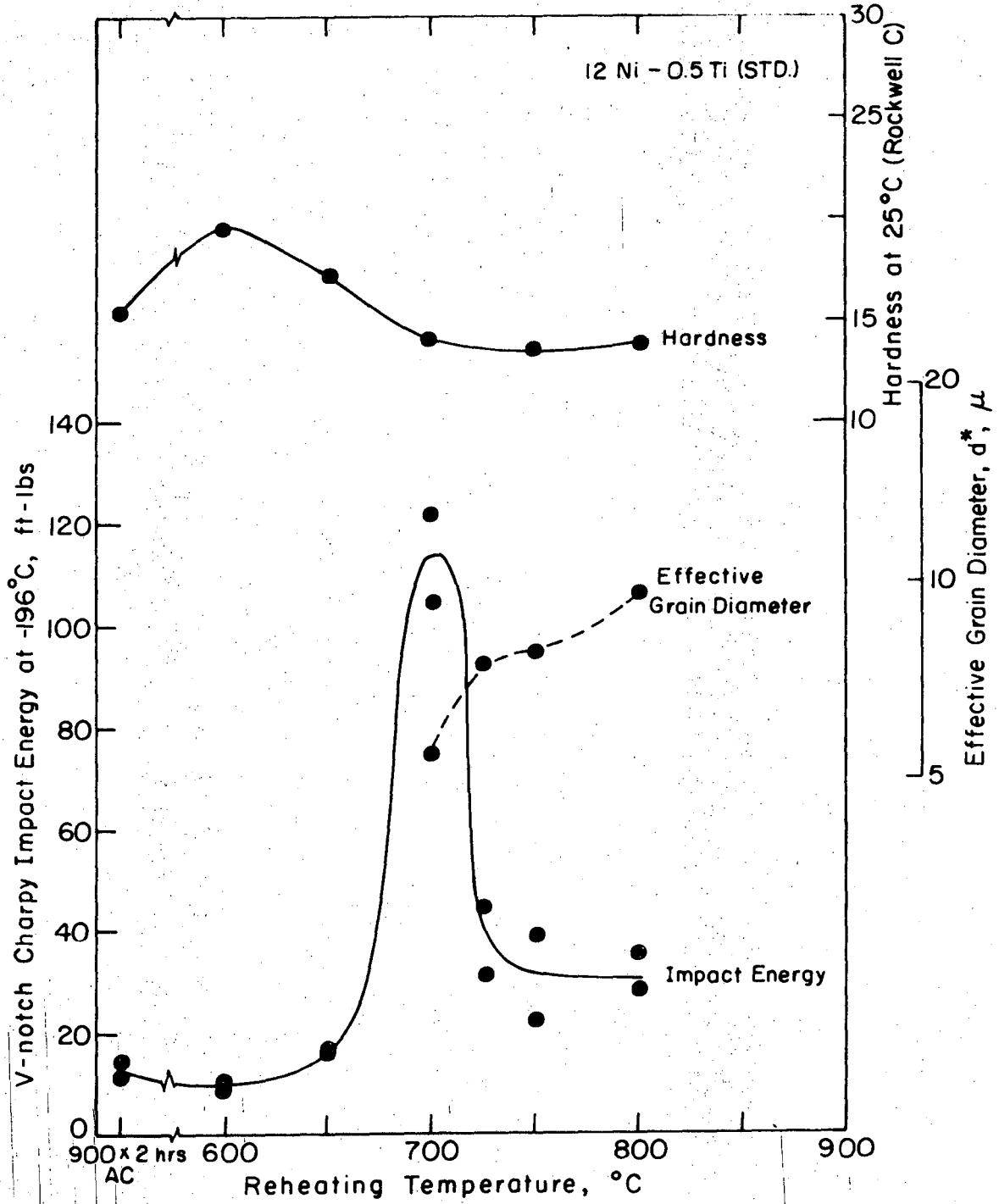

Fig. 5.

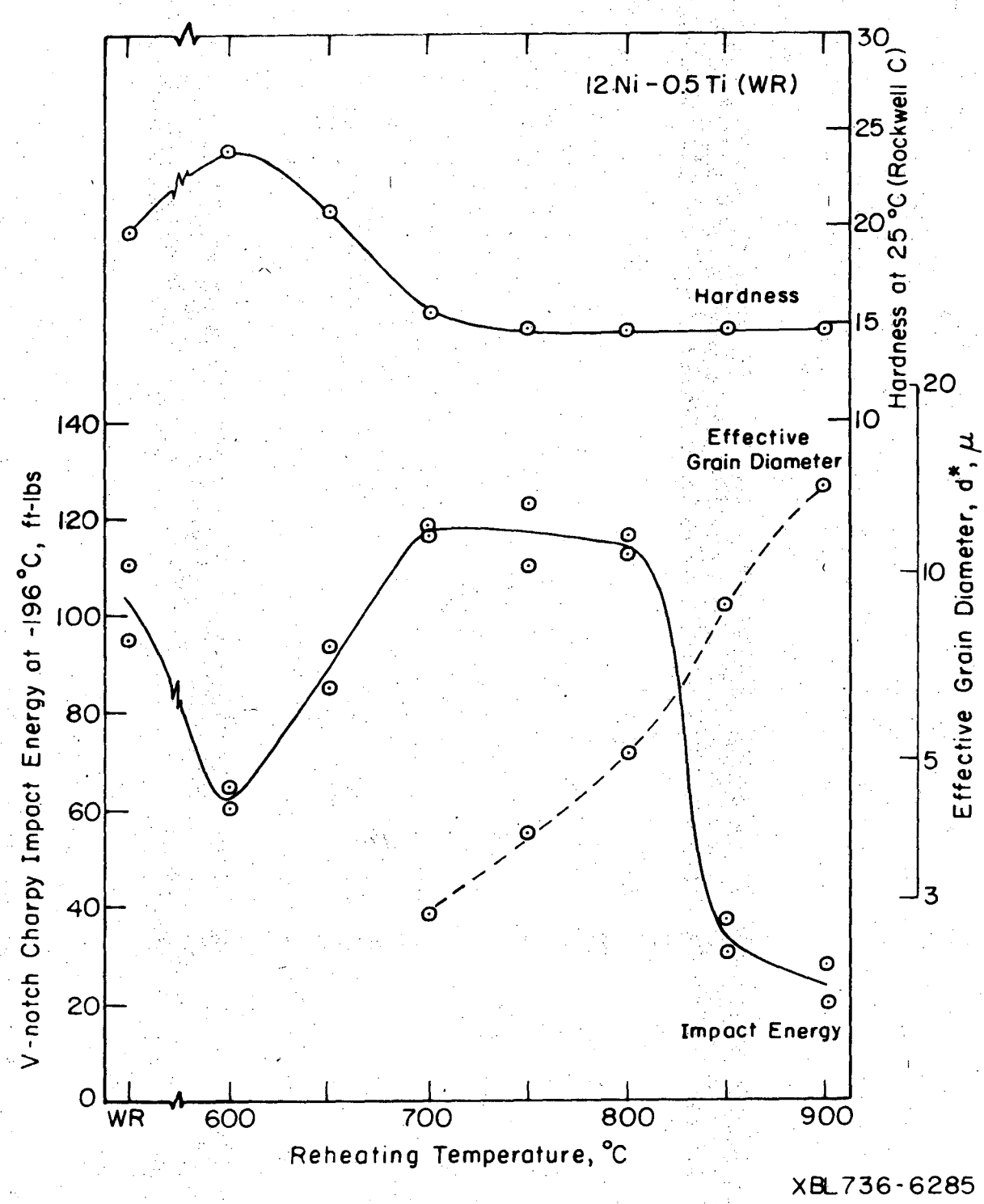
12 Ni - 0.5 Ti (WR)
Hardness
Effective
Grain Diameter
Impact Energy
V-notch Charpy Impact Energy at -196°C, ft-lbs
Hardness at 25°C (Rockwell C)
Effective Grain Diameter, d*, μ
Reheating Temperature, °C
WR
600
700
800
900
0
20
40
60
80
100
120
140
10
15
20
25
30
3
5
10
20
XBL736-6285

Fig. 6.

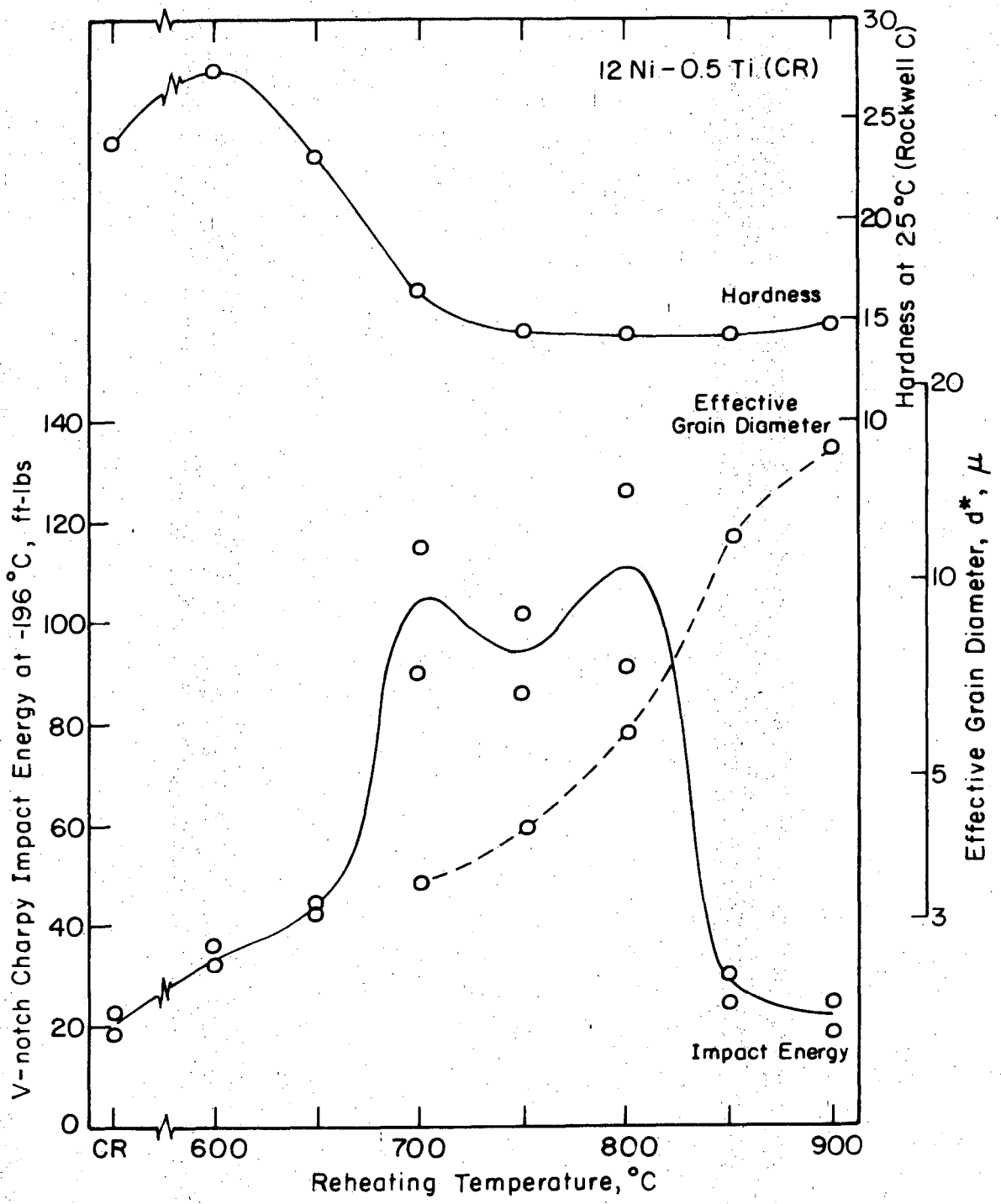

XBL 736-6286

Fig. 7.

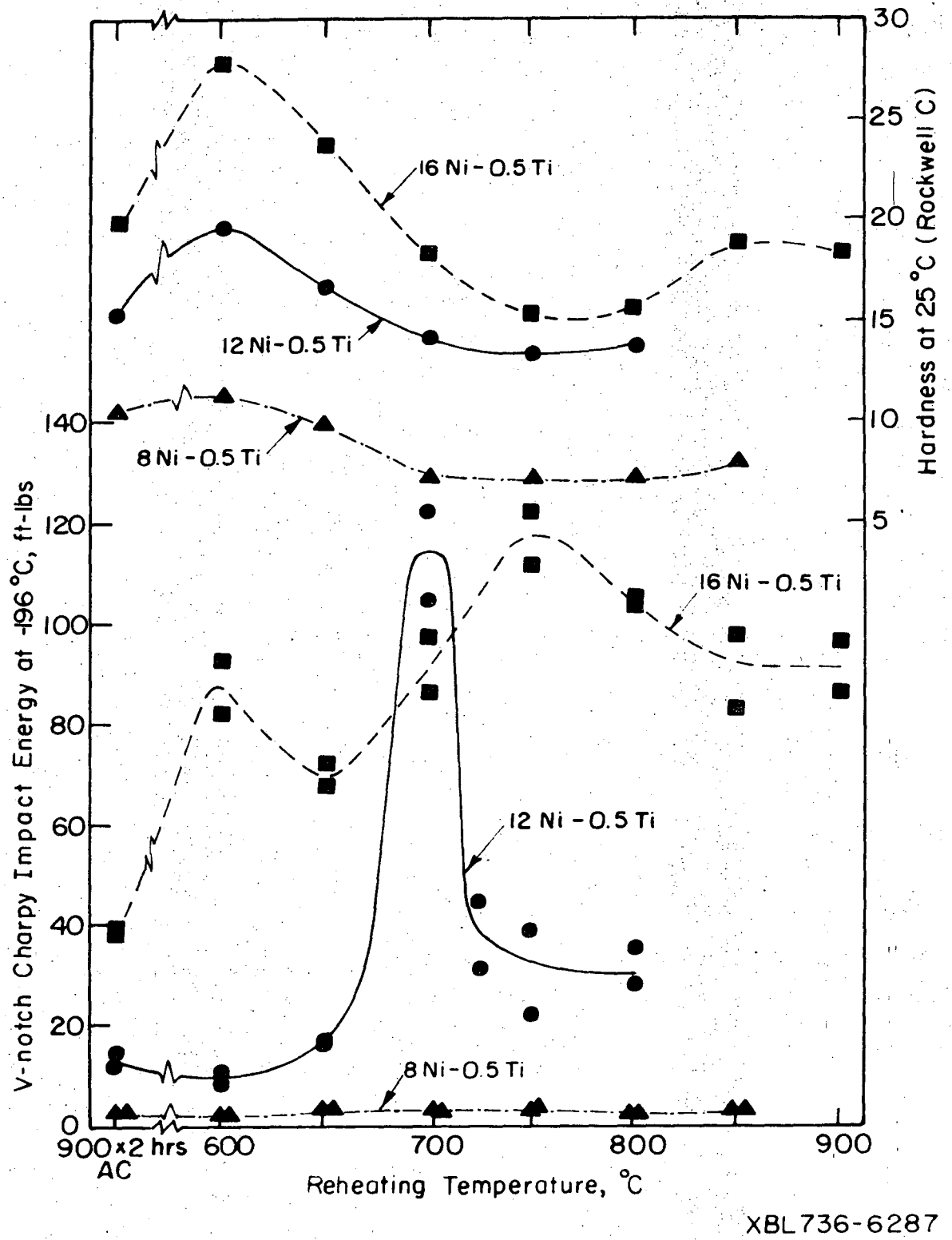
16 Ni - 0.5 Ti
12 Ni - 0.5 Ti
8 Ni - 0.5 Ti
16 Ni - 0.5 Ti
12 Ni - 0.5 Ti
8 Ni - 0.5 Ti
V-notch Charpy Impact Energy at -196 °C, ft-lbs
Hardness at 25 °C (Rockwell C)
0
20
40
60
80
100
120
140
5
10
15
20
25
30
900 x 2 hrs AC
600
700
800
900
Reheating Temperature, °C
XBL 736-6287

Fig. 8.

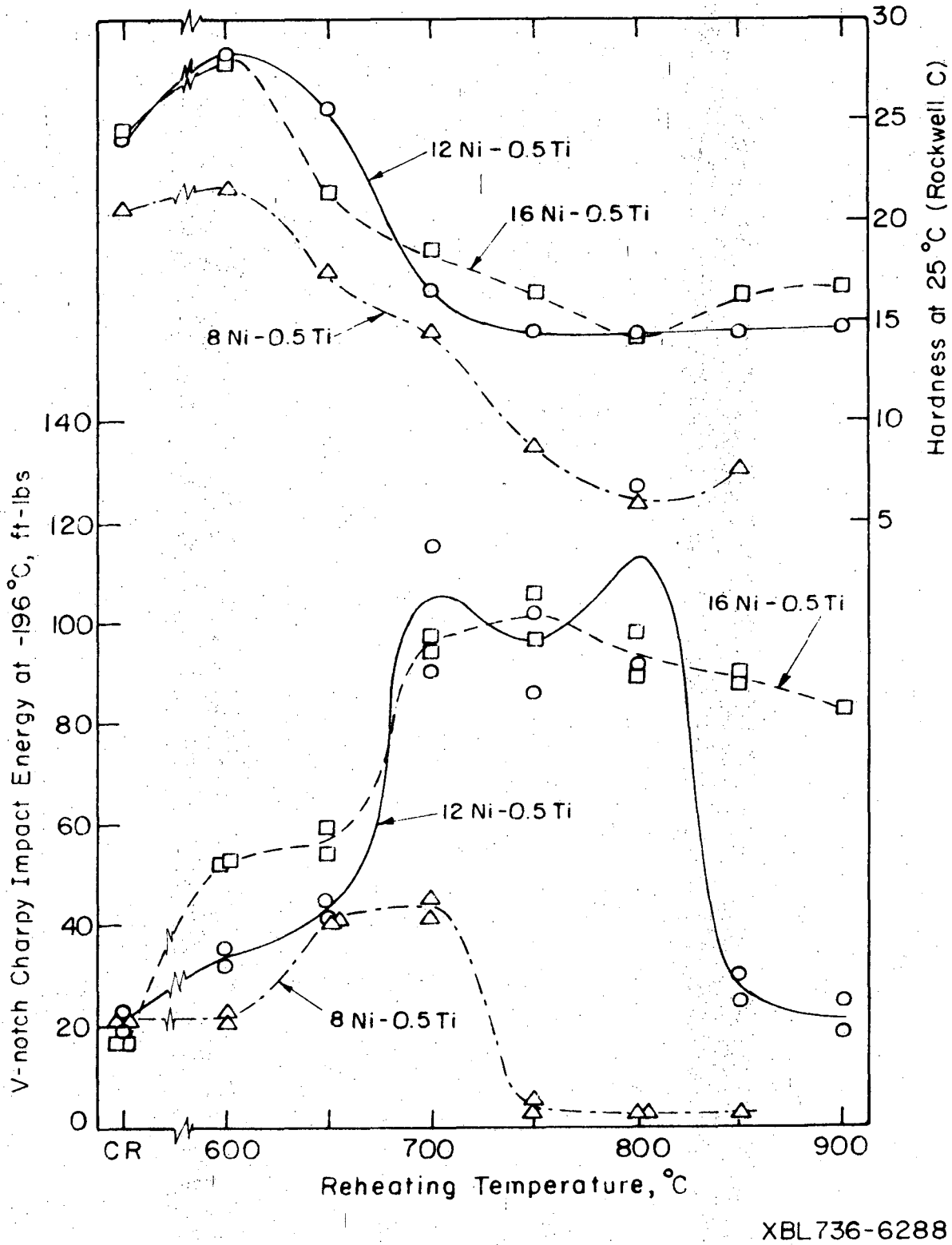

Fig. 9.

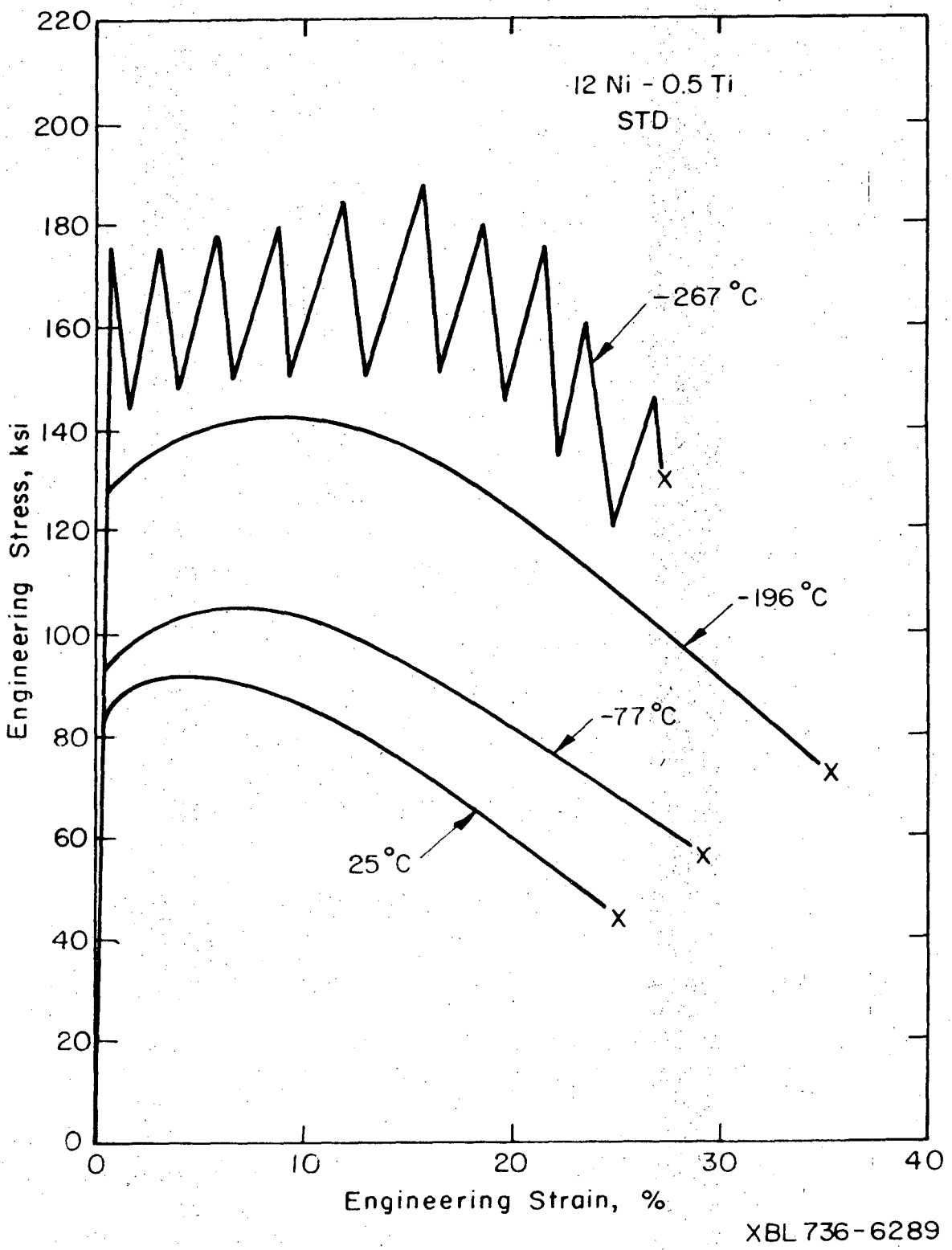
12 Ni - 0.5 Ti
STD
-267 °C
-196 °C
-77 °C
25 °C
Engineering Stress, ksi
Engineering Strain, %
0
20
40
60
80
100
120
140
160
180
200
220
0
10
20
30
40
XBL 736-6289

Fig. 10.

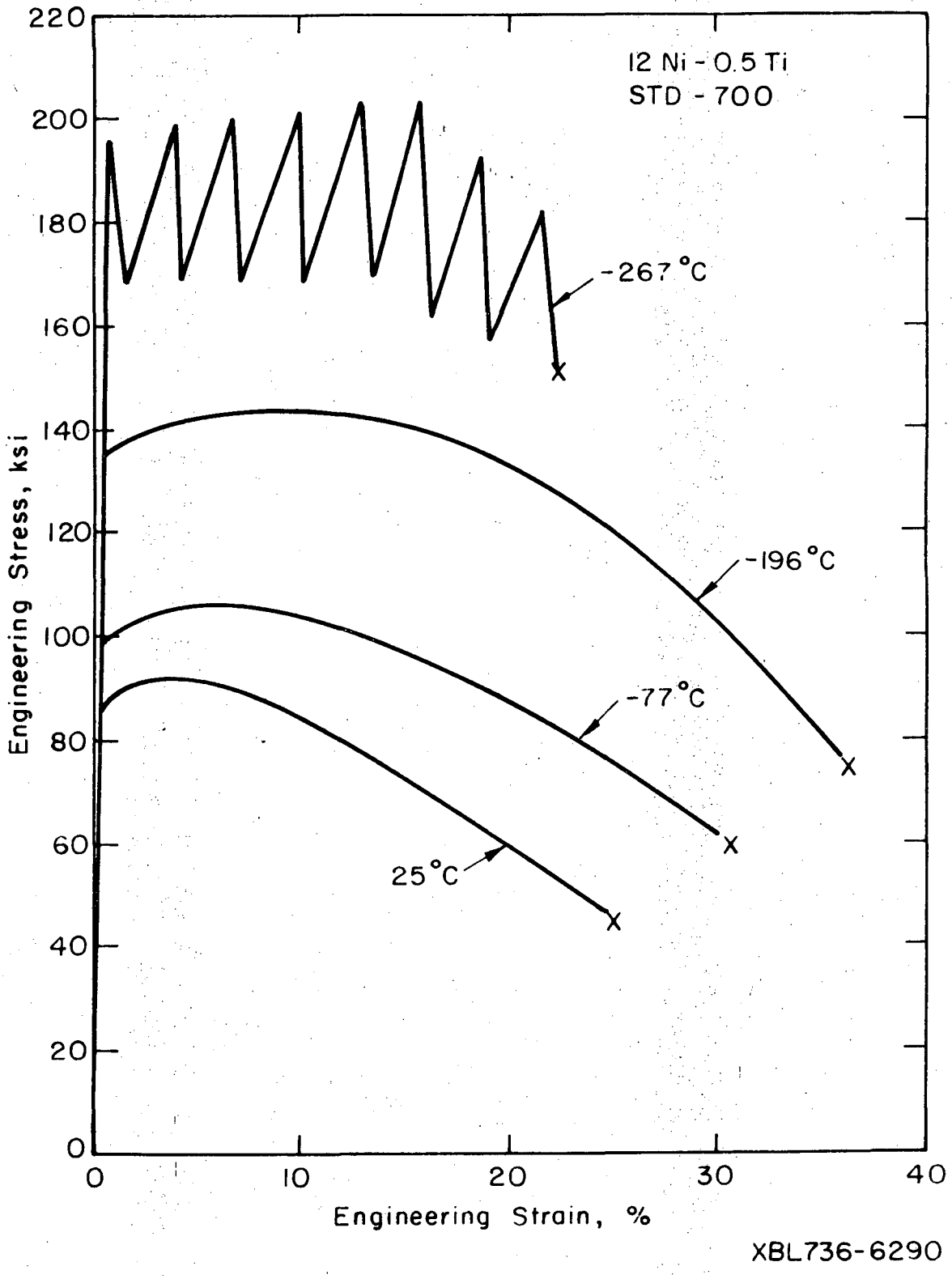
12 Ni - 0.5 Ti
STD - 700
-267 °C
-196 °C
-77 °C
25 °C
Engineering Stress, ksi
Engineering Strain, %
0
20
40
60
80
100
120
140
160
180
200
220
0
10
20
30
40
XBL736-6290

Fig. 11.

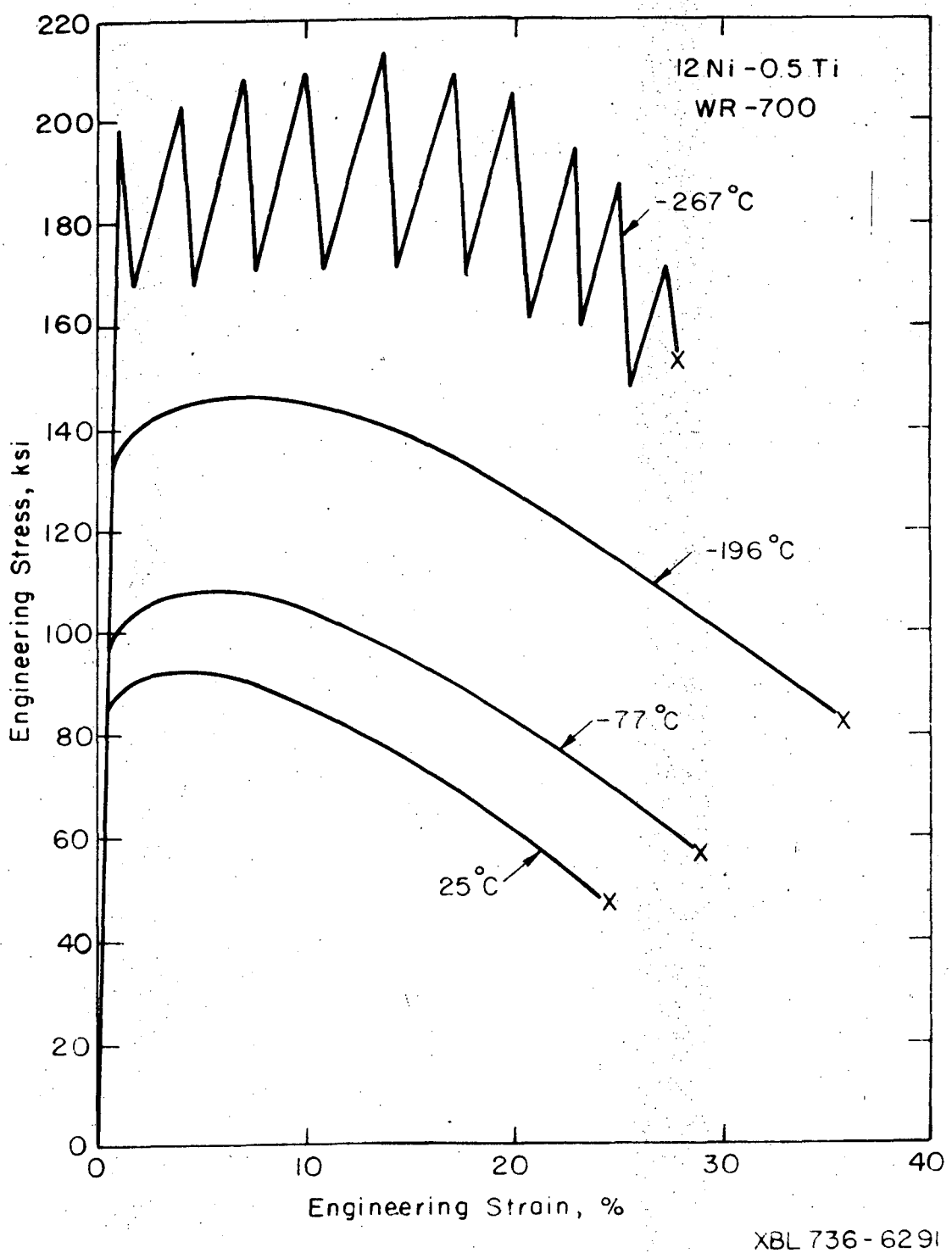
12 Ni - 0.5 Ti
WR - 700
-267 °C
-196 °C
-77 °C
25 °C
Engineering Stress, ksi
Engineering Strain, %
0
20
40
60
80
100
120
140
160
180
200
220
0
10
20
30
40
XBL 736-6291

Fig. 12.

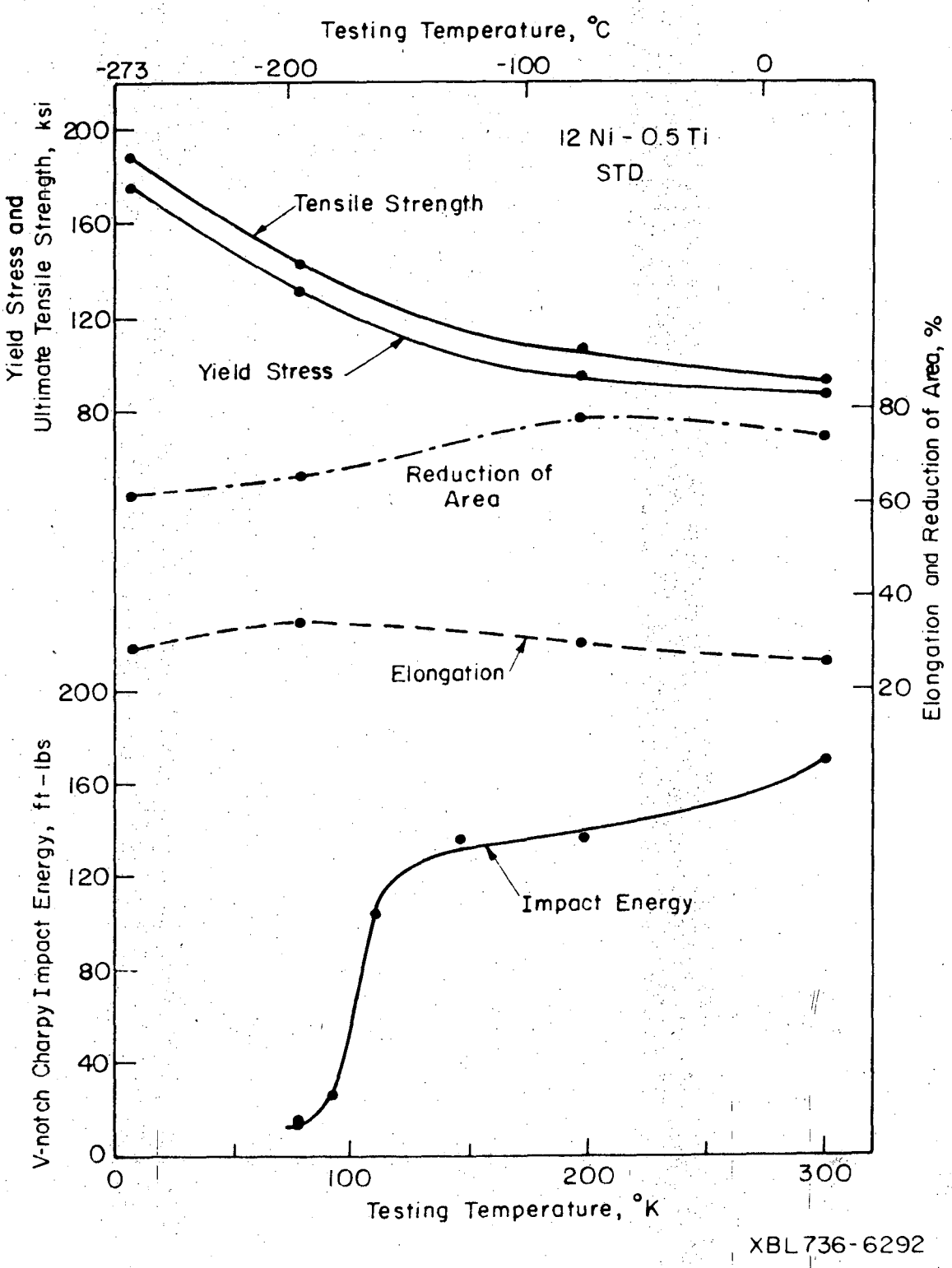
Testing Temperature, °C
-273
-200
-100
0
12 Ni - 0.5 Ti
STD
Tensile Strength
Yield Stress
Yield Stress and
Ultimate Tensile Strength, ksi
200
160
120
80
Reduction of
Area
Elongation
Elongation and Reduction of Area, %
80
60
40
20
V-notch Charpy Impact Energy, ft-lbs
200
160
120
80
40
0
Impact Energy
0
100
200
300
Testing Temperature, °K
XBL736-6292

Fig. 13.

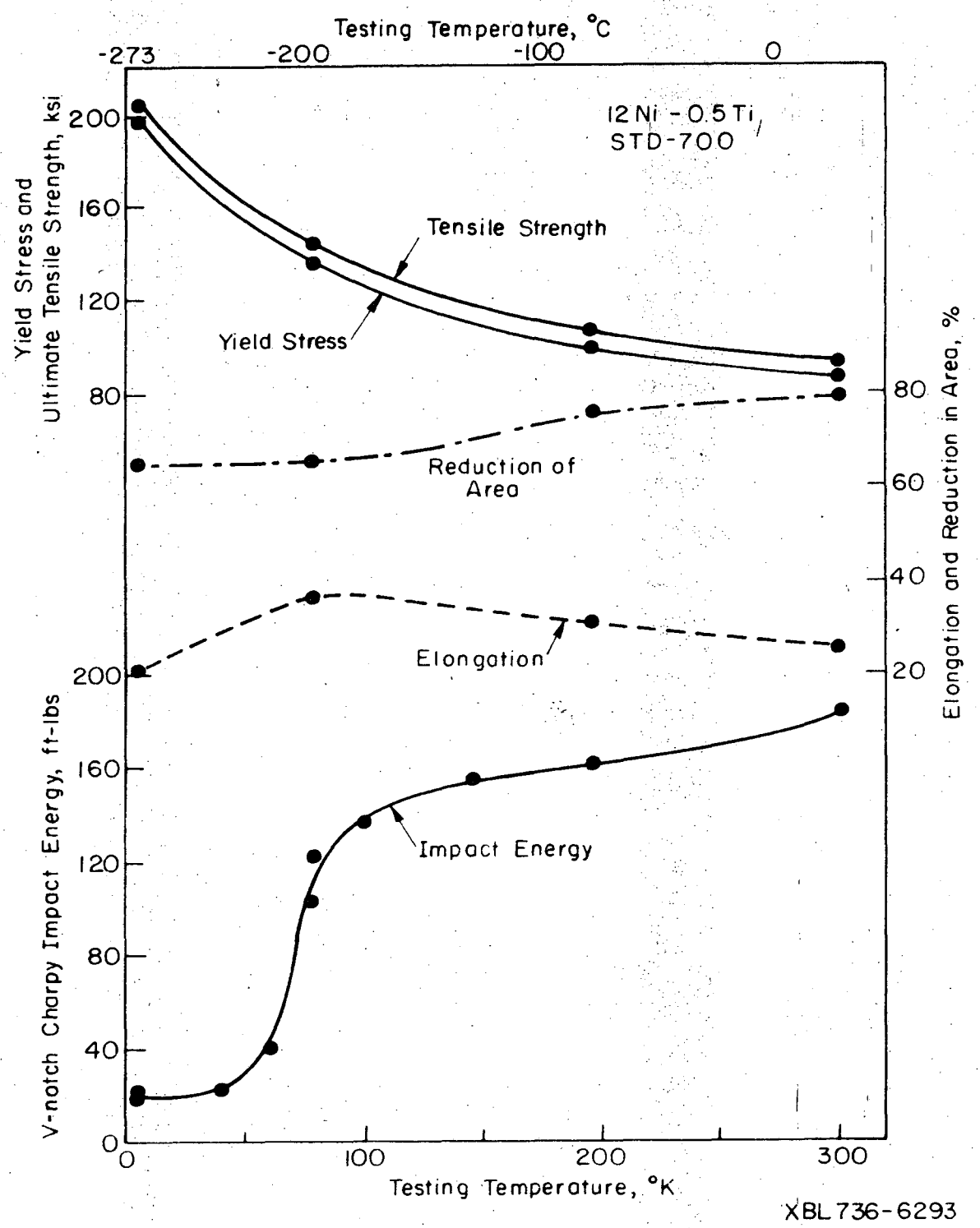
Testing Temperature, °C
-273
-200
-100
0
12 Ni - 0.5 Ti
STD-700
Tensile Strength
Yield Stress
Yield Stress and
Ultimate Tensile Strength, ksi
200
160
120
80
Reduction of
Area
60
40
Elongation
20
Elongation and Reduction in Area, %
200
160
120
80
40
0
Impact Energy
V-notch Charpy Impact Energy, ft-lbs
0
100
200
300
Testing Temperature, °K
XBL 736-6293

Fig. 14.

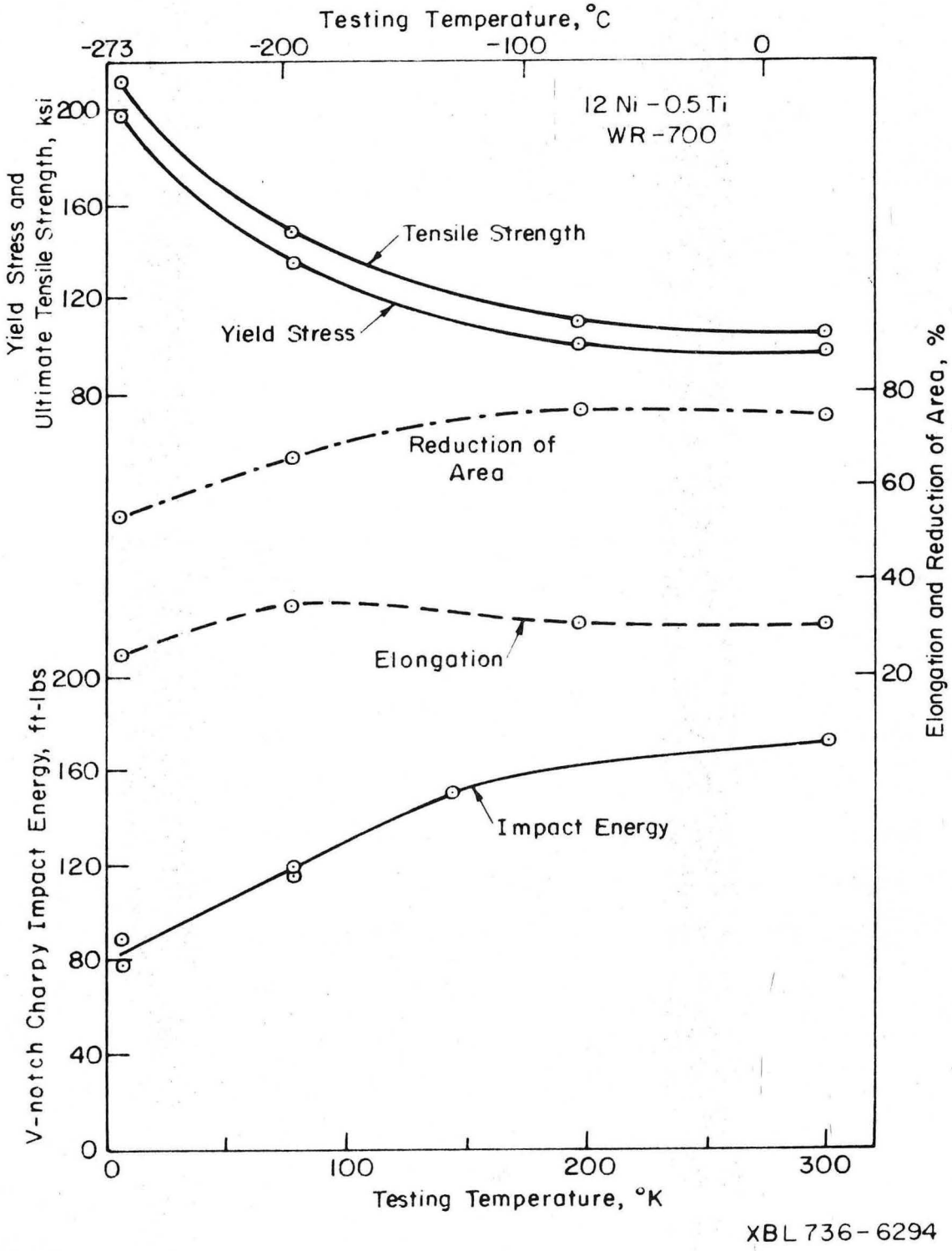

Fig. 15.

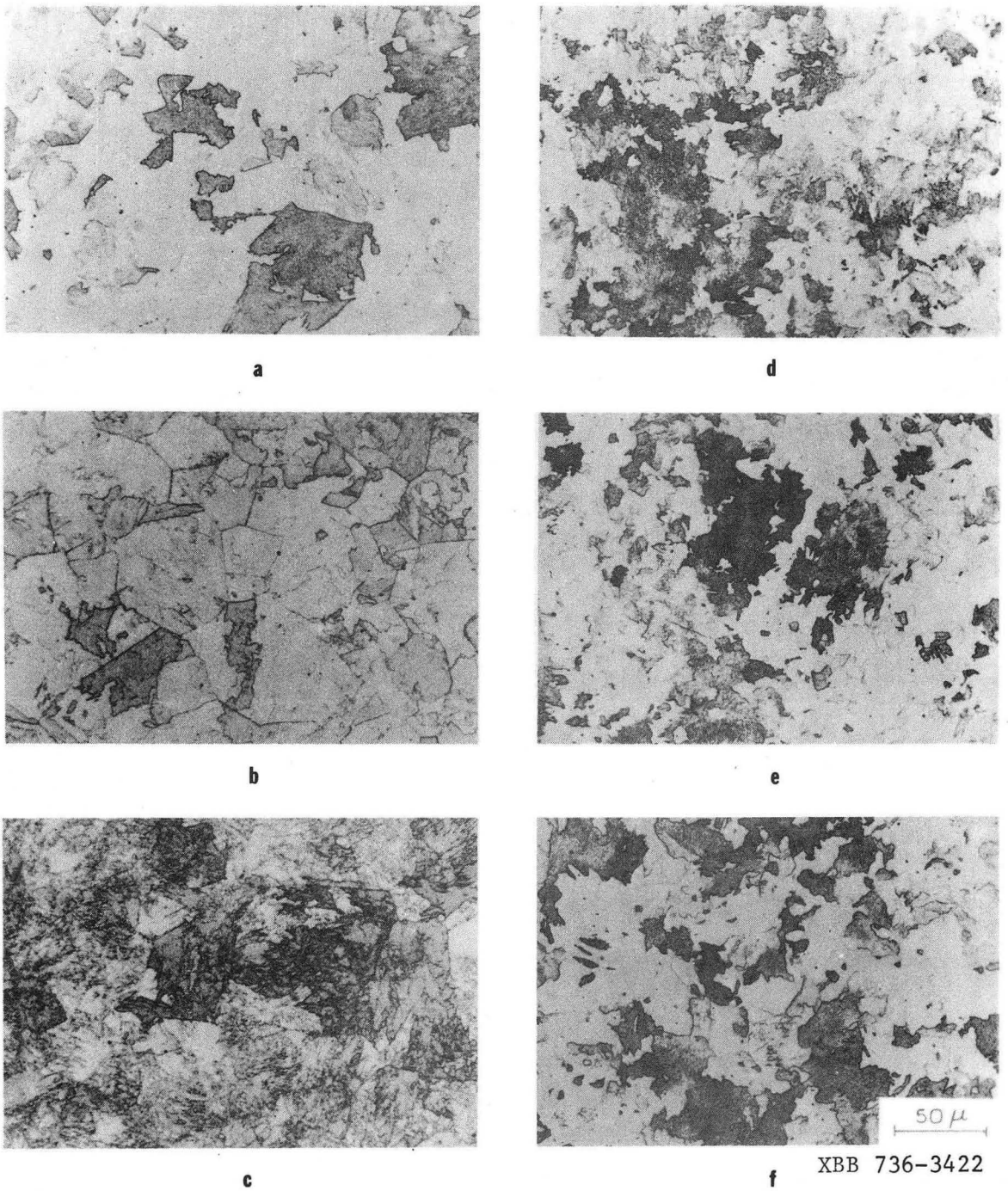

Fig. 16.

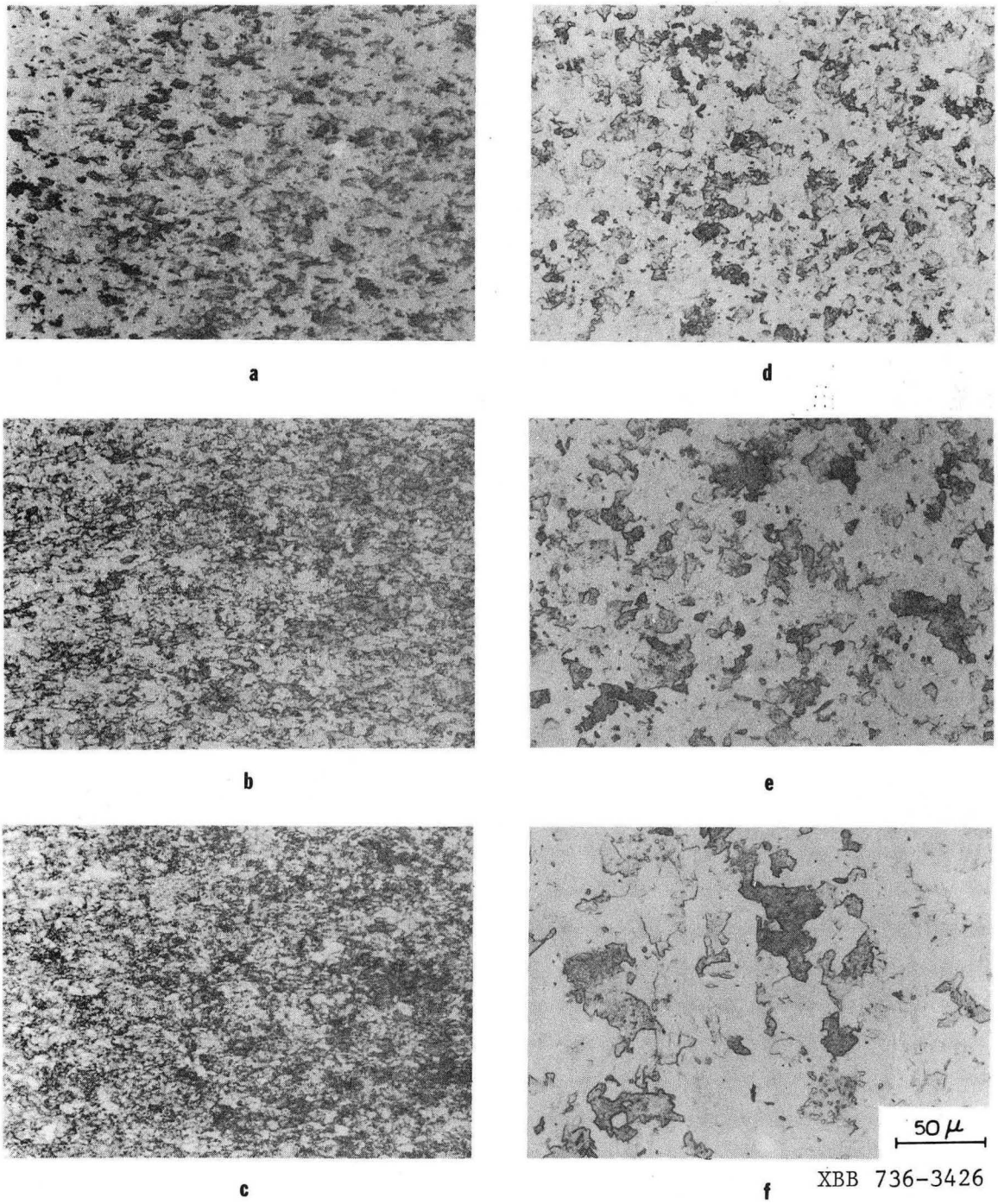

XBB 736-3426

Fig. 17.

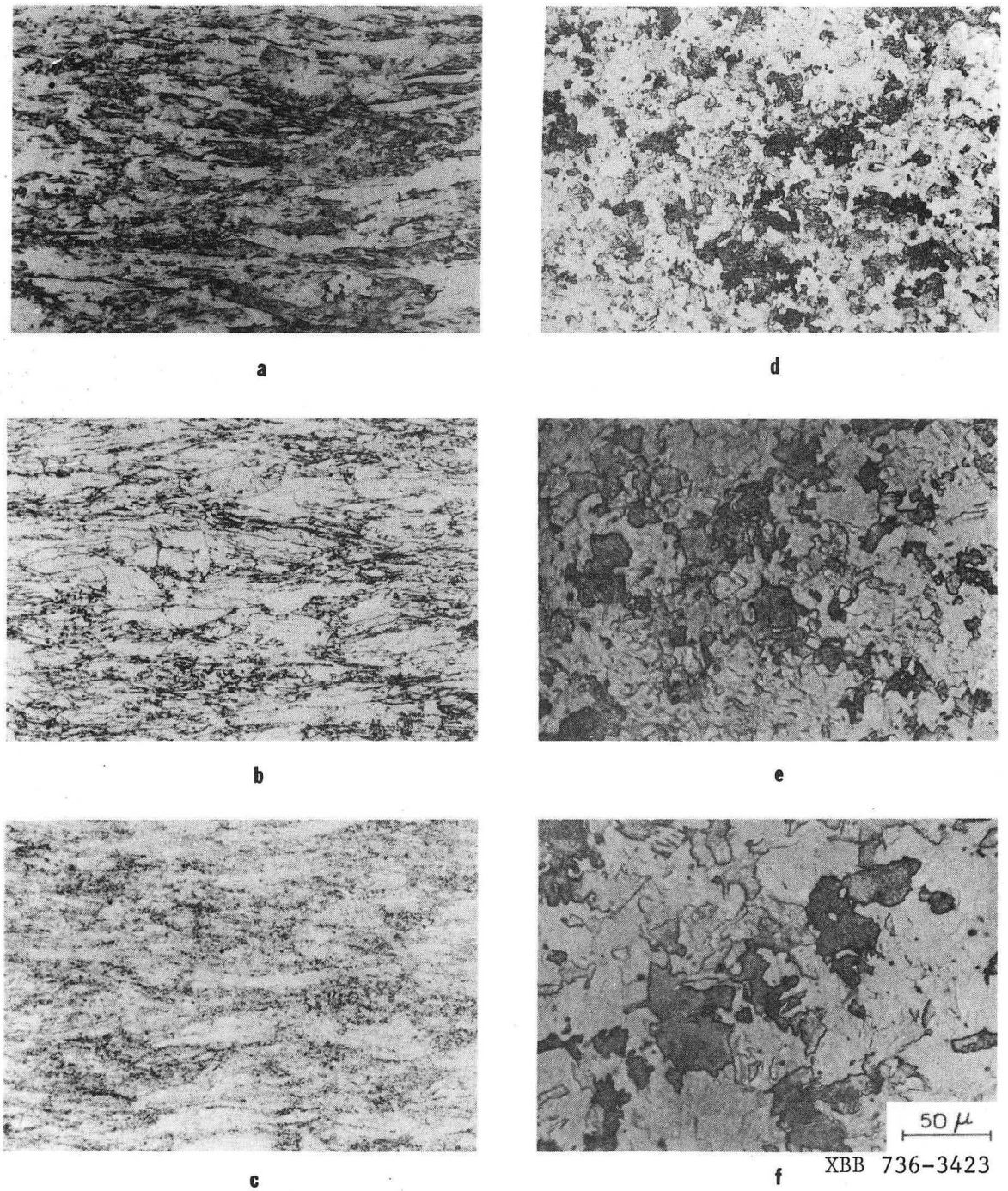

Fig. 18.

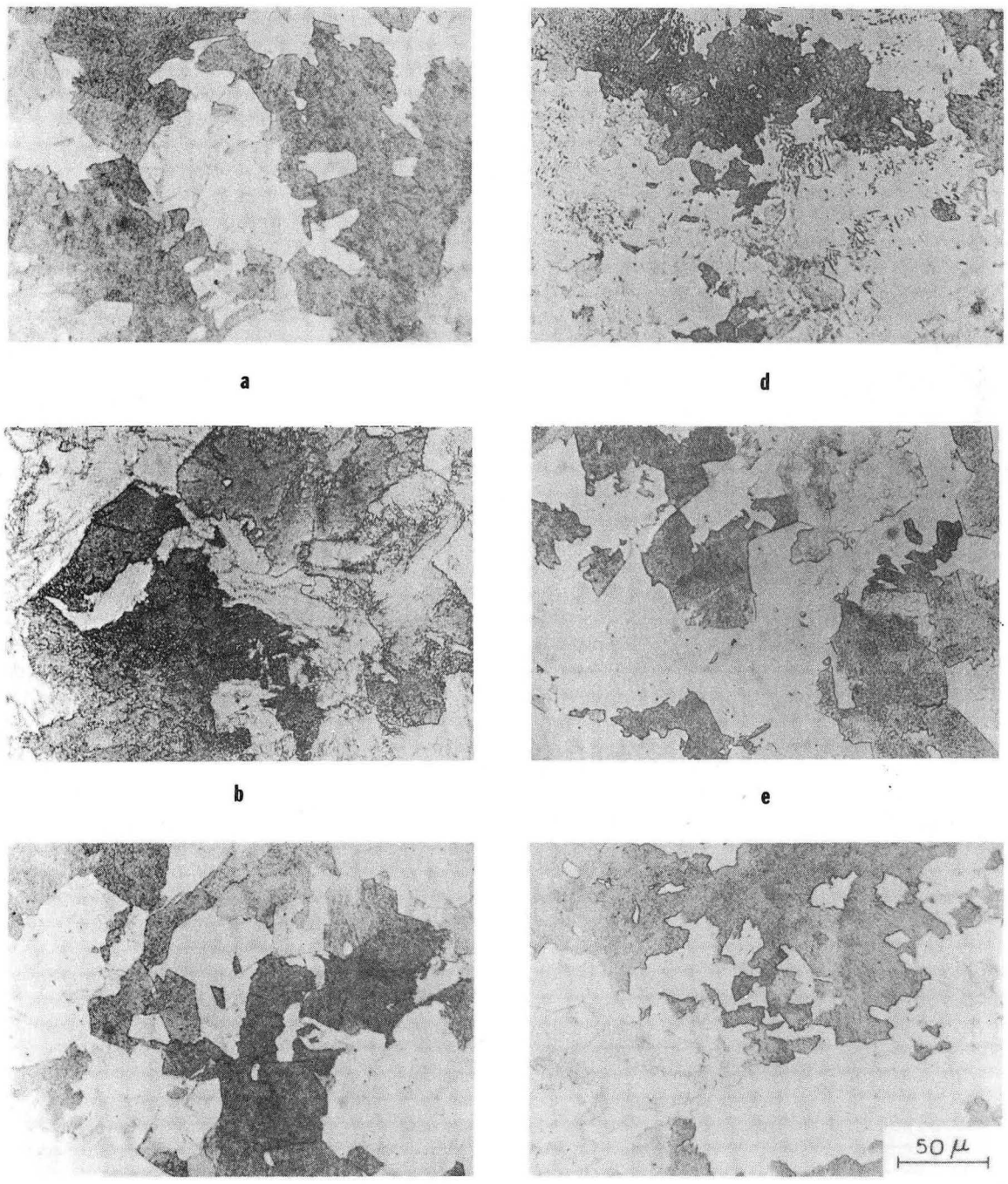

Fig. 19.

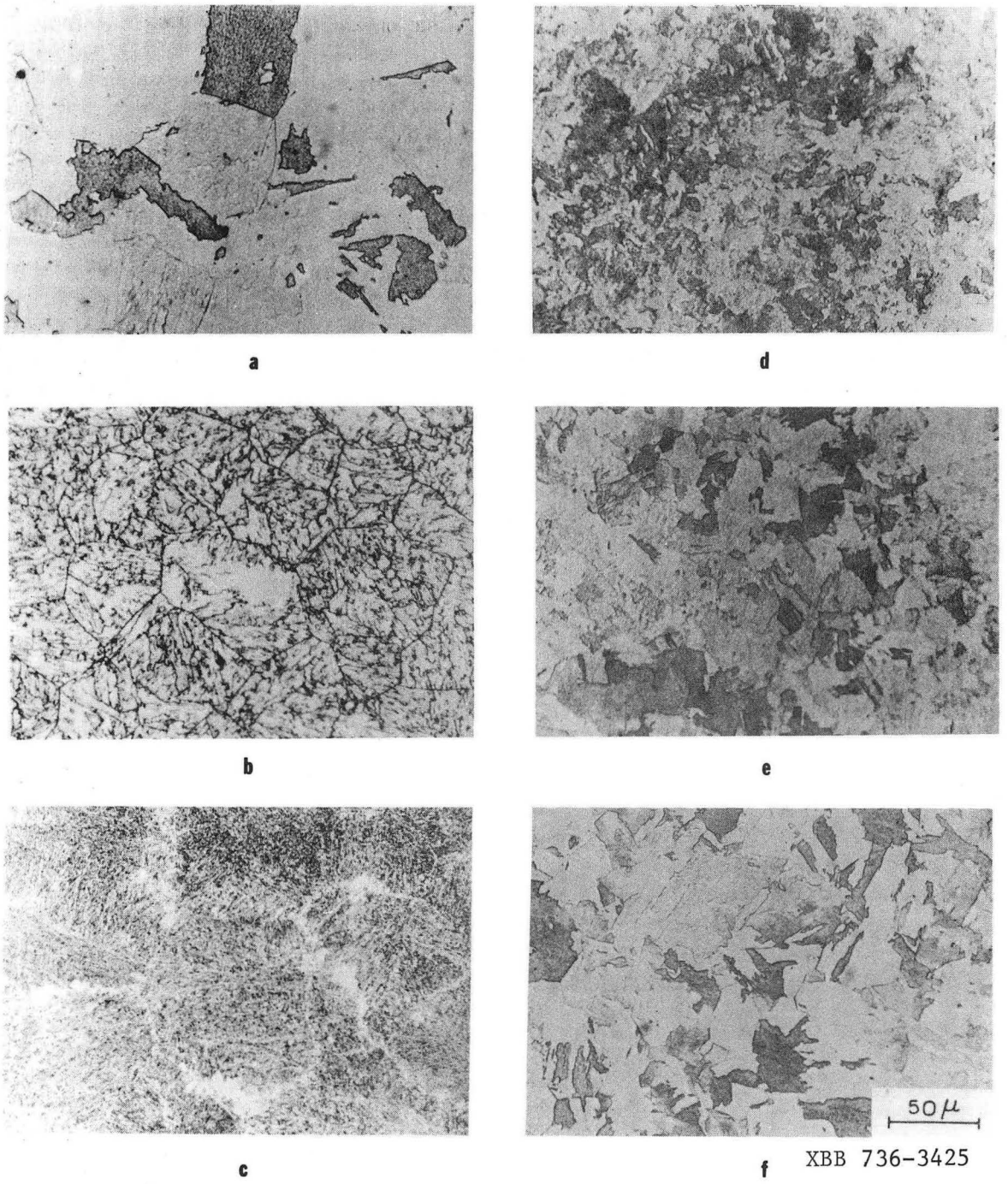

Fig. 20.

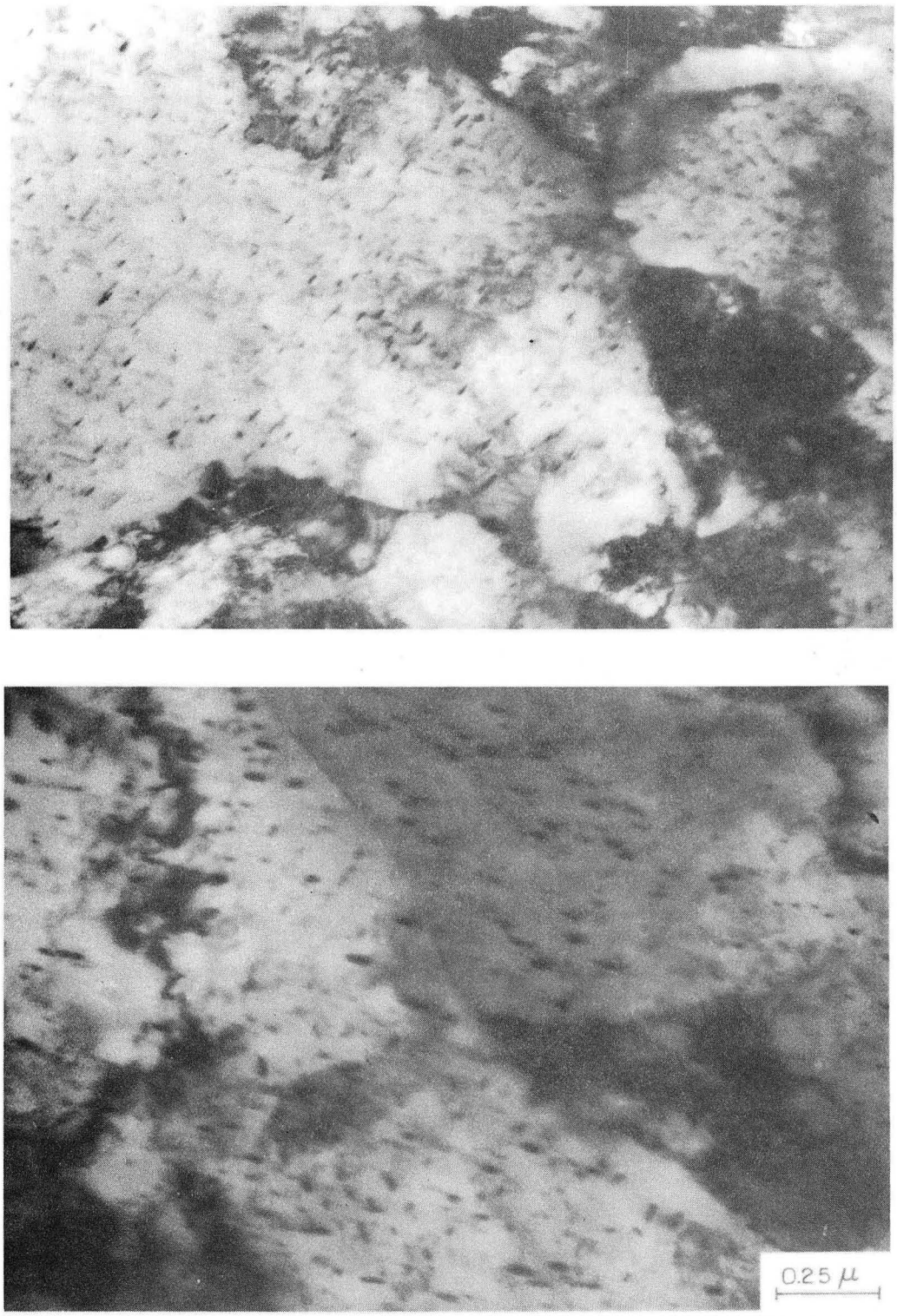

XBB 736-3419

Fig. 21.

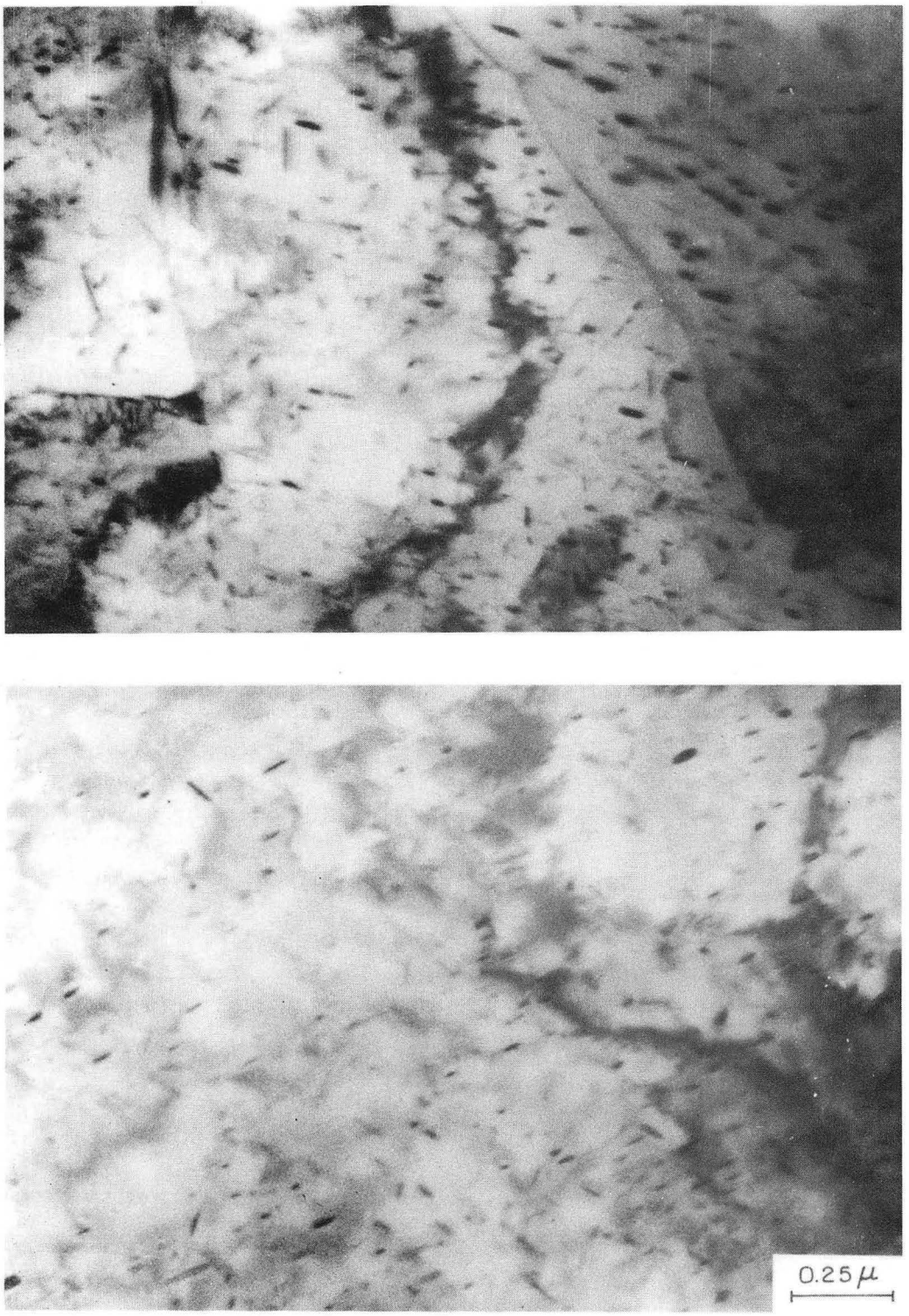

XBB 736-3418

Fig. 22.

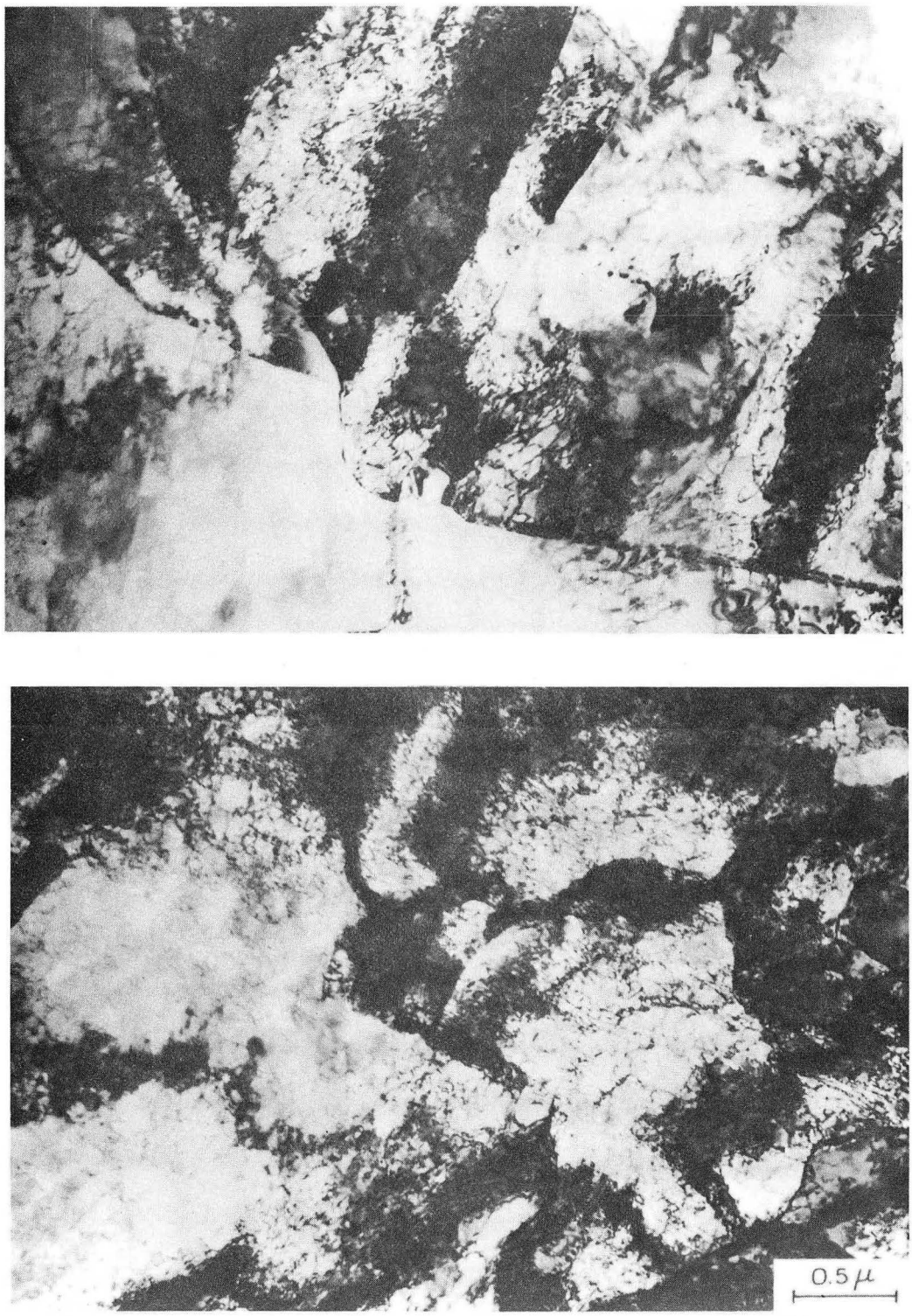

XBB 736-3417

Fig. 23.

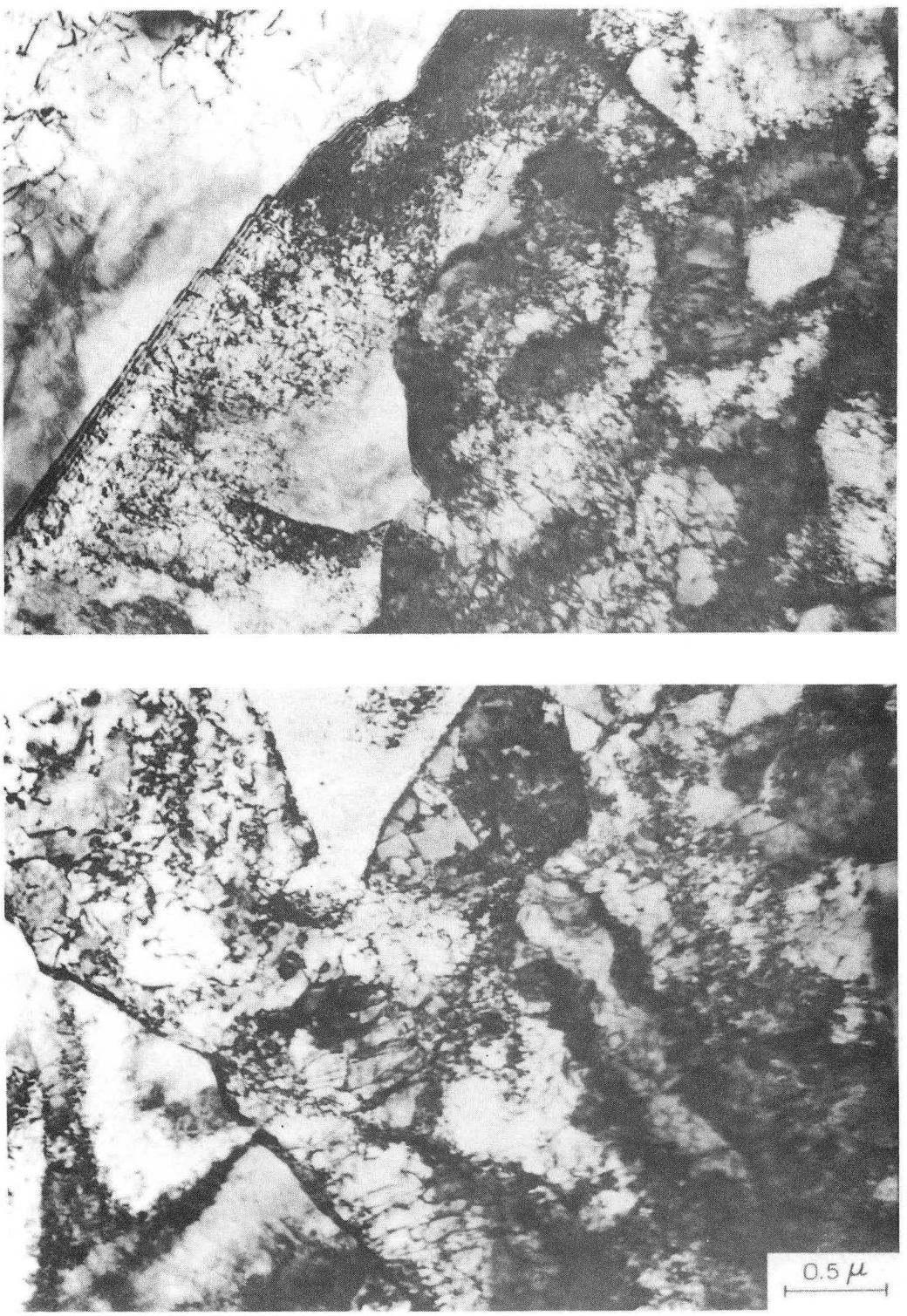

XBB 736-3416

Fig. 24.

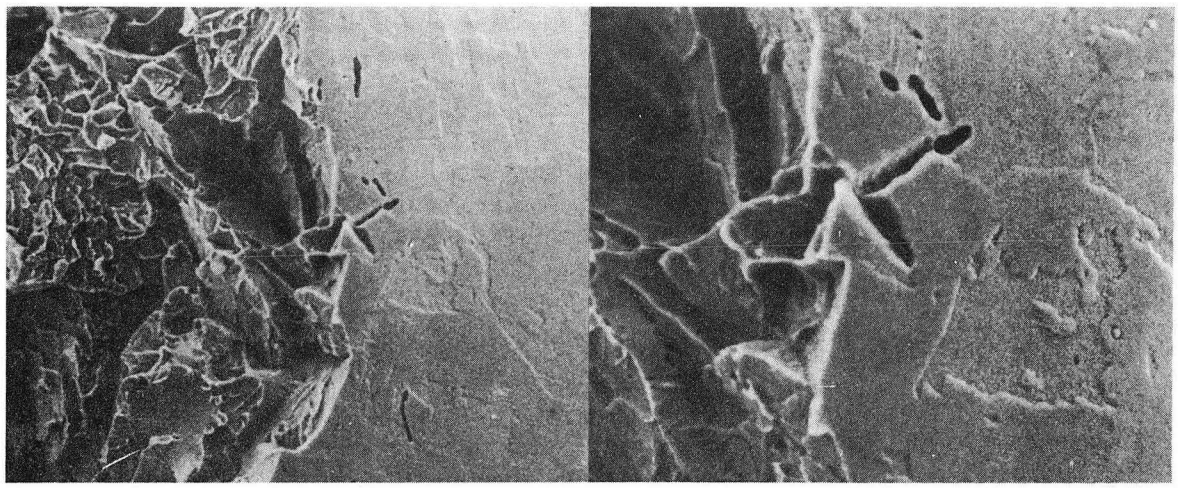

a

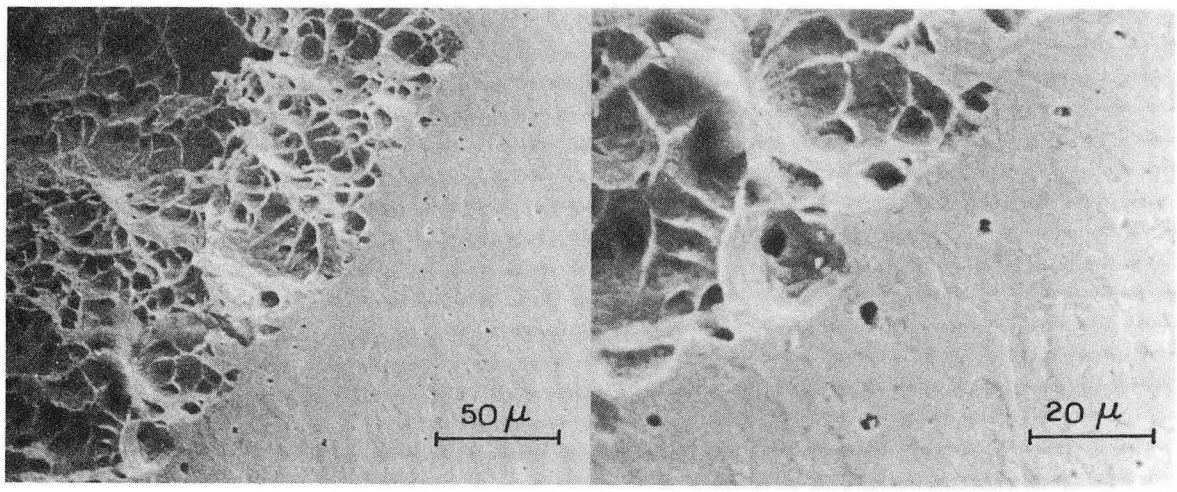

XBB 736-3433

b

Fig. 25.

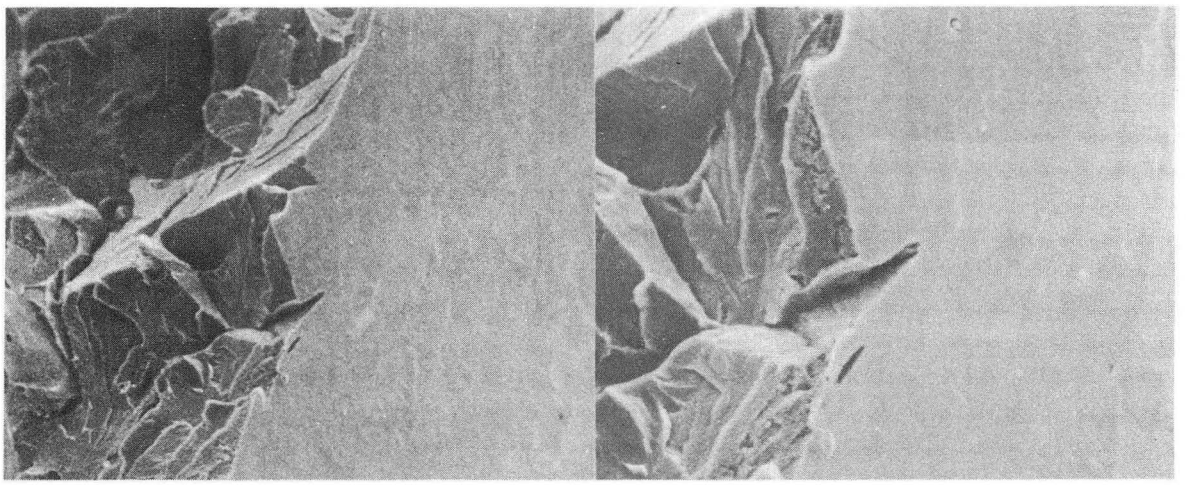

a

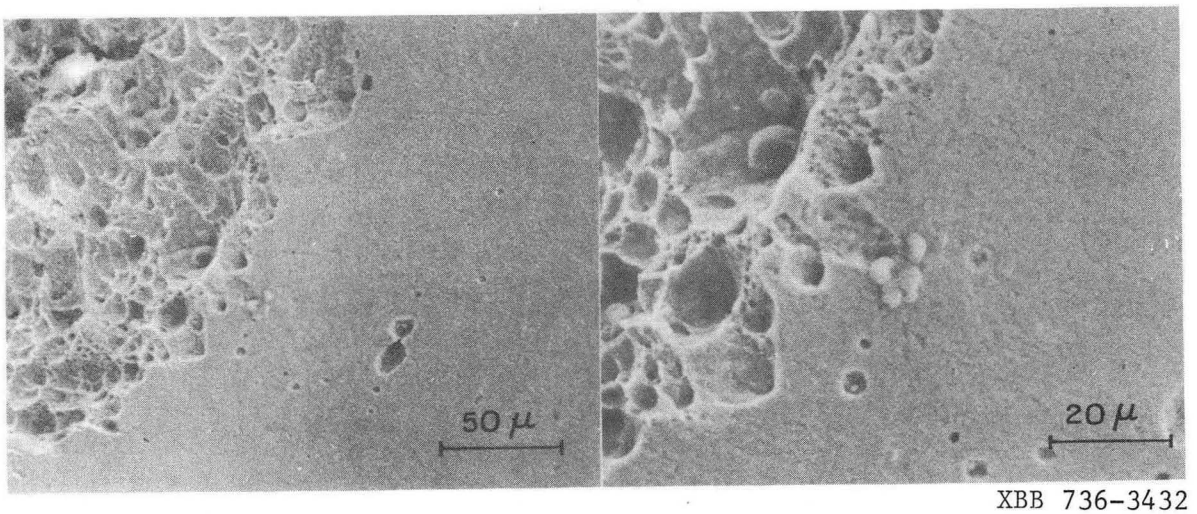

XBB 736-3432

b

Fig. 26.

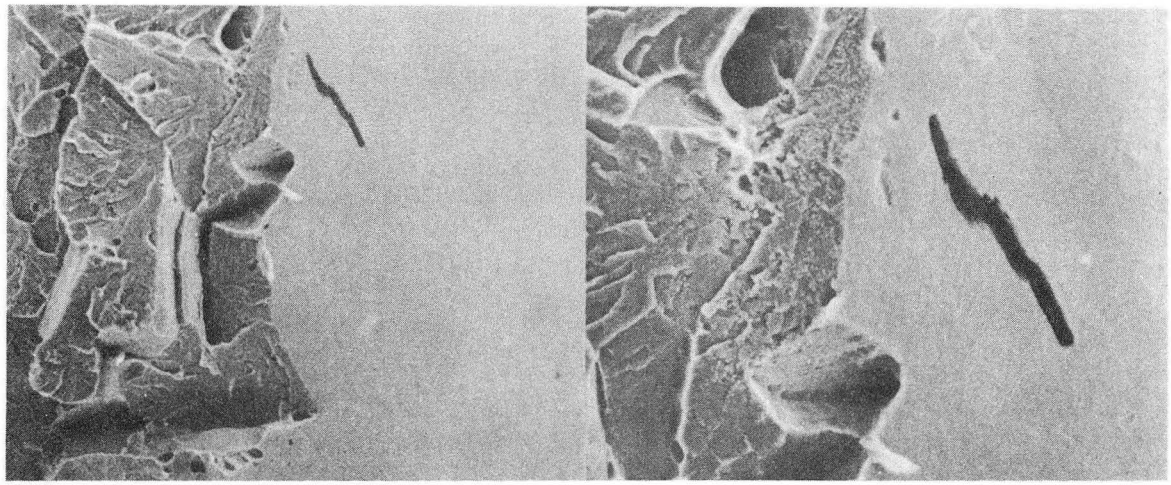

a

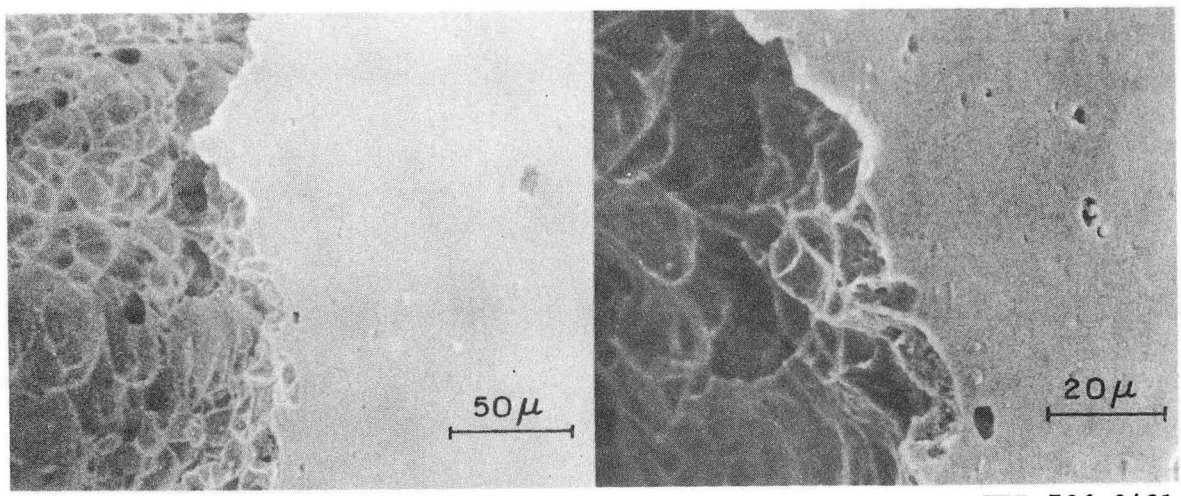

XBB 736-3431

b

Fig. 27.

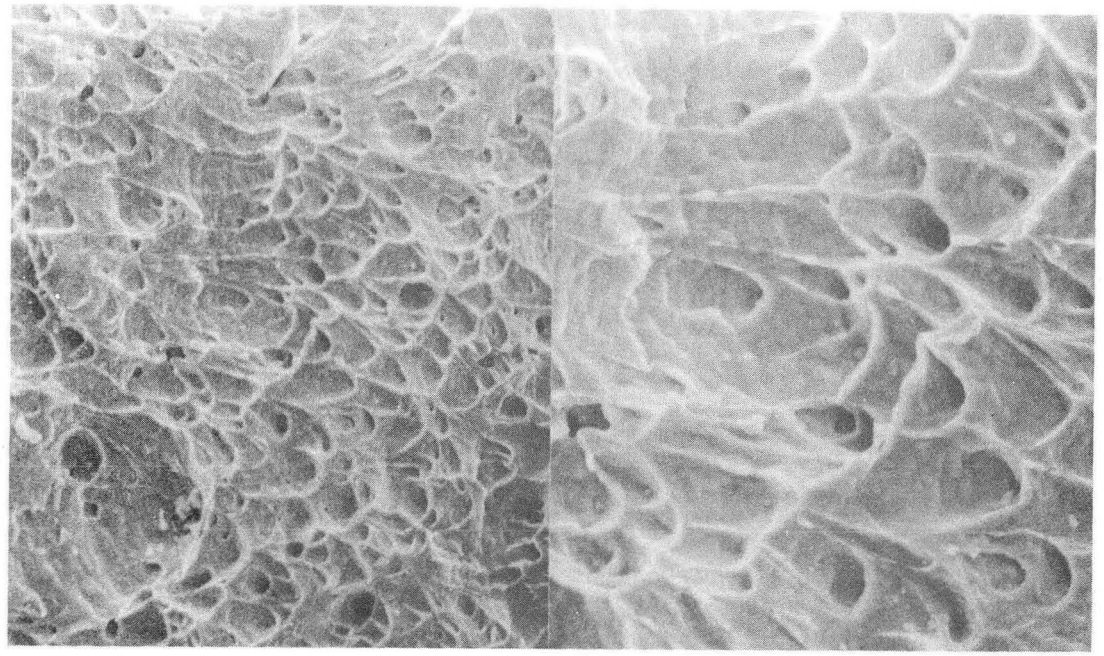

a

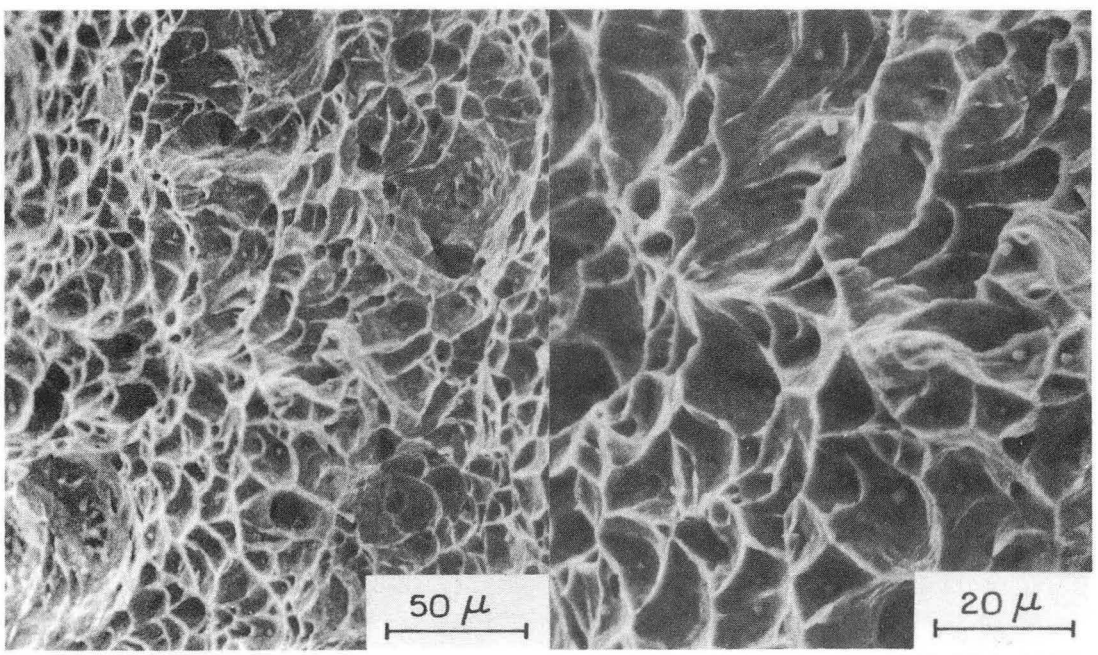

XBB 736-3429

b

Fig. 28.

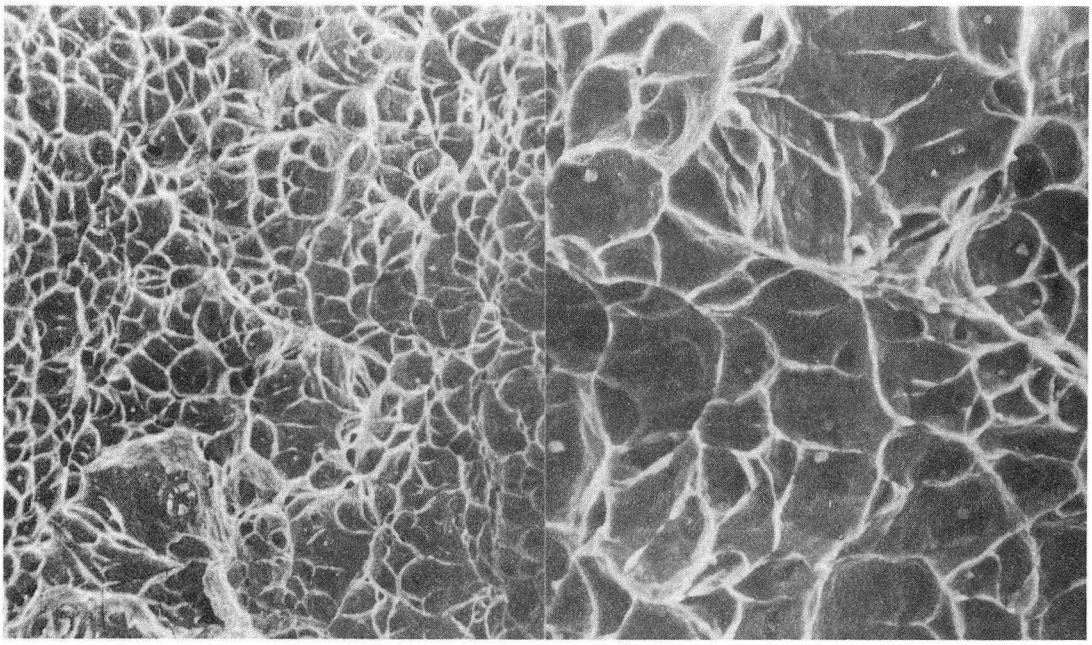

c

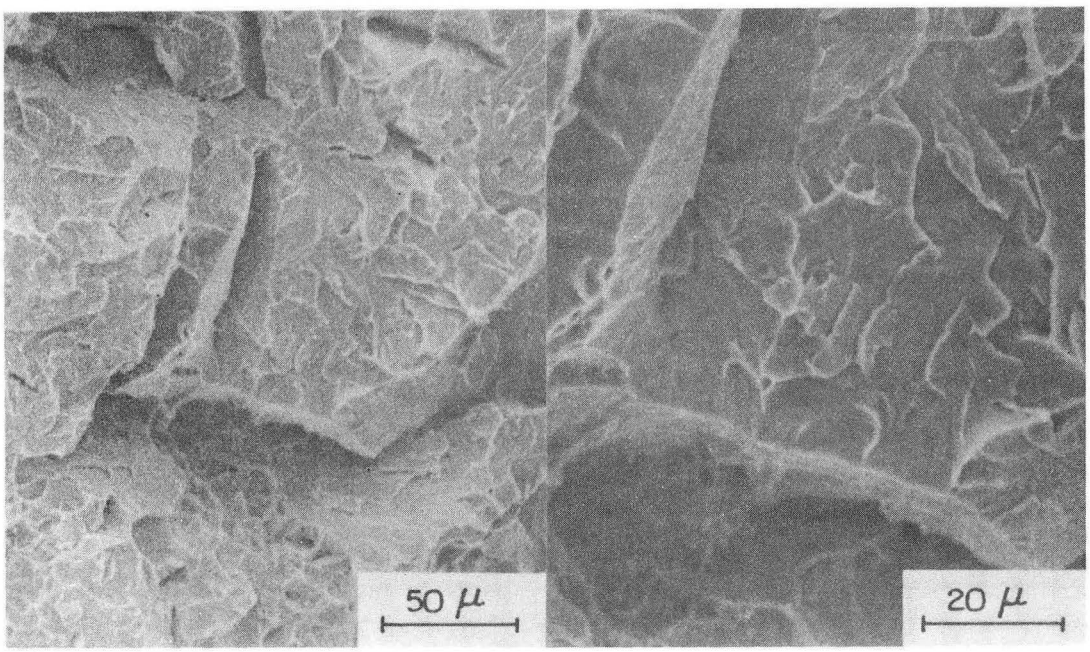

XBB 736-3435

d

Fig. 28. (Cont.)

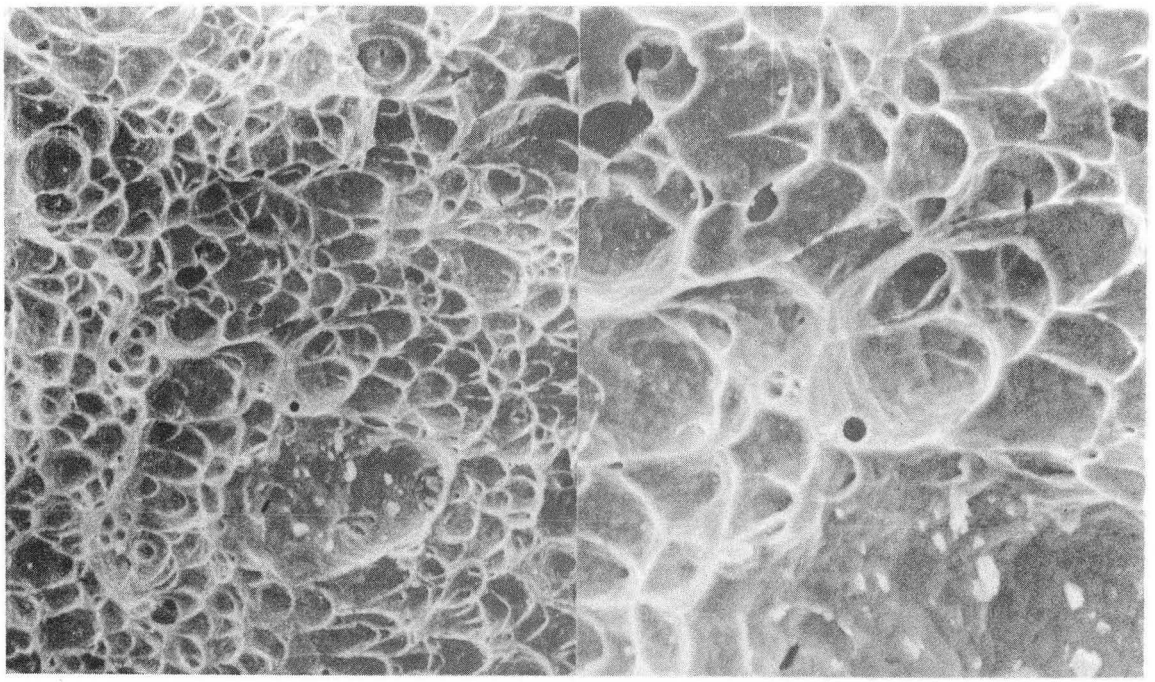

a

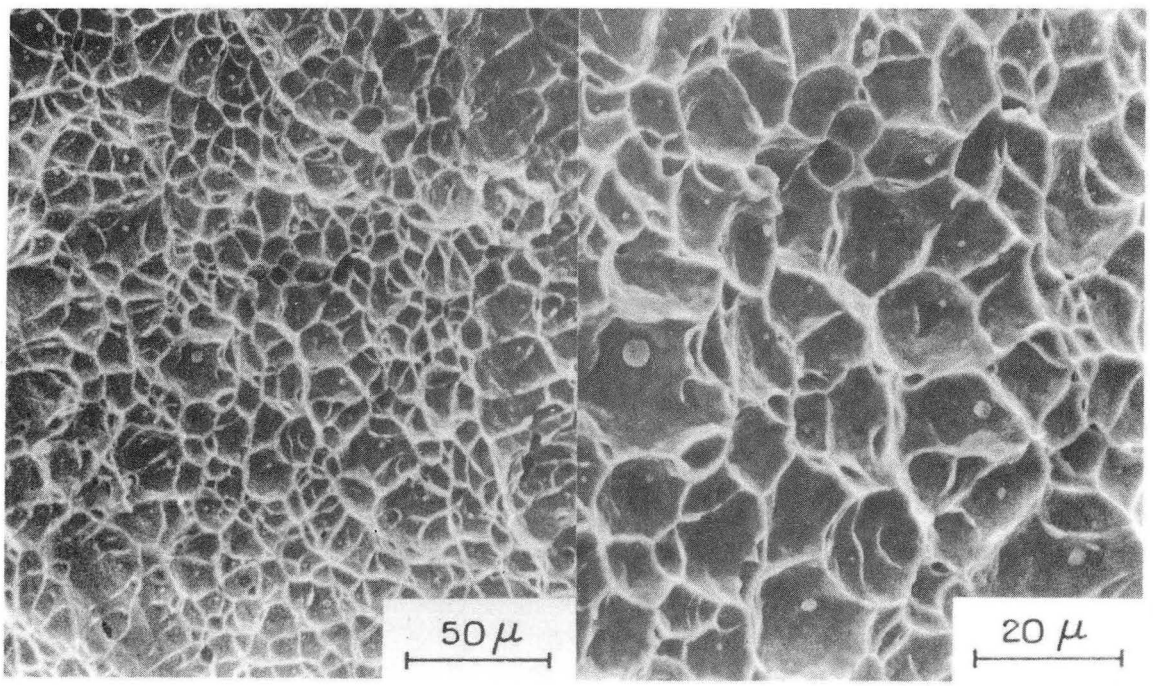

XBB 736-3428

b

Fig. 29

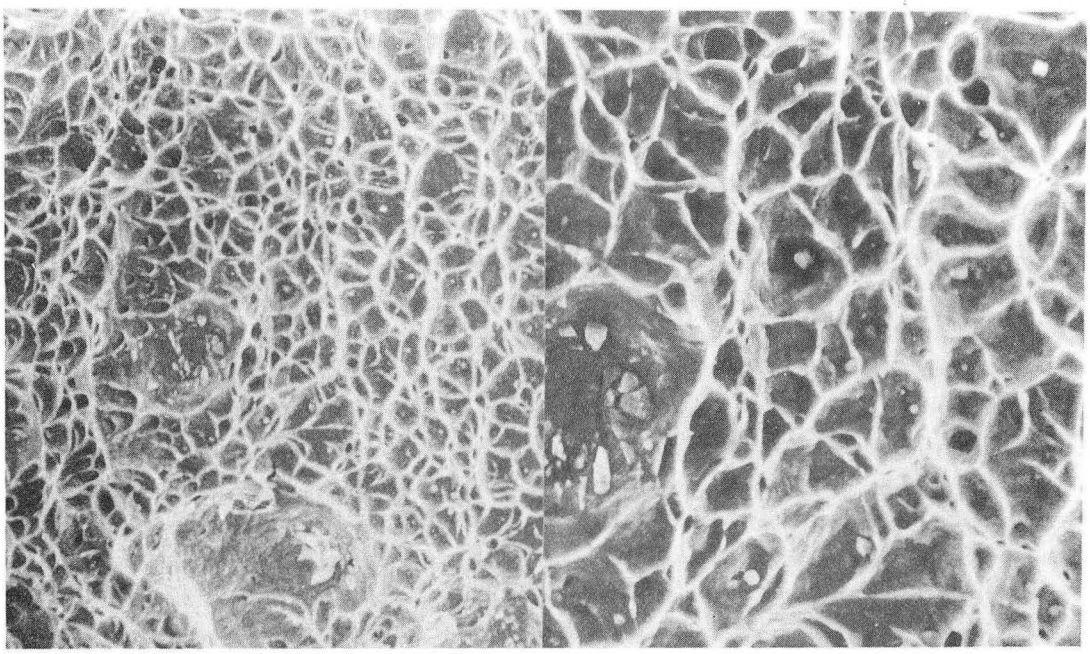

c

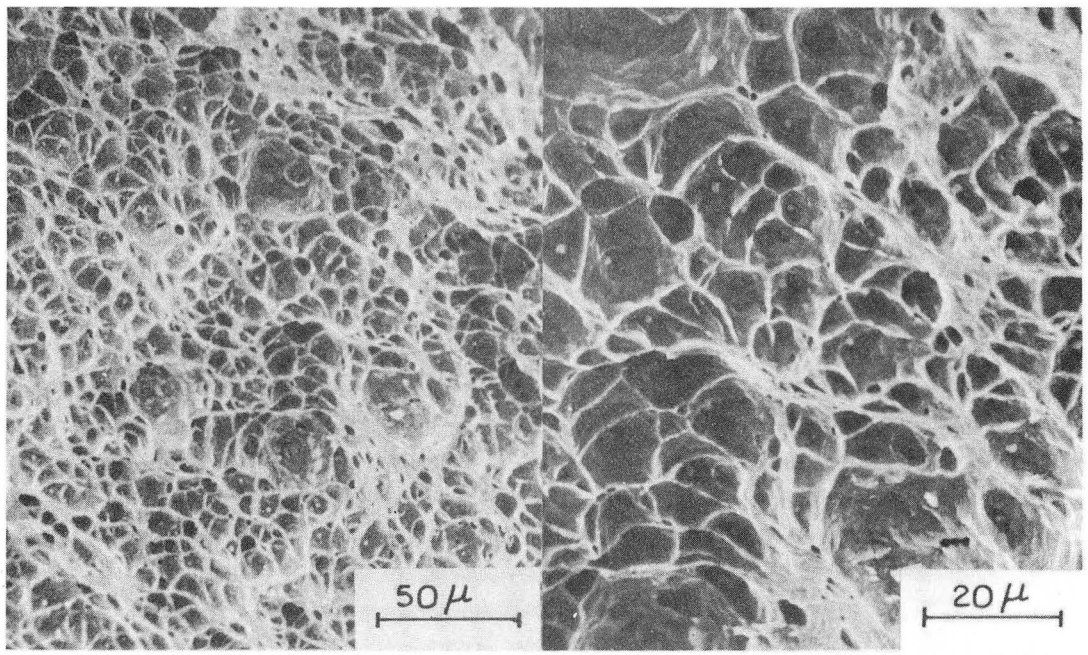

XBB 736-3434

d

Fig. 29 (Cont.)

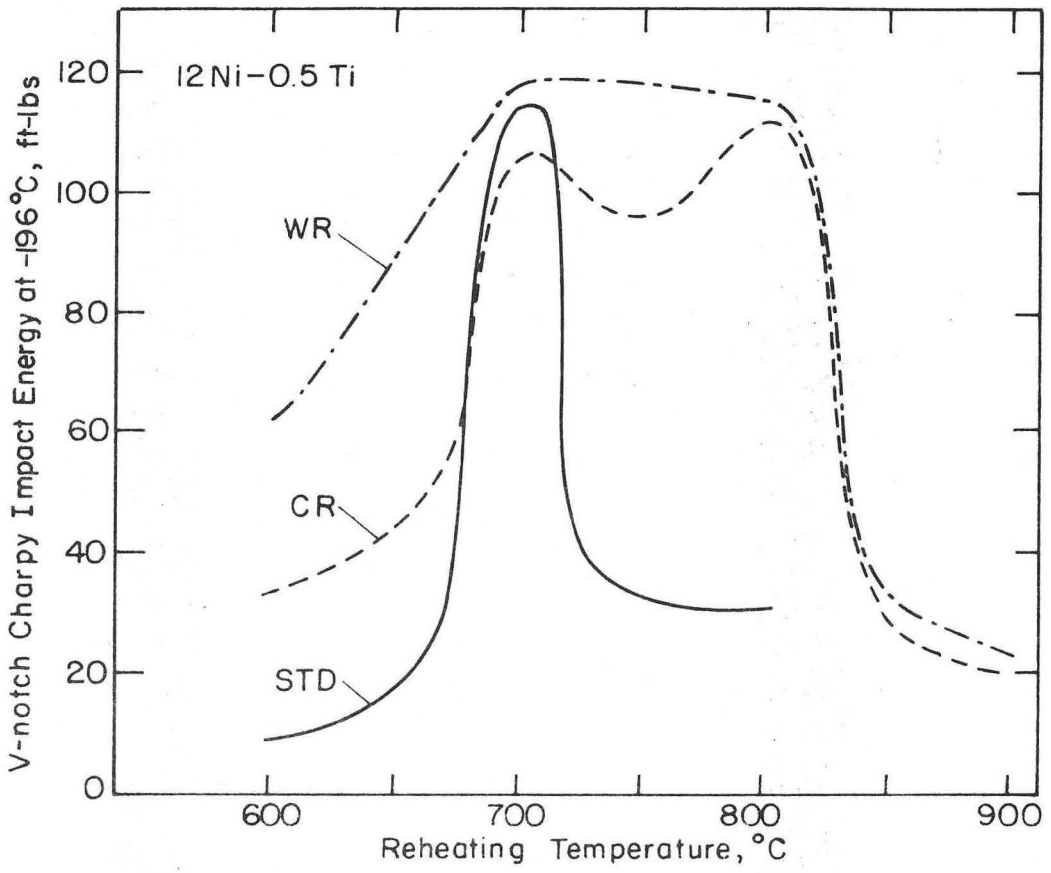
12Ni-0.5 Ti
WR
CR
STD
V-notch Charpy Impact Energy at -196°C, ft-lbs
0
20
40
60
80
100
120
600
700
800
900
Reheating Temperature, °C

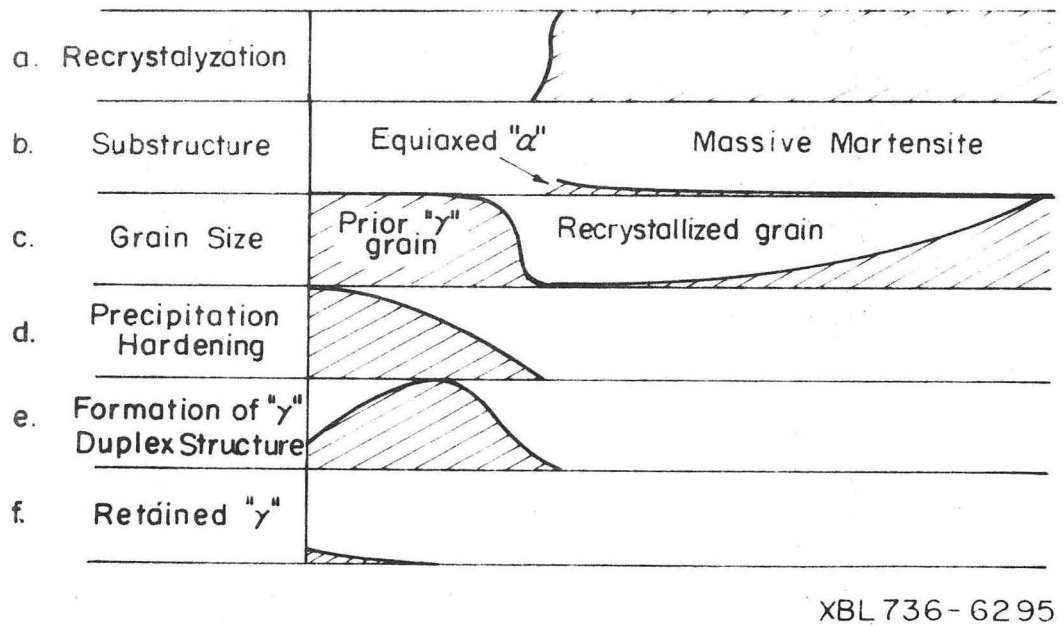
a. Recrystalyzation
b. Substructure
Equiaxed "α"
Massive Martensite
c. Grain Size
Prior "γ" grain
Recrystallized grain
d. Precipitation Hardening
e. Formation of "γ" Duplex Structure
f. Retained "γ"
XBL 736-6295

Fig. 30.

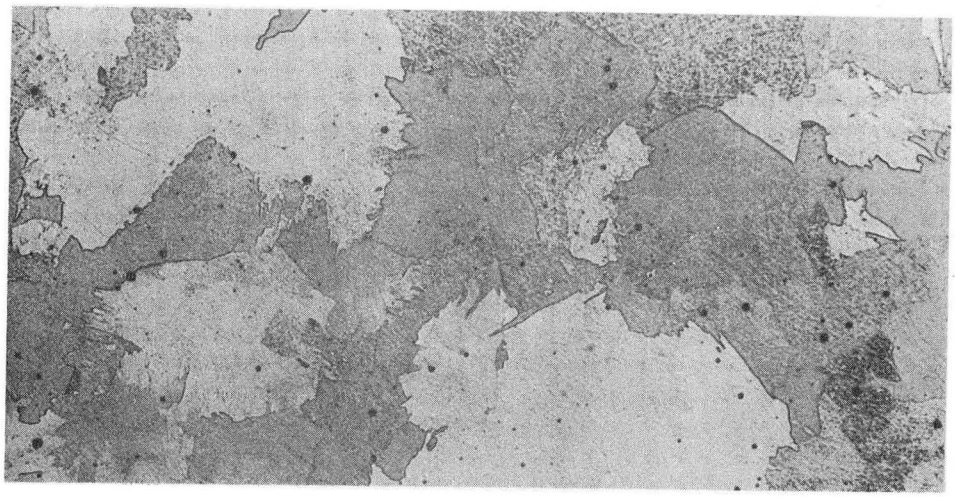

a

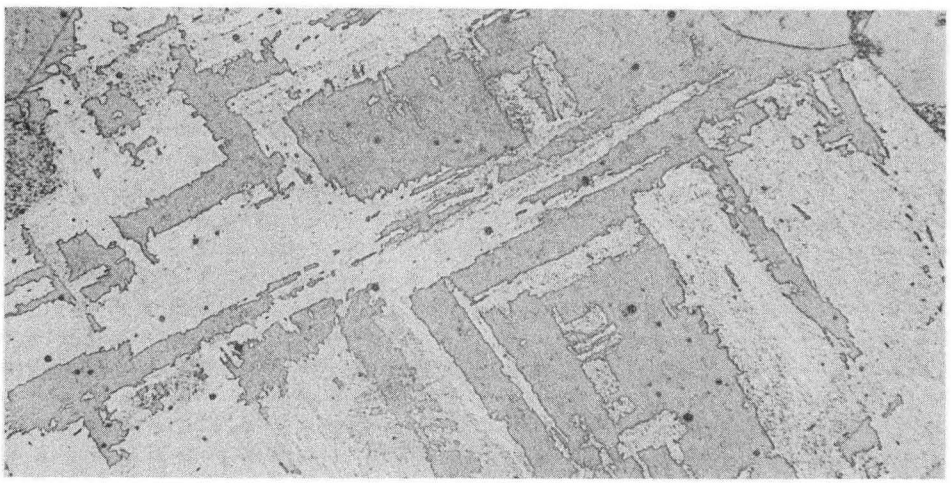

b

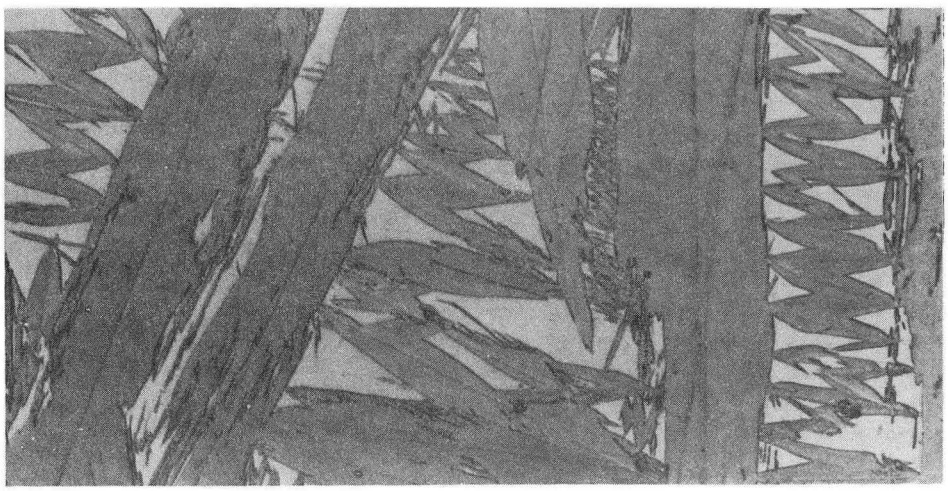

c

XBB 736-3427

Fig. 31.

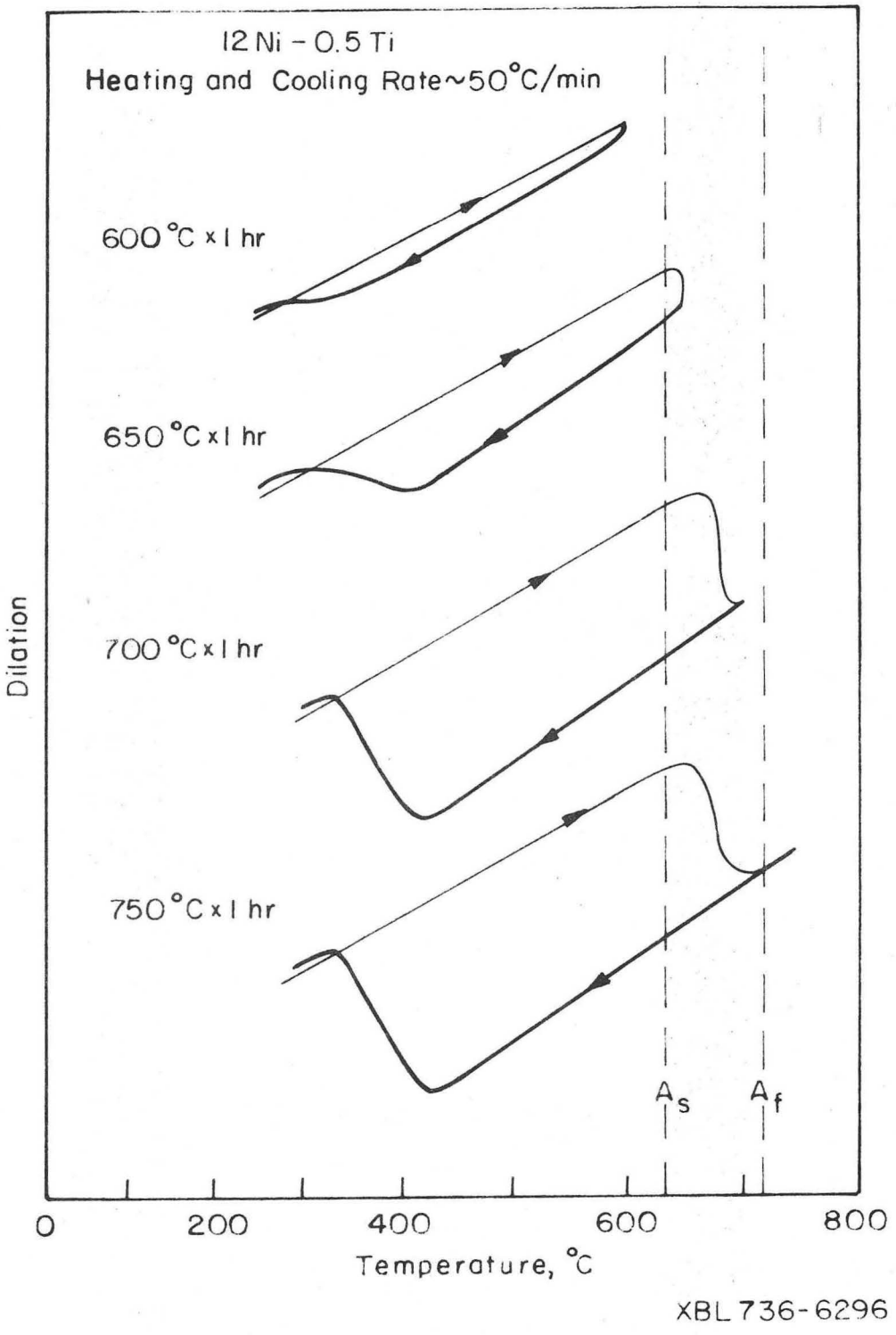
12 Ni - 0.5 Ti
Heating and Cooling Rate~50°C/min
600 °C x 1 hr
650 °C x 1 hr
700 °C x 1 hr
750 °C x 1 hr
Dilation
A_s
A_f
0
200
400
600
800
Temperature, °C
XBL 736-6296

Fig. 32.

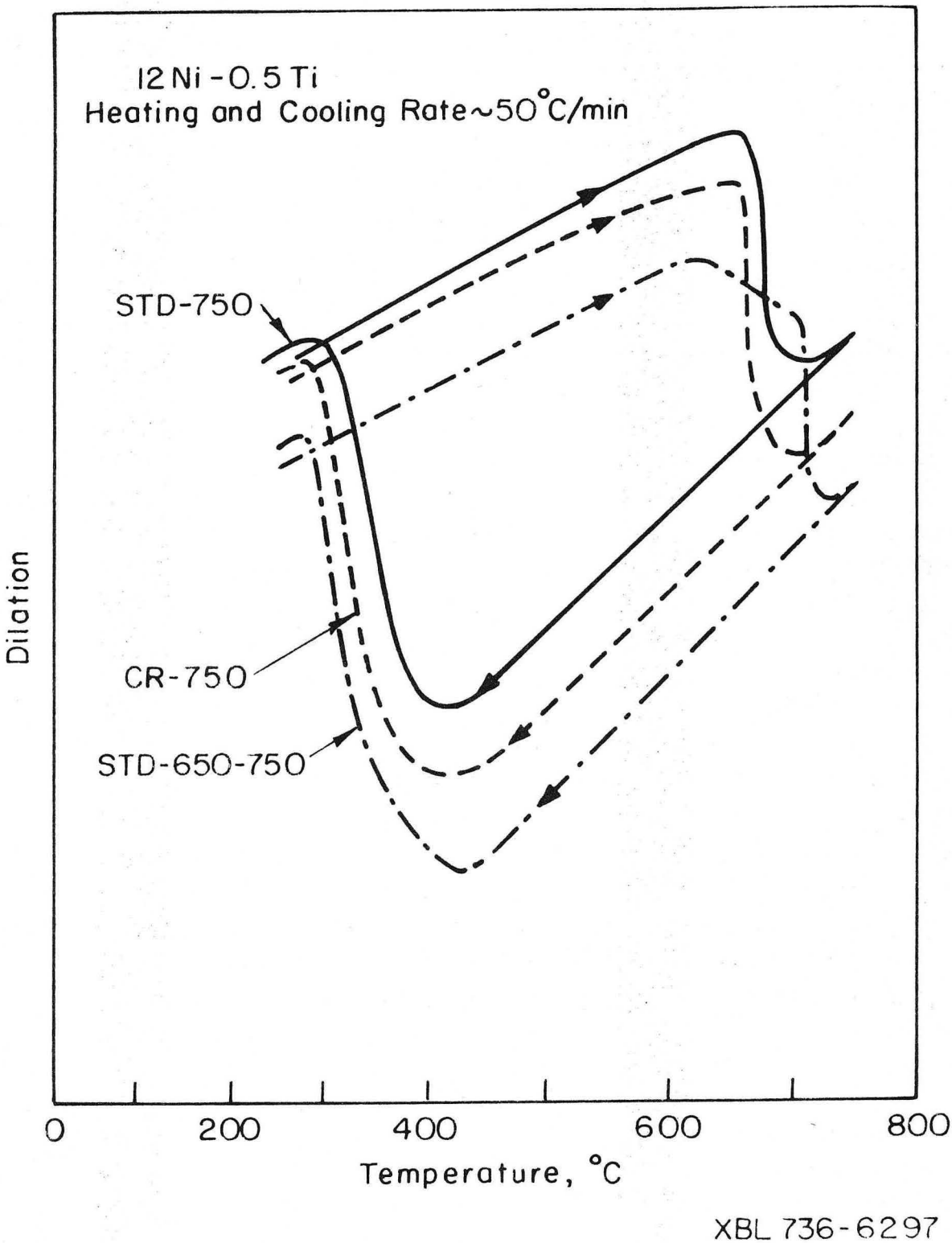

Fig. 33.

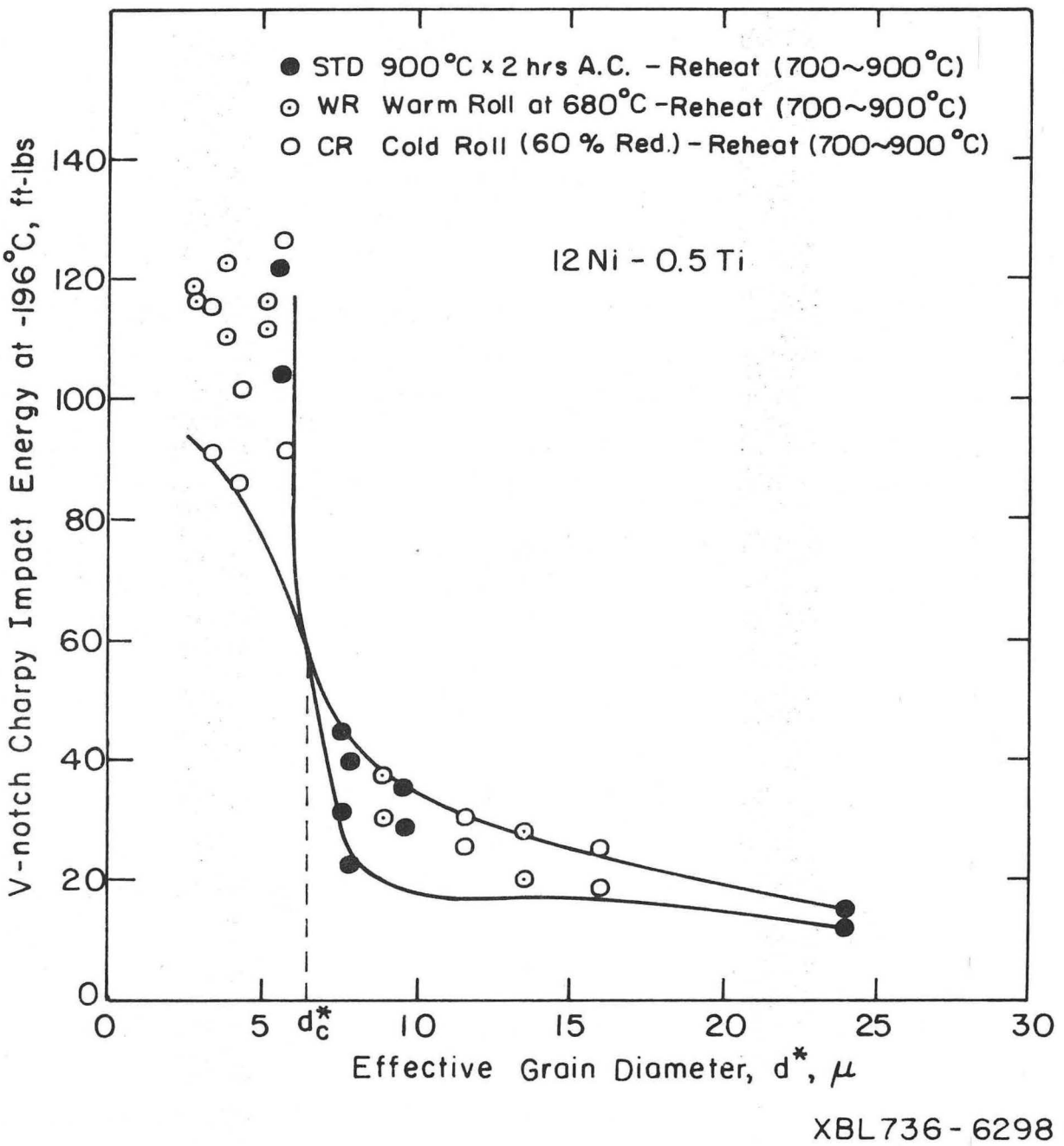
● STD 900°C x 2 hrs A.C. – Reheat (700~900°C)
⊙ WR Warm Roll at 680°C –Reheat (700~900°C)
○ CR Cold Roll (60 % Red.) – Reheat (700~900°C)
12 Ni - 0.5 Ti
V-notch Charpy Impact Energy at -196°C, ft-lbs
0
20
40
60
80
100
120
140
0
5
d_c^*
10
15
20
25
30
Effective Grain Diameter, d^*, μ
XBL736-6298

Fig. 34.

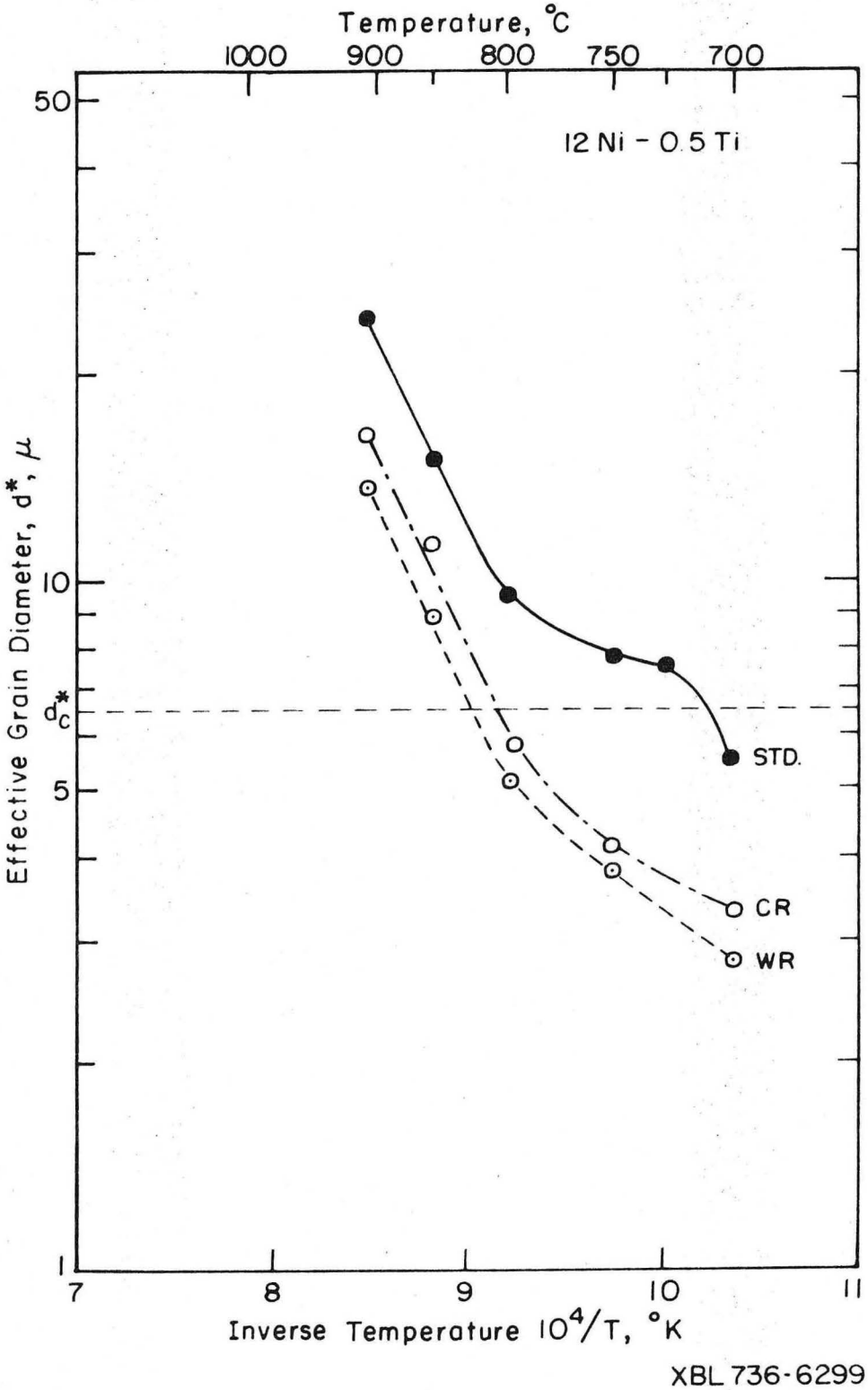
Temperature, °C
1000
900
800
750
700
12 Ni - 0.5 Ti
50
10
d_c^*
5
1
Effective Grain Diameter, d*, μ
STD.
CR
WR
7
8
9
10
11
Inverse Temperature $10^4/T$, °K
XBL 736-6299

Fig. 35.

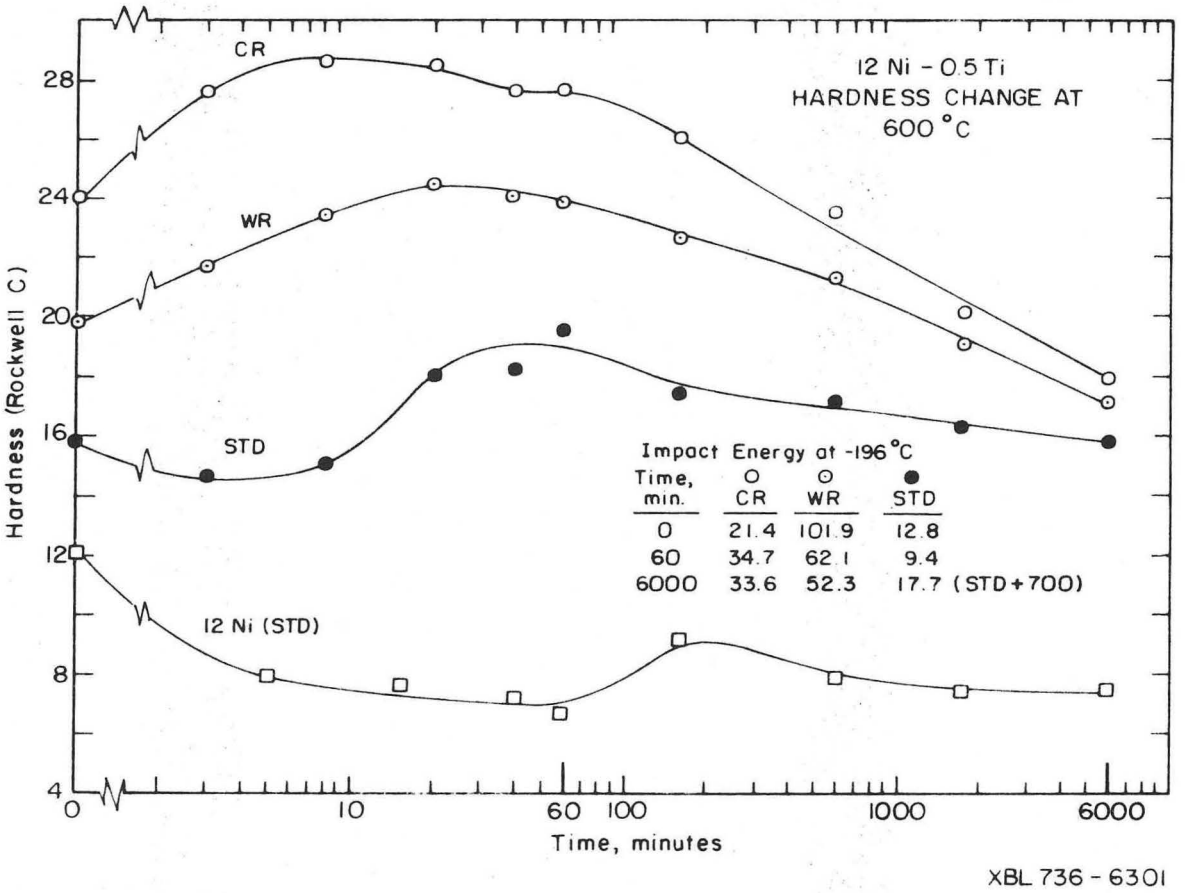
12 Ni - 0.5 Ti
HARDNESS CHANGE AT
600 °C
CR
WR
STD
12 Ni (STD)
Hardness (Rockwell C)
28
24
20
16
12
8
4
0
10
60
100
1000
6000
Time, minutes
Impact Energy at -196 °C
Time, min.
O CR
⊙ WR
● STD
0 21.4 101.9 12.8
60 34.7 62.1 9.4
6000 33.6 52.3 17.7 (STD+700)
XBL 736 - 6301

Fig. 36.

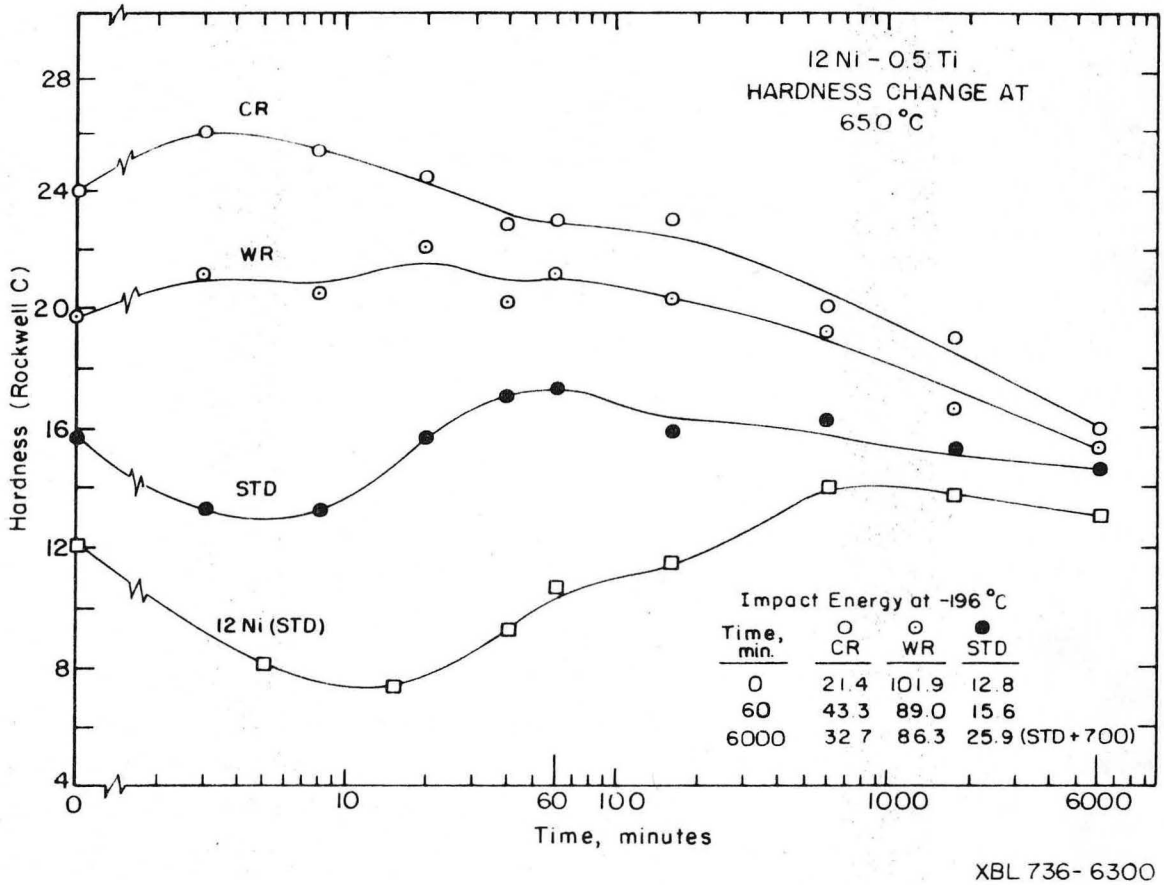
12 Ni - 0.5 Ti
HARDNESS CHANGE AT
650 °C
CR
WR
STD
12 Ni (STD)
Hardness (Rockwell C)
Time, minutes
Impact Energy at -196 °C
Time, min.
CR
WR
STD
0 21.4 101.9 12.8
60 43.3 89.0 15.6
6000 32.7 86.3 25.9 (STD+700)
XBL 736-6300

Fig. 37.

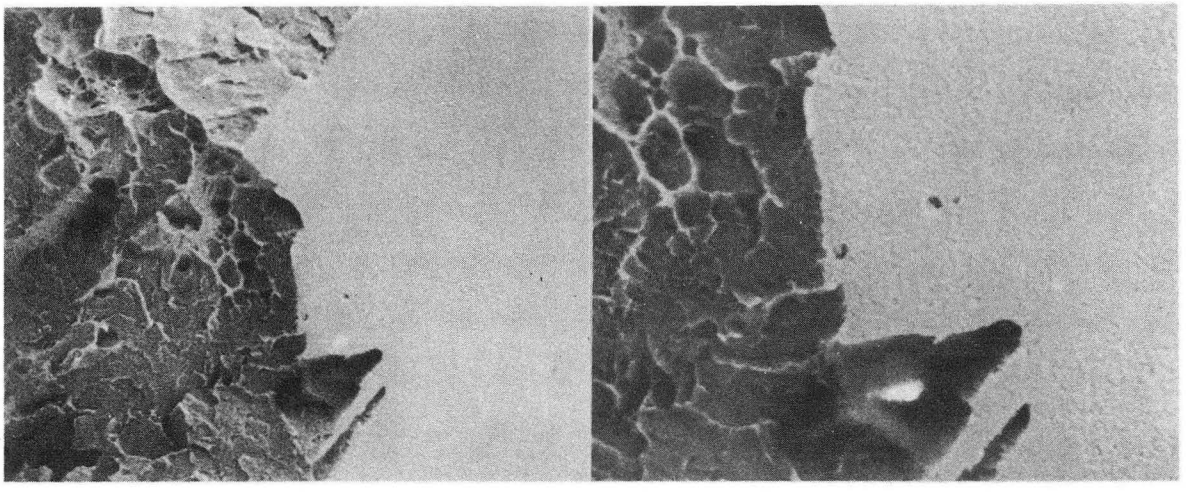

a

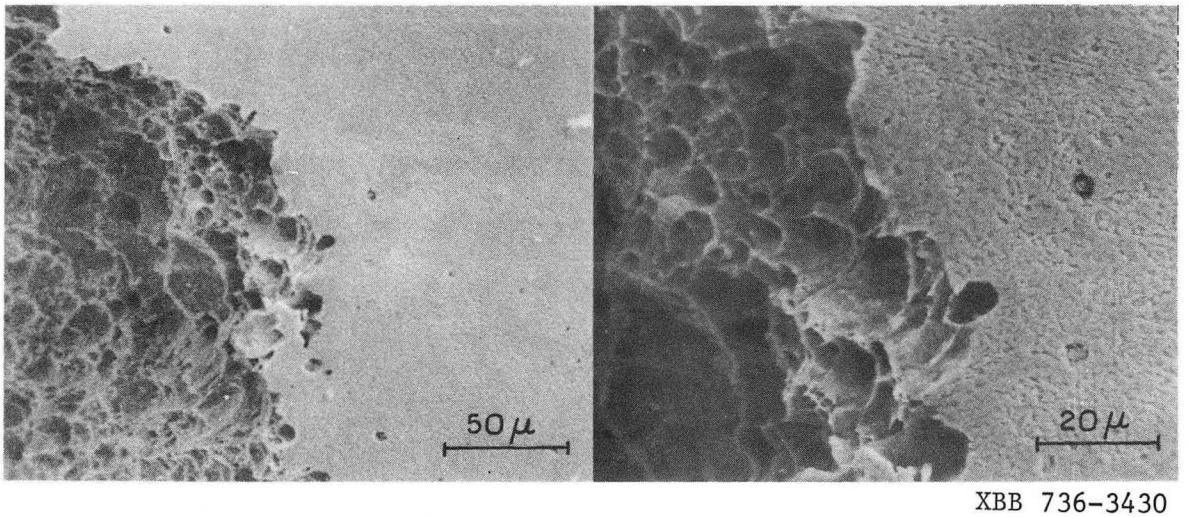

XBB 736-3430

b

Fig. 38.

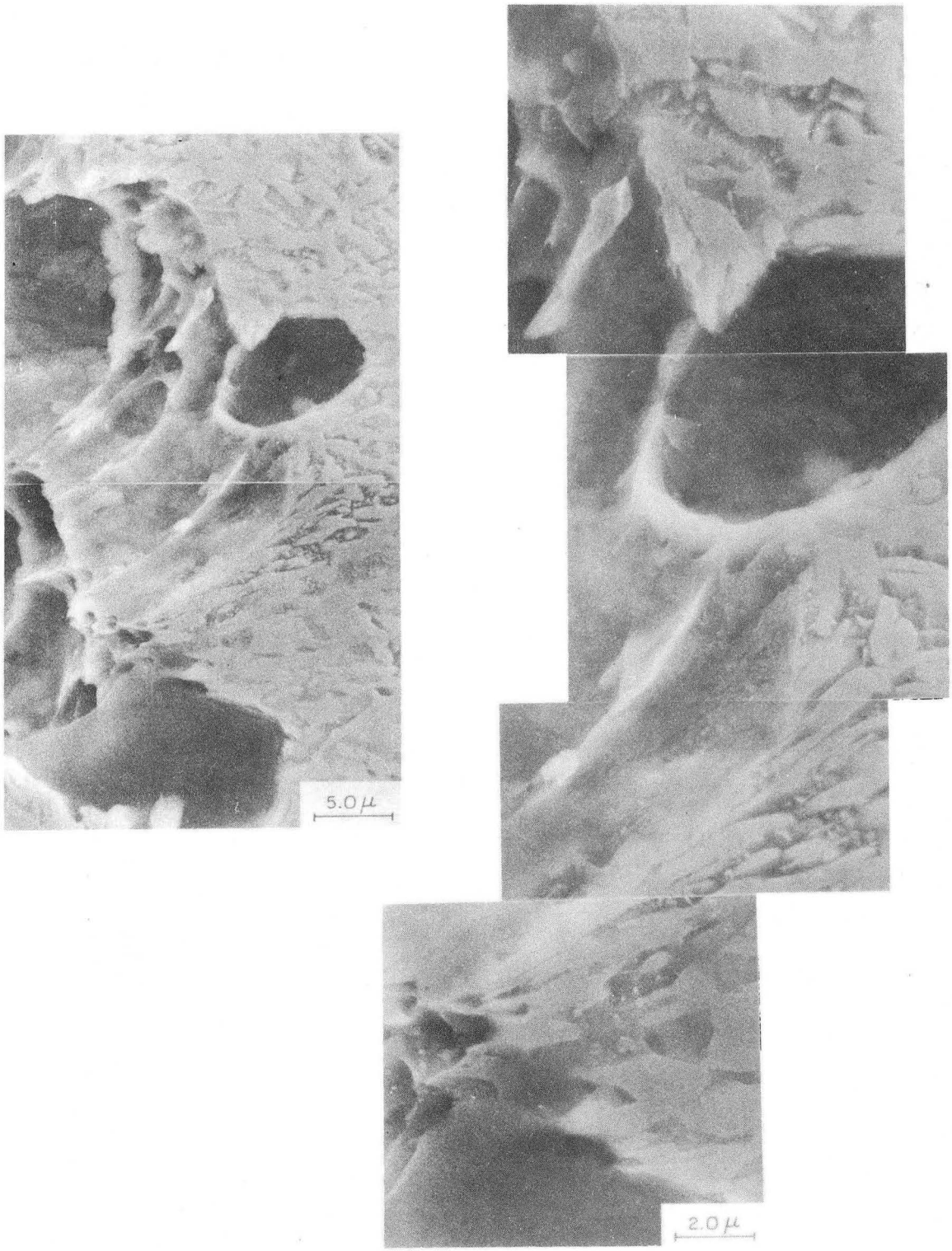

XBB 736-3420

Fig. 39.

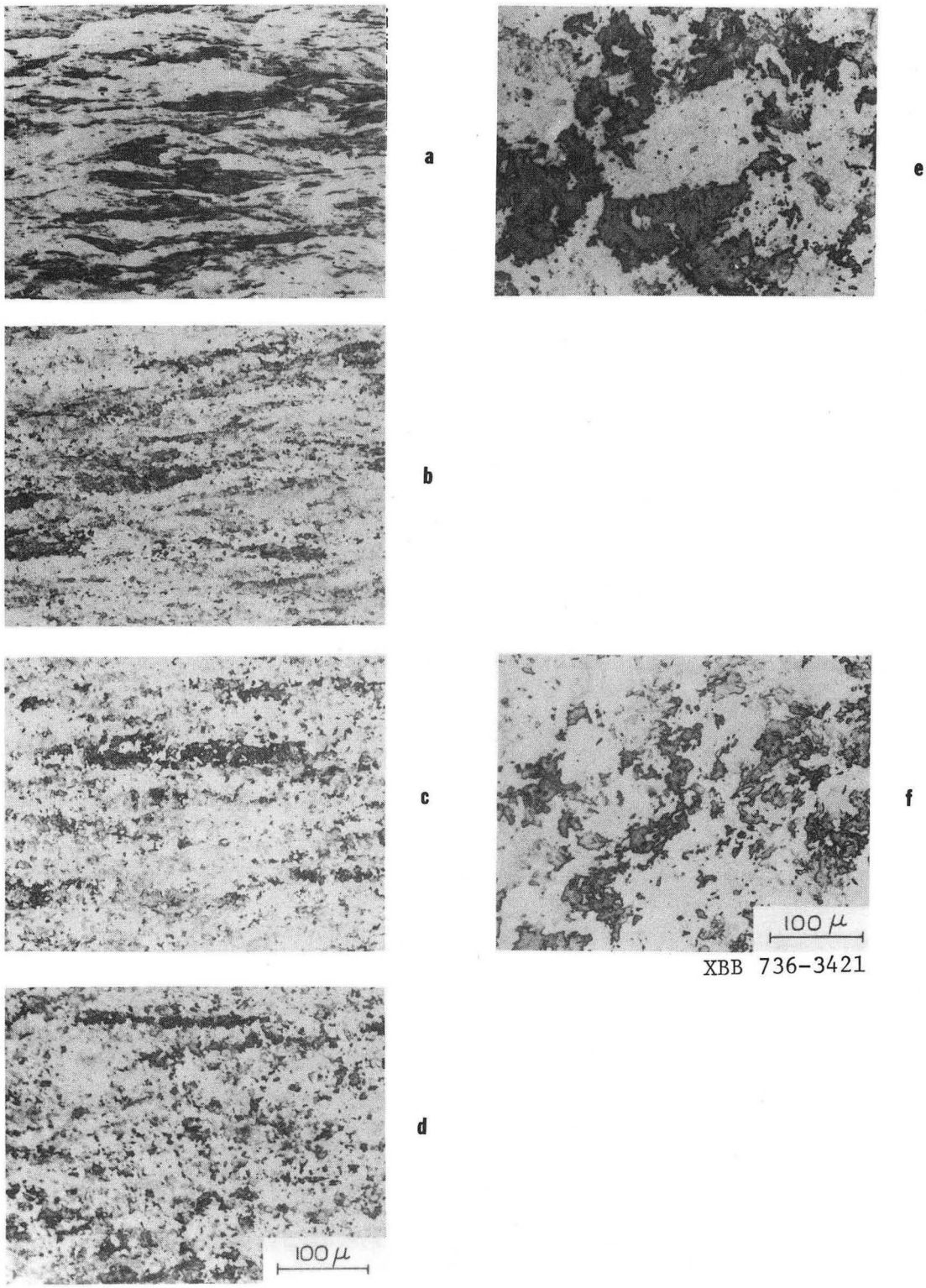

XBB 736-3421

Fig. 40.

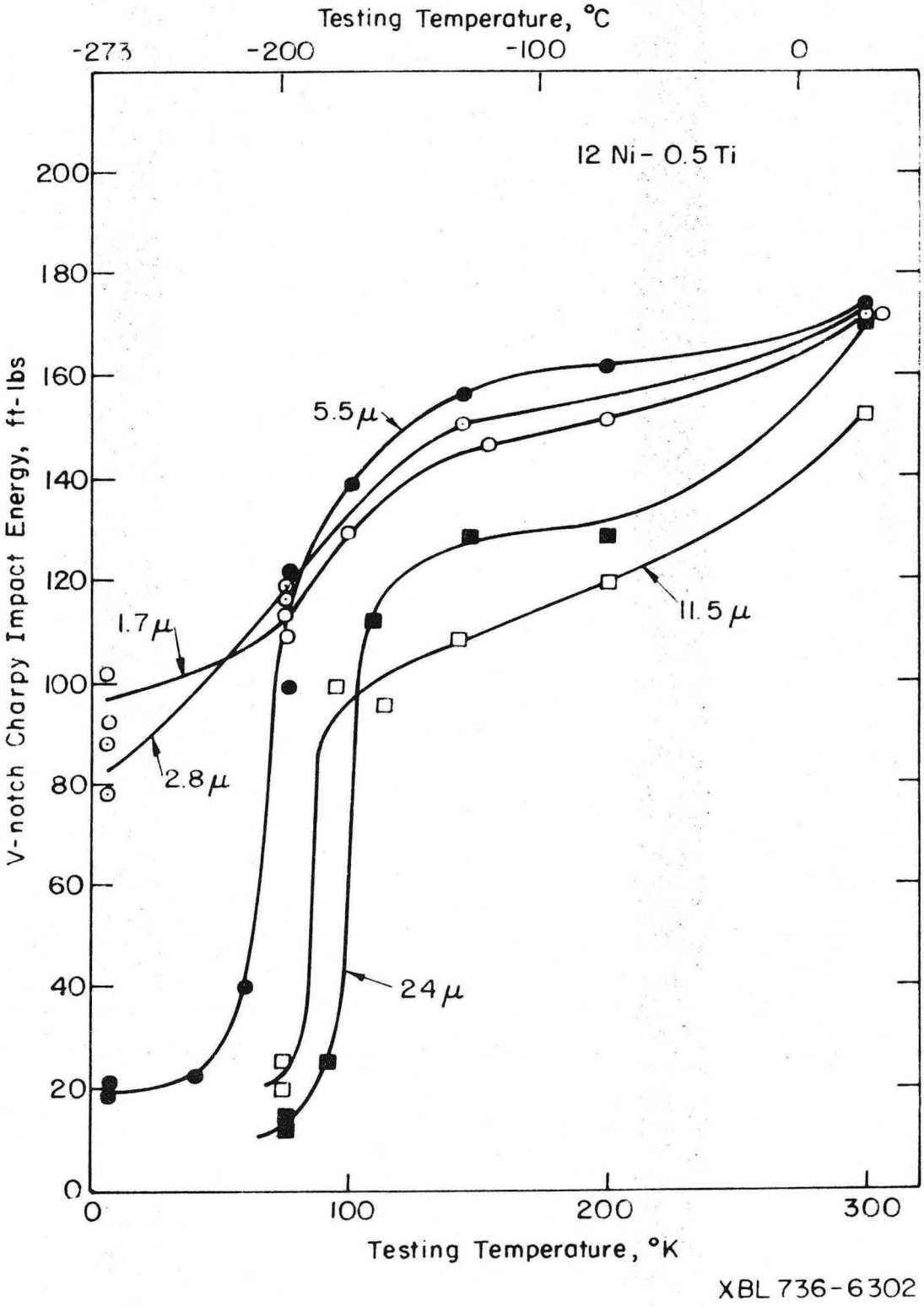

Fig. 41.

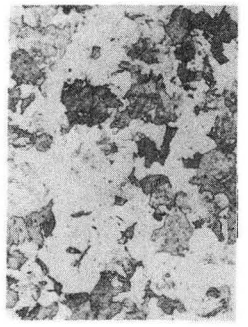

STD - 900°C x 2 hrs A.C.

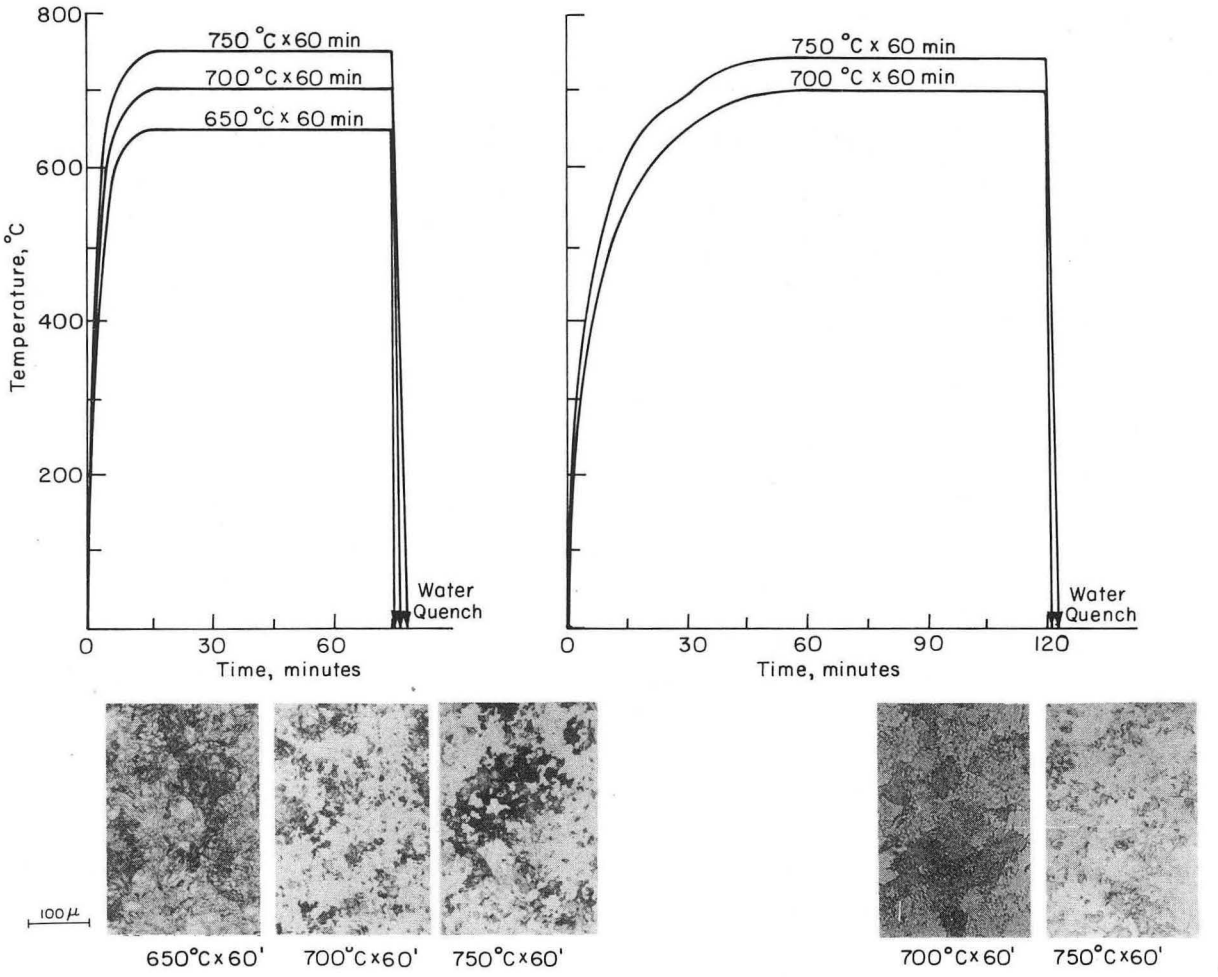

XBB 736-3562

Fig. 42.

STD -900°C x2 hrs - A.C.

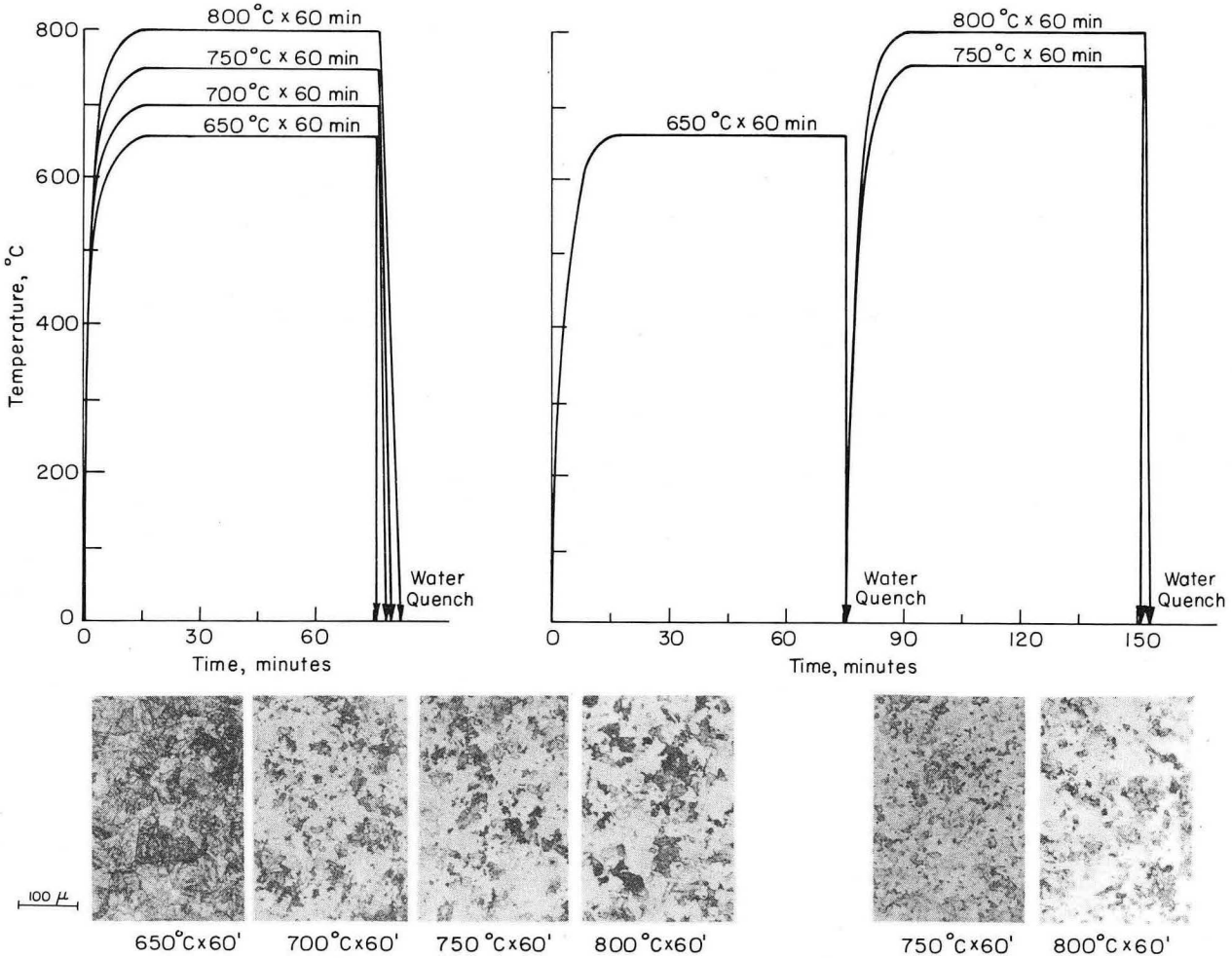

XBB 736-3563

Fig. 43.

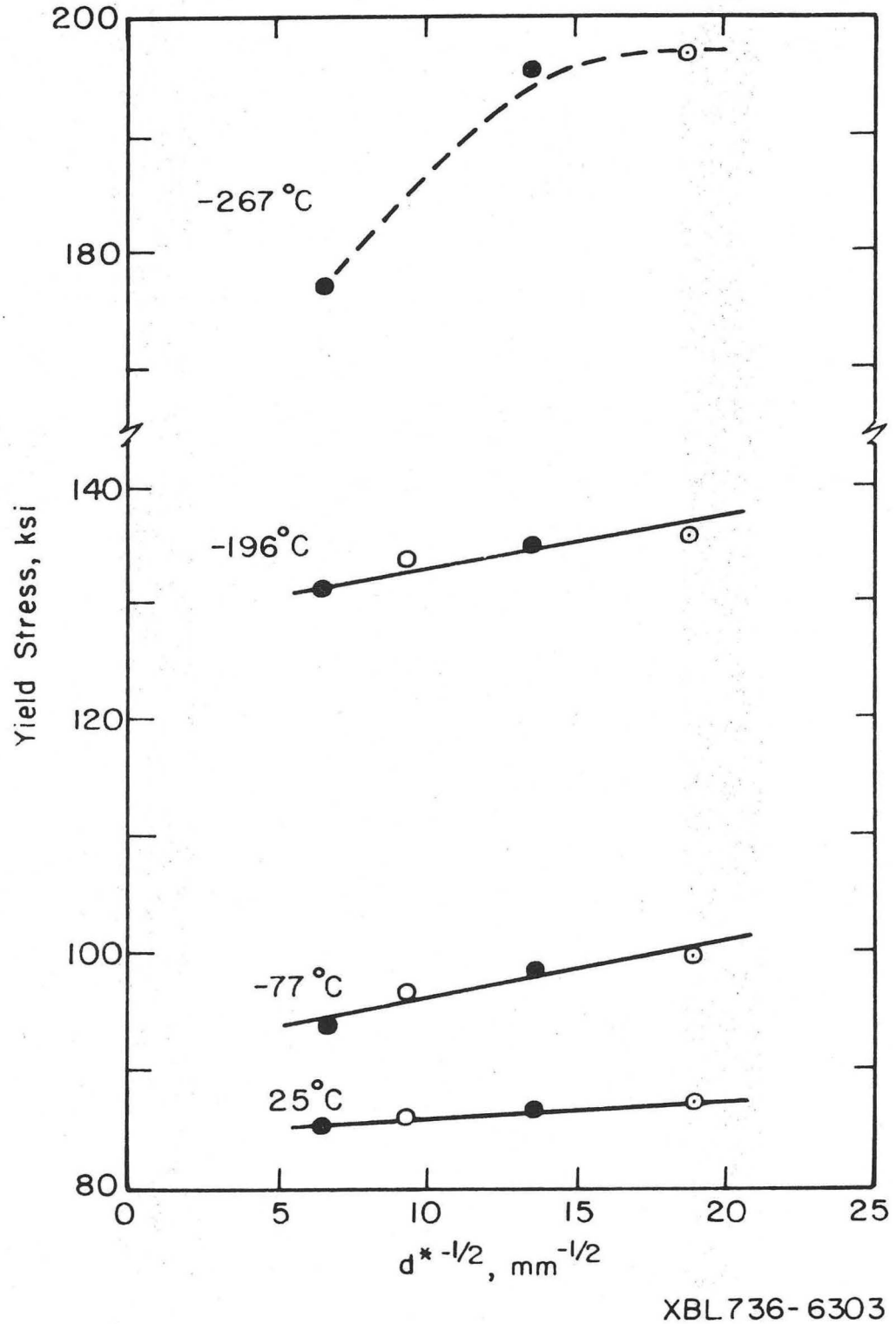
200
180
140
120
100
80
0
5
10
15
20
25
Yield Stress, ksi
d* -1/2, mm-1/2
-267 °C
-196°C
-77 °C
25°C
XBL736-6303

Fig. 44.

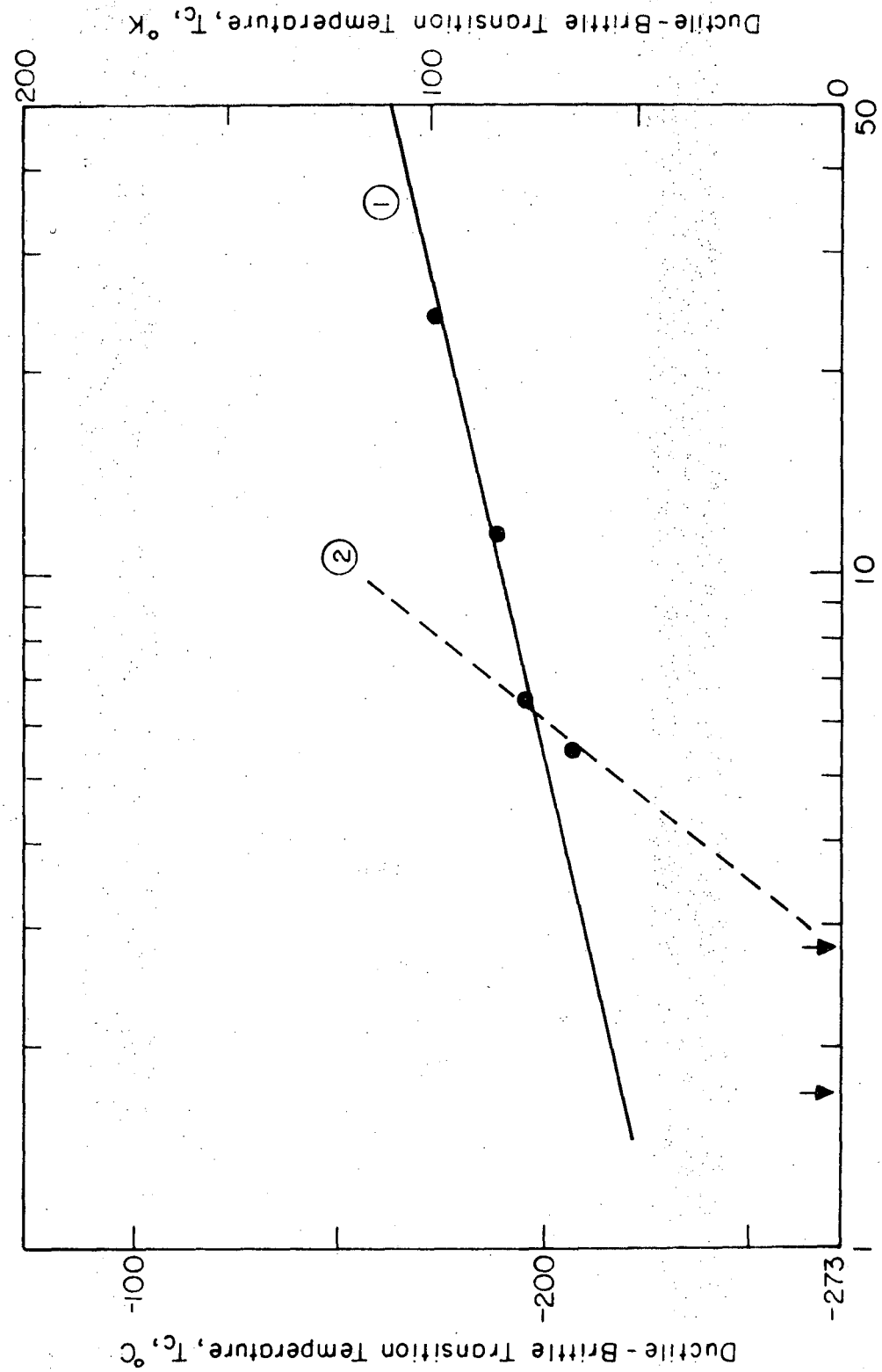
Ductile - Brittle Transition Temperature, T_c, °C
-100
-200
-273
Ductile - Brittle Transition Temperature, T_c, °K
200
100
0
50
10
Effective Grain Diameter, d^*, μ
1
2
XBL 736-6305

Fig. 45.

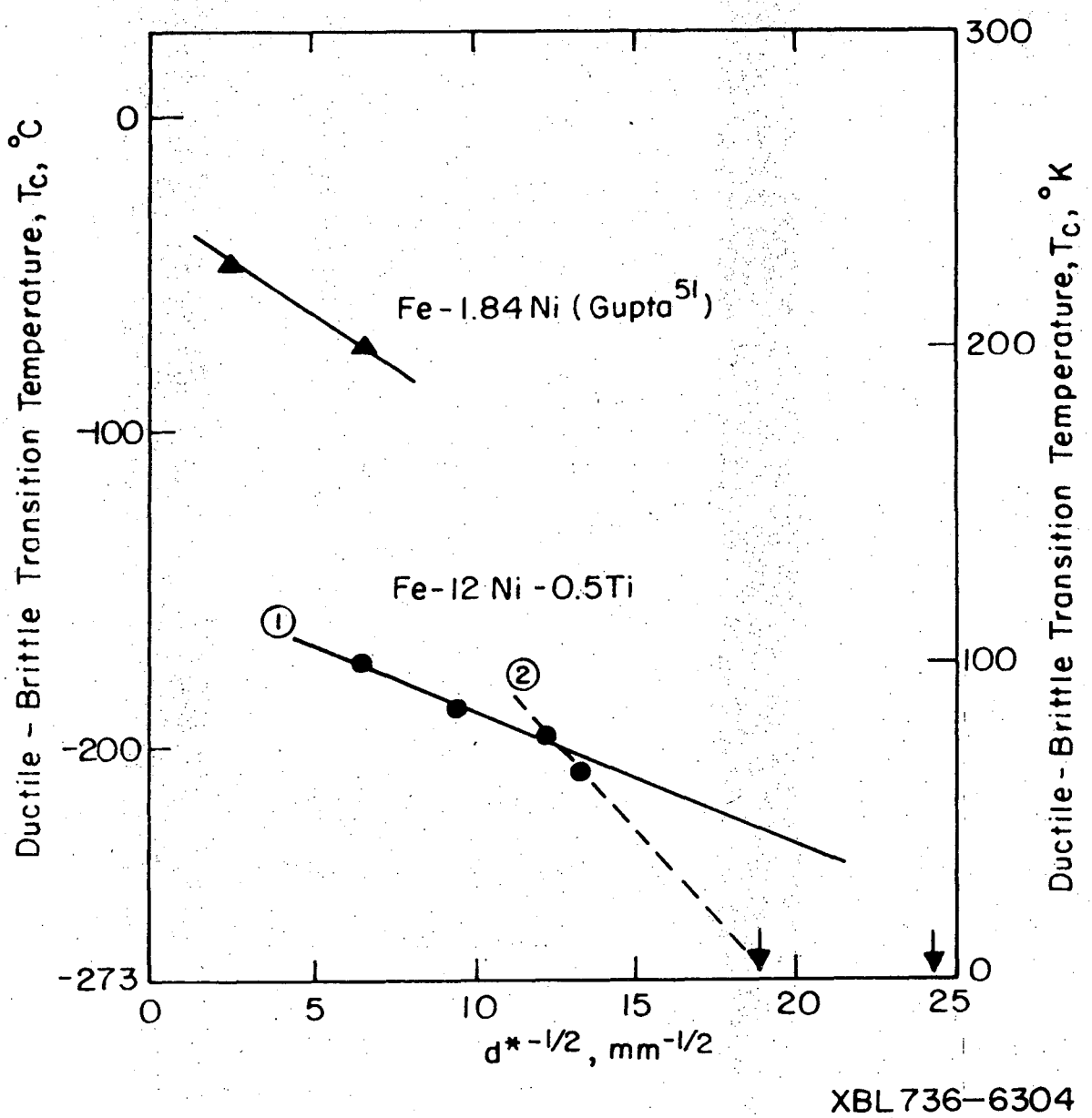
Ductile - Brittle Transition Temperature, Tc, °C
Ductile - Brittle Transition Temperature, Tc, °K
Fe - 1.84 Ni (Gupta[51])
Fe - 12 Ni - 0.5Ti
①
②
0
-100
-200
-273
300
200
100
0
0
5
10
15
20
25
d* -1/2, mm-1/2
XBL 736-6304

Fig. 46.

TECHNICAL INFORMATION DIVISION
LAWRENCE BERKELEY LABORATORY
UNIVERSITY OF CALIFORNIA
BERKELEY, CALIFORNIA 94720